



TAMPEREEN TEKNILLINEN YLIOPISTO
TAMPERE UNIVERSITY OF TECHNOLOGY

VEERA KOSKUE
NITROGEN RECOVERY FROM HYDROLYSED URINE USING
POWER-FREE MICROBIAL FUEL CELL ELECTRODIALYSIS

Master of Science Thesis

Examiners: Assistant Professor
(tenure track) Marika Kokko and
Associate Professor Stefano Fre-
guia

Examiners and topic approved by
the Dean of the Faculty of Natural
Sciences on 1st February 2017

ABSTRACT

VEERA KOSKUE: Nitrogen Recovery from Hydrolysed Urine Using Power-Free Microbial Fuel Cell Electrodialysis

Tampere University of Technology

Master of Science Thesis, 88 pages, 4 Appendix pages

April 2017

Master of Science (Tech) Degree Programme in Environmental and Energy Engineering

Major: Bioengineering

Examiners: Assistant Professor (tenure track) Marika Kokko, Associate Professor Stefano Freguia

Keywords: Nutrient recovery, nitrogen, source-separated urine, bioelectrochemistry, microbial fuel cell, electrodialysis

Nutrients, especially the most widely used macronutrients nitrogen, phosphorus and potassium, are essential for sufficient food production to feed the constantly growing human population. However, fertiliser production deals with scarce, non-renewable raw-materials and high energy consumption, which is why more efficient nutrient recovery and re-use from human waste streams should be encouraged. Human urine is an especially interesting source for nutrient recovery since it contains most of the nutrients consumed and excreted by humans.

This study focused on utilising bioelectrochemistry for nitrogen recovery from source-separated urine. The reactor design was a combination of microbial fuel cell and electrodialysis technology. The aim was to optimise the performance of both the anode and the cathode of the reactor towards a power-free nutrient recovery method. On the anodic side, the target was to enrich an acidophilic electroactive consortium, which would be able to enhance the nitrogen recovery as well as make more complete use of the high buffering capacity of urine. Of the three studied pH – 5.5, 6.5 and 7.5 – the highest one, 7.5, proved to be the most suitable one for the enriched culture, resulting in a maximum current density of 16 A m^{-2} at $E_{\text{we}} = 0 \text{ V vs. SHE}$.

On the cathodic side, an air-cathode using carbon cloth as the electrode material, carbon nanoparticles as the catalyst layer and commercial PTFE spray as diffusion layers was developed. Of the different layer materials tested, the best performance was obtained using acid-pre-treated nitrogen-doped carbon nanotubes as the catalyst and four layers of WD-40 PTFE spray as the diffusion layers. With this combination, an onset potential of $+0.1 \text{ V vs. SHE}$ for the reduction reaction was obtained and the maximum current reached in a cyclic voltammetry test was 25 A m^{-2} at -0.6 V vs. SHE .

When the best performing anode and cathode were combined in a reactor, current densities in the range of $1\text{--}2 \text{ A m}^{-2}$ were obtained at short circuit. When the cell voltage was increased to 0.5 V , the current production approximately doubled, but further increase in cell voltage did not have a notable effect on the current density obtained. Based on the preliminary studies, higher current densities should have been obtained, which indicates that further optimisation in the reactor configuration and operation is needed.

TIIVISTELMÄ

VEERA KOSKUE: Typen talteenotto hydrolysoituneesta virtsasta energiaomavaraisen elektrokonsentraation avulla
Tampereen teknillinen yliopisto
Diplomityö, 88 sivua, 4 liitesivua
Huhtikuu 2017
Ympäristö- ja energiatekniikan diplomi-insinöörin tutkinto-ohjelma
Pääaine: Bioengineering
Tarkastajat: Assistant Professor (tenure track) Marika Kokko, Associate Professor Stefano Freguia

Avainsanat: Ravinteiden talteenotto, typpi, erilliskerätty virtsa, bioelektrokemia, mikrobipolttokenno, elektrodialyysi

Ravinteet, erityisesti eniten käytetyt makroravinteet typpi, fosfori ja kalium, ovat välttämättömiä takaamaan riittävän ruoantuotannon alati kasvavalle ihmiskunnalle. Lannoitteiden tuotantoon liittyy kuitenkin ongelmia, kuten raaka-aineiden uusiutumattomuus ja rajallisuus sekä korkea energiankulutus. Tämän takia ravinteiden talteenotto ja kierrätys ihmisten jätevirroista on suositeltavaa. Ihmismvirtsa on erityisen kiinnostava jätevirta ravinteiden talteenoton kannalta, sillä se sisältää suurimman osan ihmisten kuluttamista ja erittämistä ravinteista.

Tämä työ keskittyi bioelektrokemiallisten menetelmien hyödyntämiseen typen talteenotossa erilliskerätystä virtsasta. Käytetty reaktori oli yhdistelmä mikrobipolttokenno- ja elektrodialyysitekniikkaa. Tavoitteena oli optimoida sekä anodin että katodin toiminta niin, että energiaomavarainen ravinteidentalteenotto olisi mahdollista. Anodin osalta tavoitteena oli rikastaa alhaisessa pH:ssa viihtyvä mikrobipopulaatio, joka pystyisi edistämään typen talteenottoa ja hyödyntämään virtsan korkeaa puskurikapasiteettia entistä tehokkaammin. Kolmesta tutkitusta pH:sta – 5.5, 6.5 ja 7.5 – korkein eli 7.5 osoittautui sopivimmaksi rikastetulle populaatiolle. Korkein saavutettu virrantiheys oli 16 A m^{-2} potentiaalilla 0 V vs. SHE.

Katodiksi suunniteltiin ja valmistettiin ilmakatodi käyttäen hiilikangasta elektrodimateriaalina, hiilinanomateriaaleja katalyyseina ja kaupallista PTFE-suihketta diffuusiokerroksina. Paras tulos saavutettiin käyttämällä hapolla esikäsiteltyjä hiilinanoputkia katalyyseina ja neljää kerrosta WD-40-suihketta diffuusiokerroksina. Hapen pelkistymisreaktion alkamispotentiaali tällä yhdistelmällä oli +0.1 V vs. SHE ja korkein saavutettu virrantiheys 25 A m^{-2} potentiaalilla -0.6 V vs. SHE.

Kun parhaiksi todetut anodi ja katodi yhdistettiin, reaktorin tuottama virrantiheys ilman potentiaalil lisäystä oli noin $1\text{--}2 \text{ A m}^{-2}$. Kun kennon potentiaali kasvatettiin 0.5 V:iin, virrantiheys tuplaantui. Tämän jälkeen potentiaalil kasvatuksella ei ollut suurta vaikutusta reaktorin tuottamaan virrantiheyteen. Alustavien kokeiden perusteella korkeampien virrantiheyksien olisi pitänyt olla saavutettavissa, mikä viittaa siihen, että reaktorin rakenteessa ja operoinnissa on vielä optimoimisen varaa.

PREFACE

In February 2016, I heard about a Master's Thesis position that would include a 2–3-month exchange in Australia. I applied and was accepted. Along the way, a lot happened: the exchange period was lengthened to 6 months, which meant that I would be writing my whole thesis in Australia (which I quite obviously did not mind doing), but at the same time I ran into some problems and delays both with funding and the visa process. I ended up investing quite a lot of my own time and money into this thesis project, but after spending these six months on the other side of the world, I can honestly say that it was totally worth it.

Of course, I could not have done this on my own. First and foremost, I want to thank my fellow UGold project members at AWMC: my supervisors Stefano Freguia and Pablo Ledezma for excellent guidance and teaching me more than I could ever have imagined; my mentor Johannes Jermakka for always having the time and answers to all my questions; and Juliette Monetti for peer support and fun times in and outside the lab. Many thanks also to my supervisor at TUT, Marika Kokko, for helping me especially with the writing process and always being only one e-mail away. In addition, sincere thanks to professor Jukka Rintala at TUT for all the help and support throughout the process.

Thank you TUT and Maa- ja vesitekniikan tuki ry for the stipends I was granted that helped make this experience possible.

From the bottom of my heart, I want to thank every single person I met at AWMC for being so extremely nice and making me feel welcome. You truly made my time in Brisbane unforgettable. Similar thanks also go to all the people I got to know during my seven years at TUT for making my study time the best time of my life.

Last but not least, I want to thank my family for life-long love and support. And Samu, thank you for always making me laugh, even when there are 15,000 km between us.

Brisbane, 8.4.2017

Veera Koskue

CONTENTS

1	INTRODUCTION	1
2	NUTRIENT RECOVERY FROM DOMESTIC WASTEWATERS	3
2.1	Nutrient cycle from agriculture to domestic wastewaters.....	3
2.2	Need for nutrient recovery and recycling	4
2.2.1	Phosphorus.....	4
2.2.2	Nitrogen	5
2.2.3	Sources for nutrient recovery.....	6
2.3	Nutrient recovery from source-separated urine	7
2.3.1	Characteristics of source-separated urine	7
2.3.2	Recovery of phosphorus	10
2.3.3	Recovery of nitrogen	10
2.3.4	Decentralised wastewater treatment	11
3	BIOELECTROCHEMISTRY AS A NOVEL TECHNIQUE FOR NITROGEN RECOVERY FROM WASTEWATERS	13
3.1	Bioelectrochemical systems.....	13
3.1.1	Microbial fuel cells	15
3.1.2	Electrodialysis.....	17
3.1.3	Combining MFC and ED technology	19
3.1.4	Enhanced oxygen reduction at the air-cathode	21
3.1.5	Cyclic voltammetry for analysing BES performance	23
3.2	Bioelectrochemical methods for nitrogen recovery from urine	24
3.3	The UGold project	27
3.4	Research objectives.....	29
4	MATERIALS AND METHODS.....	30
4.1	Enrichment of a neutrophilic electroactive consortium	30
4.1.1	Reactor configuration and start-up	30
4.1.2	Continuous operation and pH adjustment.....	33
4.1.3	Sampling	34
4.1.4	Microbial community analysis using DNA pyrosequencing	35
4.2	Development of an efficient air-cathode.....	35
4.2.1	Cathode preparation.....	35
4.2.2	Cathode performance analyses	37
4.3	Operation of UGold reactors with air-cathodes	38
4.3.1	Reactor configuration and start-up	38
4.3.2	Operation with air-cathode	39
4.3.3	Sampling	42
4.4	Analyses and calculations	43
5	RESULTS	44
5.1	Enrichment of neutrophilic electroactive consortia	44

5.1.1	Electrochemical measurements.....	44
5.1.2	Microbial community analyses.....	51
5.1.3	Buffer capacity.....	53
5.2	Enhanced ORR at the air-cathode.....	55
5.2.1	Catalyst coating.....	55
5.2.2	PTFE coating.....	59
5.3	Operation of UGold reactor with air-cathodes.....	62
5.3.1	Enrichment of anodic biomass.....	62
5.3.2	Operation with air-cathodes.....	65
6	DISCUSSION.....	72
6.1	Enrichment of the neutrophilic consortium.....	72
6.2	Performance of the catalyst materials.....	74
6.3	Performance of PTFE as diffusion layer and operation of UGold reactor with air-cathode.....	76
7	CONCLUSIONS.....	78
7.1	Concluding remarks.....	78
7.2	Outlook.....	79
	REFERENCES.....	81

APPENDIX A: Composition of the trace element solution

APPENDIX B: Photo of struvite formation on the cathode in the enrichment experiments

APPENDIX C: Ion species distribution at different pH

LIST OF FIGURES

<i>Figure 2.1.1 Cycle of N fertilisers from production to human excreta. Values are calculated based on data from several sources (FAO 2016; Friedler et al. 2013; Sutton et al. 2013).</i>	4
<i>Figure 3.1.1 Operating principle of an MFC.</i>	15
<i>Figure 3.1.2 Operating principle of a stacked ED system.</i>	18
<i>Figure 3.1.3 ORR at the air-cathode (A) via the 2-electron pathway and (B) via the 4-electron pathway, facilitated by a catalyst layer on the water-facing side and diffusion layer(s) on the air-facing side.</i>	21
<i>Figure 3.1.4 Typical shape of a turnover (i.e. all proteins involved in the pathway are oxidized and reduced multiple times (LaBelle & Bond 2010)) CV with scan rate 1 mV s^{-1} (Harnisch & Freguia 2012). Onset potential for the oxidation reaction (dashed line) and peak anodic current (solid line) are marked with red.</i>	23
<i>Figure 3.3.1 Operating principle of the UGold reactor. The flow of urine is presented in orange and the flow of electrons in blue.</i>	27
<i>Figure 4.1.1 Photos of (A) the anodes constructed for the enrichment reactors, and (B) the experimental set-up when operating the enrichment reactors in continuous mode.</i>	31
<i>Figure 4.1.2 Schematic picture of the reactor configuration (from above) used in the enrichment experiments. In batch mode, the ports for flow in and out were also sealed.</i>	31
<i>Figure 4.2.1 The small-scale air-cathode reactor used in the preliminary tests for different cathode catalyst and PTFE materials.</i>	38
<i>Figure 4.3.1 Schematic picture of the reactor configuration when operating UGold reactors with air-cathodes.</i>	40
<i>Figure 4.3.2 Photos of the UGold reactors operated with air-cathodes.</i>	41
<i>Figure 4.3.3 Schematic picture of the experimental set-up when operating UGold reactors with air-cathodes. pH sampling points are marked with red.</i>	42
<i>Figure 5.1.1 Current density and influent and effluent pH of A5.5 during enrichment experiments.</i>	45
<i>Figure 5.1.2 Current density and influent and effluent pH of A6.5 during enrichment experiments.</i>	46
<i>Figure 5.1.3 Current density and influent and effluent pH of A7.5 during enrichment experiments.</i>	46
<i>Figure 5.1.4 CVs conducted individually to the two anodes in A5.5 after re-start on day 30: (A) Anode 1, meaning the anode moved from A6.5, and (B) Anode 2, meaning the anode originally in the reactor. Days when measurements were conducted are presented in brackets.</i>	48

<i>Figure 5.1.5 CVs conducted individually to the two anodes in A6.5 after the re-start on day 75: (A) Anode 1, meaning the anode moved from A7.5, and (B) Anode 2, meaning the completely new one. Days when measurements were conducted are presented in brackets.....</i>	<i>49</i>
<i>Figure 5.1.6 CVs conducted individually to the two anodes in A7.5 after the re-start on day 63: (A) Anode 1, meaning the original anode in the reactor, and (B) Anode 2, meaning the completely new one. Days when measurements were conducted are presented in brackets.....</i>	<i>50</i>
<i>Figure 5.1.7 Heat map summarising the relative abundancies of different bacteria in the biomass samples. For clarity, only bacteria present at $\geq 2\%$ in at least one of the samples are presented.</i>	<i>51</i>
<i>Figure 5.1.8 Quality control (QC) statistics of the four different runs.....</i>	<i>53</i>
<i>Figure 5.2.1 CVs conducted for the NCNT-coated cathode in two different buffers immediately after the deposition and in ammonia buffer the following day (marked “overnight”).CVs conducted for plain carbon cloth in both buffers are included for comparison.....</i>	<i>56</i>
<i>Figure 5.2.2 CVs conducted for the NG-coated cathodes in ammonia buffer immediately after the deposition, in both buffers the following day, and in a more dilute ammonia buffer 21 days after the deposition (also tested with a larger range). CVs conducted for plain carbon cloth in both buffers are included for comparison.....</i>	<i>57</i>
<i>Figure 5.2.3 A summary of the CVs in phosphate buffer for the rest of the catalyst materials tested. All CVs were conducted after an overnight drying period. CVs conducted for plain carbon cloth in both buffers are included for comparison.</i>	<i>58</i>
<i>Figure 5.2.4 A summary of the CVs in ammonia buffer for the rest of the catalyst materials tested. All CVs were conducted after an overnight drying period. CVs conducted for plain carbon cloth in both buffers are included for comparison.</i>	<i>59</i>
<i>Figure 5.2.5 CVs conducted for Acid-NCNT and PVDF-PAC with different amounts of Ezy Glide PTFE spray in phosphate or ammonia buffer. Control means a cathode with no catalyst coating and 4 layers of WD-40 PTFE spray, measured in 0.1 M ammonia buffer.....</i>	<i>60</i>
<i>Figure 5.2.6 CVs conducted in ammonia buffer for (A) Acid-NCNT and (B) PVDF-PAC with varying numbers of layers of WD-40 PTFE spray. Control means a cathode with no catalyst coating and 4 layers of WD-40 PTFE spray, measured in 0.1 M ammonia buffer.....</i>	<i>61</i>
<i>Figure 5.3.1 Current density (calculated as the averages of nine consecutive data points) and feed, anode and cathode pH of (A) UGold1 and (B) UGold2 during the enrichment of biomass at the anode.</i>	<i>63</i>
<i>Figure 5.3.2 CVs conducted at the start-up and after the enrichment for the anodes in (A) UGold1 and (B) UGold 2.</i>	<i>65</i>

<i>Figure 5.3.3 Current density produced by UGold1 at different applied cell voltages when operated with air-cathode. Blue area represents the time period when recirculation from cathode to anode was used.</i>	<i>66</i>
<i>Figure 5.3.4 Current density produced by UGold2 at different applied cell voltages when operated with air-cathode. Blue area represents the time period when recirculation from cathode to anode was used.</i>	<i>67</i>
<i>Figure 5.3.5 Biomass growing on the cathode of UGold2 at the end of the air-cathode experiments.....</i>	<i>68</i>
<i>Figure 5.3.6 Measured cathode and anode potentials and influent, effluent and middle chamber pH of (A) UGold1 and (B) UGold2 during the operation with air-cathodes.....</i>	<i>69</i>
<i>Figure 5.3.7 CVs conducted for the anodes and the cathodes in (A) UGold1 and (B) UGold2. The voltammogram of Acid-NCNT with 4xWD-40 in the preliminary experiments is included for comparison.</i>	<i>71</i>

LIST OF TABLES

<i>Table 2.3.1 Typical compositions of fresh and hydrolysed urine</i>	<i>8</i>
<i>Table 4.1.1 Compositions of the synthetic hydrolysed urine feeds. Green, red and blue values represent changes made to the feed compositions during the experiments.</i>	<i>32</i>
<i>Table 4.2.1 Tested catalyst materials and different parameters used</i>	<i>36</i>
<i>Table 5.1.1 Changes made to operation conditions in the three enrichment reactors during the experiments</i>	<i>44</i>
<i>Table 5.1.2 Ion species distribution of main buffering compounds at different pH</i>	<i>54</i>

ABBREVIATIONS AND SYMBOLS

ACE	Australian Centre for Ecogenomics
AEM	Anion exchange membrane
AWMC	Advanced Water Management Centre
Ag/AgCl	Silver/silver chloride electrode, has a constant potential of -0.197 V vs. SHE
BES	Bioelectrochemical system
BW	Blackwater, sanitary wastewater
CA	Chronoamperometry
Ca	Calcium
Cd	Cadmium
CE	Counter electrode
CEM	Cation exchange membrane
COD	Chemical oxygen demand
CV	Cyclic voltammetry
DL	Diffusion layer
EAM	Electrochemically active microorganisms
EC	Electric conductivity
ED	Electrodialysis
EET	Extracellular electron transfer
EMF	Electromotive force
EPD	Electrophoretic deposition
EPS	Extracellular polymer substance
GHG	Greenhouse gas
GW	Greywater, domestic wastewater generated e.g. via shower, kitchen sink and washing machine
H ₂	Hydrogen gas
H ⁺	Proton
HAP	Hydroxyapatite
HCO ₃ ⁻	Bicarbonate
HRT	Hydraulic retention time
IBDU	Isobutylaldehydediurea
IBU	Isobutyraldehyde
K	Potassium
LSV	Linear sweep voltammetry
MAP	Magnesium-ammonium phosphate, a.k.a. struvite
MEC	Microbial electrolysis cell
MFC	Microbial fuel cell
Mg	Magnesium
N	Nitrogen
N ₂	Nitrogen gas
Nr	Reactive nitrogen
Na	Sodium
NCNT	Nitrogen-doped carbon nanotube
NCP	Nitrogen-doped carbon powder
NG	Nitrogen-doped graphene
NH ₃	Ammonia
NH ₄ ⁺	Ammonium

NMP	N-Methyl-2-Pyrrolidone
OCV	Open circuit voltage
ORR	Oxygen reduction reaction
P	Phosphorus
PAC	Powdered activated carbon
PEM	Proton exchange membrane
PTFE	Polytetrafluoroethylene
PVDF	Polyvinylidene fluoride
QC	Quality control
RE	Reference electrode
RO	Reverse osmosis
SHE	Standard hydrogen electrode
TAN	Total ammonia nitrogen, $\text{NH}_3 + \text{NH}_4^+$
WE	Working electrode
WWTP	Wastewater treatment plant
E	Electric potential [V]
E_{cell}	Cell potential [V]
E_{emf}	Cell potential [V]
E_{emf}^θ	Cell potential under standard conditions [V]
E_{we}	Working electrode potential [V]
I	Electric current [A]
R	Universal gas constant [$\text{J mol}^{-1} \text{K}^{-1}$]
T	Absolute temperature [K]
u	Ion mobility [$10^{-1} \text{m}^2 \text{s}^{-1} \text{V}^{-1}$]
ΔG_r	Gibb's free energy [J]
ΔG_r^θ	Gibb's free energy at standard conditions [J]
Π	Reaction quotient [-]

1 INTRODUCTION

Worldwide chemical fertiliser usage keeps increasing in order for the agriculture to be able to respond to the nutritional need of the constantly growing world population (Sutton et al. 2013). However, at the same time the production of the fertilisers suffers from unsustainability and increasing costs due to the depletion of nutrient resources and high energy consumption related to their production (Pronk & Koné 2009; Sutton et al. 2013). Furthermore, the environmental effects of the fertiliser industry are also drawing more and more attention (Cai et al. 2013; Erisman & Larsen 2013). Thus, actions are needed to recover and reuse nutrients, especially the most important macronutrients phosphorus, nitrogen and potassium, from human-generated waste streams in a more efficient way.

Domestic wastewaters are an interesting source for nutrient recovery since humans do not accumulate nutrients in their bodies; therefore, the amount of nutrients we consume as food will also be excreted into the wastewaters (Jönsson & Vinnerås 2013). Most of these nutrients will end up in human urine, which makes it an especially interesting recovery source for nutrients (Friedler et al. 2013). In order to best take advantage of this, source separation of domestic wastewaters e.g. by using urine-diverting toilets and waterless urinals is required. Furthermore, novel techniques for nutrient recovery from urine need to be introduced since traditional wastewater treatment methods only tend to focus on removing the nutrients from wastewaters, not recovering them in a reusable form (Booker et al. 1999).

Struvite precipitation from urine is an efficient method to recover phosphorus and it is widely considered the most promising nutrient recovery technique (Ledezma et al. 2015; Maurer et al. 2006). Struvite formation will also help recover some of the nitrogen in the urine. However, due to the 1:1 stoichiometric ratio for N:P in struvite and since nitrogen is present at much higher concentrations than phosphorus in urine, the majority of nitrogen remains in the dilute liquid phase. (Friedler et al. 2013; Ledezma et al. 2015) Therefore, other methods are needed to achieve more complete nitrogen recovery.

Utilisation of bioelectrochemical systems can be seen as an intriguing option for nitrogen recovery from source-separated urine. Bioelectrochemical systems benefit from the high electric conductivity and buffering capacity of urine compared to other wastewaters (Udert et al. 2006). Contrary to other available recovery methods, they rarely require addition of chemicals and can even be operated with no external power source.

In this work, the focus was on developing a novel technique for the recovery of nitrogen from source-separated urine using a combination of microbial fuel cell and electro dialysis technology. The work was carried out as a part of the UGold project at the Advanced Water Management Centre of the University of Queensland in Brisbane, Australia.

2 NUTRIENT RECOVERY FROM DOMESTIC WASTEWATERS

All plant and animal growth and development need to be supported by several key elements, nutrients. The three major nutrients that are needed in the greatest supply, and are therefore called macronutrients, are phosphorus (P), nitrogen (N), and potassium (K). (Sutton et al. 2013) Of these three, N is typically needed in largest amounts and it is the yield-limiting nutrient for most crops. P, on the other hand, can limit crop development in low-fertility soils. (Jönsson & Vinnerås 2013)

Nutrients are lost from soils not only by the harvested crops but also due to leaching and erosion as well as N losses to the atmosphere by volatilisation. Thus, to maintain the fertility of the arable lands, similar amounts of nutrients need to be added to the soil as are removed from it. This is typically done by using chemical fertilisers. (Jönsson & Vinnerås 2013)

2.1 Nutrient cycle from agriculture to domestic wastewaters

Worldwide production of different types of N, P and K fertilisers in 2014 was approximately 113.3 million tonnes for N, 53.3 million tonnes for P, and 41.4 million tonnes for K in nutrients. Similarly, the amounts of N, P and K consumed as fertilisers in 2014 were 108.9 million tonnes, 46.7 million tonnes, and 37.7 million tonnes, respectively. (FAO 2016) The efficiency at which plants are able to uptake nutrients depends on many factors, such as soil properties and the plant being cultivated (Syers et al. 2008). In total, nutrient use in agriculture is very inefficient: on average over 80 % of N and 25–75 % of P are lost to the environment during the full chain (Sutton et al. 2013). The main reasons for nutrient losses in the plant growth period are e.g. naturally occurring denitrification (for N), retainment in soil, or flushing with rainwaters (Erisman & Larsen 2013).

Adult human bodies do not accumulate nutrients. Thus, the amount of nutrients humans consume through eating plants equals the amount that will be excreted and end up in both urine and faeces. (Jönsson & Vinnerås 2013) Average amounts of N_{tot} , P_{tot} and K excreted in urine are 11, 0.93 and 2.6 g person⁻¹ d⁻¹, respectively, and 1.5, 0.6 and 0.9 g person⁻¹ d⁻¹ in faeces, respectively (Friedler et al. 2013). As an example, the cycle of N fertiliser from production to human excreta is presented in Figure 2.1.1.

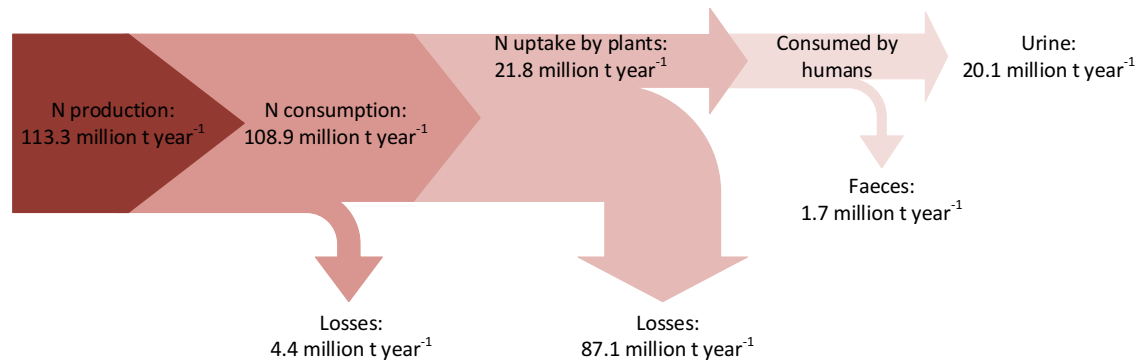


Figure 2.1.1 Cycle of N fertilisers from production to human excreta. Values are calculated based on data from several sources (FAO 2016; Friedler et al. 2013; Sutton et al. 2013).

So far, traditional wastewater treatment methods have mainly been focusing on removing nutrients from wastewaters to prevent them from getting into the environment, but not so much effort has been put into their possible recovery and further use. Typical nutrient removal technologies include biological nitrification/denitrification or anammox (i.e. anaerobic ammonium oxidation) for N and precipitation with metal salts for P. With both techniques, the nutrient is made unrecoverable for fertiliser use. (Booker et al. 1999) However, it would be beneficial both from an economical and environmental point of view to make more direct use of nutrients contained in waste streams.

2.2 Need for nutrient recovery and recycling

P is a mined nutrient and its availability is therefore dependent on finite mineral deposits. There is no alternative for P as an essential plant nutrient, which is why it needs to be recycled back to agriculture to secure adequate food production also in the future. (Pronk & Koné 2009; Sutton et al. 2013) N, on the other hand, is abundant in nature as N₂ gas but its conversion into a form suitable for fertilising purposes is energy demanding. Therefore, recovery and recycling of N from waste streams is also highly beneficial. (Pronk & Koné 2009)

K is also acquired through mining (Sutton et al. 2013), which makes its situation and need for recovery similar to P. However, the recovery of K has been studied very little compared to the other two main nutrients, P and N. This is most likely because of its similar nature and properties to another element present in wastewaters, sodium (Na), which makes its recovery more complex. Recovery of K is beyond the scope of this thesis and is therefore not discussed in detail here.

2.2.1 Phosphorus

Phosphate rock, which is the main source of P used in fertilising industry, is a scarce and non-renewable natural resource. As the amount of existing phosphate rock grows

smaller and smaller, the cost of it increases. In order to secure sufficient food production in the future with the continuously growing world population, actions are needed to efficiently recover P from wastewaters and other waste streams. (Cordell 2013)

In addition to its importance for the food production industry, another driving factor for P recovery from wastewaters is its influence on the environment. Most of the world's phosphate rock reserves are high in cadmium (Cd) which will end up in the final fertiliser products alongside P. Cd accumulation in soil is a serious problem especially in Europe, which is why limits for the Cd concentrations in fertilisers have been set up. (Jönsson & Vinnerås 2013) P production from phosphate rock also results in heavy metal pollutants and even radioactive by-products. The production process naturally requires energy and when using fossil fuels, significant greenhouse gas (GHG) emissions are generated. Phosphate rock being one of the most traded commodities in the world, also emissions caused by its transport play an important role in its effect on the environment. (Cordell et al. 2009)

Furthermore, P is known to cause eutrophication when entering water bodies. (Cordell et al. 2009) Eutrophication further leads to issues such as reduction of biodiversity and replacement of dominant species, increased water toxicity, and increased turbidity, resulting in decreased lifespan of the water bodies (Cai et al. 2013). Therefore, it needs to be efficiently removed from wastewater streams. Recovery of P from waste streams would decrease the carbon emissions caused by its generation from phosphate rock, and if the recovery of it could be carried out decentralised close to the final utilisation location, also the transport emissions would be diminished.

2.2.2 Nitrogen

N exists in numerous different forms on Earth's atmosphere, hydrosphere and biosphere and, contrary to P, can be considered the most abundant element on Earth. N compounds can be roughly divided into two groups: reactive and nonreactive. The nonreactive form of N is N_2 , nitrogen gas, naturally found in the Earth's atmosphere. Reactive N, N_r , comprises of the rest of the N compounds which are either biologically, photochemically or radiatively active. These include inorganic reduced forms of N, e.g. ammonia (NH_3) and ammonium (NH_4^+), inorganic oxidised forms, e.g. nitrogen oxides (NO_x), nitric acid (HNO_3), nitrous oxide (N_2O), and nitrate (NO_3^-) as well as organic compounds, e.g. urea, amines, proteins, and nucleic acids. (Galloway et al. 2003)

Only very few organisms can utilise the nonreactive atmospheric N_2 directly (Erisman & Larsen 2013). Thus, when producing nitrogen fertilisers, N_2 needs to be converted into a more readily available form of N, NH_3 , via the commonly used Haber-Bosch process. In N_2 , there is a strong triple bond holding the two N atoms together, and breaking that bond requires a large amount of energy. (Galloway et al. 2003) In fact, N production contributes to 2 % of the worldwide energy use (Sutton et al. 2013). Furthermore,

as this energy is generated with fossil fuels, it also results in significant GHG emissions. The production of chemical fertilisers is responsible for 1.2 % of total GHG emissions in the world, of which most is due to N fertiliser production. N fertiliser production has the greatest potential for GHG emission savings for all fertiliser products (contributing to 85 % of all the possible savings). (Jönsson & Vinnerås 2013)

In recent years, the production of Nr from N_2 has been much more rapid than Nr conversion back to N_2 through denitrification. This has led to the accumulation of Nr in the environment. (Erisman et al. 2013; Galloway et al. 2003) Nr is easily transported through hydrologic and atmospheric transport processes, which makes the problem global. It can also be assumed that the production and accumulation of Nr is only going to increase in the future which will be detrimental for the environment in several ways. Alongside P, it causes eutrophication in water bodies. (Galloway et al. 2003) Nr can also be responsible e.g. for the depletion of ozone in the atmosphere, thus contributing to climate change, the formation of acidic rains, and the decreasing quality of ground and surface waters used as drinking water (Erisman & Larsen 2013).

As mentioned above, wastewater treatment plants (WWTPs) typically use a combined nitrification/denitrification process or alternatively anammox (i.e. anaerobic ammonium oxidation) for the removal of N from wastewaters and thus release it back to the atmosphere as N_2 (Booker et al. 1999; Erisman & Larsen 2013; Kuntke et al. 2012). From there, it once again needs to be converted to NH_3 via the energy-intensive Haber-Bosch process to use for food production. This is naturally an unnecessary and unsustainable step in the N cycle and it would be more reasonable to recover N from wastewaters in a form that could be more directly recycled back to agriculture.

2.2.3 Sources for nutrient recovery

As mentioned before, practically all the nutrients consumed by humans will end up in domestic wastewaters. From there, they can be recovered at different stages of the wastewater treatment process. There are also several different recovery techniques that can be applied.

A relatively simple practice is to use the wastewater directly as a growing platform for plants or microorganisms that can later be harvested and used as fertiliser or feed. For example, microalgae have been found to be able to utilise nutrients in wastewaters. The algae grown on the wastewater nutrients can later be cultivated and used for e.g. biofuel production due to their high lipid content. After the lipid extraction, the remaining biomass can also be further used as an N-rich animal feed or fertiliser. (Cai et al. 2013) Another option for nutrient recovery with easier harvesting is to cultivate plants, such as duckweed, on the wastewater nutrients. Similarly to microalgae, cultivation of duckweed also results in a protein-rich biomass that can be used e.g. as animal feed. (El-Shafai et al. 2007)

Conventional WWTPs often anaerobically digest the sludge produced in the wastewater treatment process, which results in the formation of a digestate rich in both ammonia and phosphate. The concentrations of both N and P are in the range of 0.5–1 g L⁻¹. (Booker et al. 1999; Siegrist et al. 2013) P can be recovered from the supernatant e.g. by addition of lime which will result in precipitation of P (Booker et al. 1999). N, on the other hand, can be recovered e.g. through ammonia stripping (Siegrist et al. 2013). Recovery of both nutrients together through struvite precipitation is also an option (see Chapter 2.3.1). However, it will require addition of chemicals into the supernatant to control pH and balance the ratio of P, N and magnesium (Mg) in the liquid for enhanced precipitation. (Booker et al. 1999)

Instead of the conventional way of collecting all wastewaters together and thus mixing them with each other, it is also possible to collect different wastewater streams separately. That way, the more nutrient-rich streams can be kept separate and dilution caused by the other streams and e.g. excess flushing water is prevented. Especially urine contains high concentrations of the key nutrients N and P and is therefore an interesting source for nutrient recovery.

2.3 Nutrient recovery from source-separated urine

Domestic wastewaters consist of multiple sub-streams. These can be divided into two main categories: blackwater (BW), meaning sanitary wastewaters, and greywater (GW), which covers the rest of the domestic wastewaters, generated e.g. via shower, kitchen sink and washing machine. In more detail, BW can be further divided into two major sub-streams, yellowwater (urine) and brownwater (faeces, toilet paper, and carrier flushwater). Source separation of sanitary wastewaters means the individual collection of these different wastewater streams e.g. through the use of urine diverting toilets. (Friedler et al. 2013)

2.3.1 Characteristics of source-separated urine

Urine contains large amounts of key nutrients used in agriculture, and they even exist in similar proportions to those needed by most plants (Table 2.3.1). 79 % of N, 47 % of P and 71 % of K that end up in domestic wastewaters are originally contained in urine. (Friedler et al. 2013) This makes urine an intriguing fertiliser. However, urine only contributes to 1 % of the total volume of wastewaters (Kuntke et al. 2012). Therefore, when urine is collected together with other domestic wastewaters, the nutrient concentrations have already been diluted approximately 100-fold when they reach the WWTP, which makes their recovery or removal more complicated (Ledezma et al. 2015). In addition to nutrients, urine also contains most of the micropollutants excreted by humans (Udert et al. 2003a; Udert et al. 2003b), such as synthetic hormones, pharmaceuticals, and their metabolites (Udert et al. 2006). Therefore, it is reasonable to separate urine from other

wastewater streams to facilitate more efficient nutrient recovery as well as micropollutant removal.

Table 2.3.1 Typical compositions of fresh and hydrolysed urine

Parameter	Unit	CONCENTRATION						
		FRESH URINE			HYDROLYSED URINE			
Reference		Udert et al. 2003 ^a	Udert et al. 2003 ^b	Ciba Geigy 1981 ^c	Udert et al. 2003	Udert et al. 2006 ^d	Kirchmann & Petterson 1995 ^e	Kirchmann & Petterson 1995 ^f
pH	-	6.0	7.2	6.2	9.0	9.1	9.0	8.9
N _{tot}	g _N m ⁻³	-	-	9200	-	9200	1795	2610
TAN	g _N m ⁻³	386	254	616	1720	8100	1691	2499
Urea	g _N m ⁻³	8750	5810	7200	73	0	-	-
P _{tot}	g _P m ⁻³	559	367	496	76	540	210	200
COD _{tot}	g _{O2} m ⁻³	9700	8150	-	1650	10000	-	-
Carbonate	g _C m ⁻³	≤5	-	-	966	3200	-	-
K	g _K m ⁻³	2250	2170	2160	770	2200	875	1150
Mg	g _{Mg} m ⁻³	121	77	92	1	0	1.6	1.5
Ca	g _{Ca} m ⁻³	168	129	160	28	0	16	13
Na	g _{Na} m ⁻³	3730	2670	2800	837	2600	982	938
S	g _S m ⁻³	1350 ^g	748 ^g	1056	292 ^g	1500 ^g	225	175
Cl	g _{Cl} m ⁻³	5230	3830	3840	1400	3800	2500	2235

^a Urine collected from piping between toilet and collection tank

^b Urine collected from collection tank

^c Values calculated assuming an average urine volume of 1.25 L person⁻¹ d⁻¹ (Udert et al. 2003b)

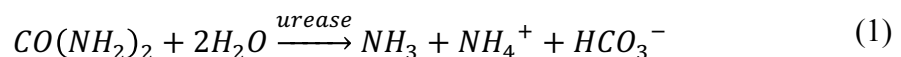
^d Simulated values

^e Urine collected from households

^f Urine collected from a school

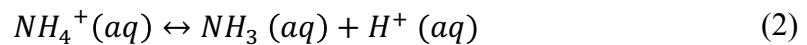
^g Only sulfate (SO₄²⁻) taken into account

Urine contains dissolved salts, making it a saline solution. During storage and transportation, the properties of urine change due to the occurrence of different kinds of processes, such as urea hydrolysis, precipitation, and volatilisation. (Friedler et al. 2013) Thus, there is a difference between urine being treated right after collection or after storage (Table 2.3.1). In fresh urine, most of the N present is fixed as urea (CO(NH₂)₂). During storage and transportation of urine, bacteria present in the urine produce an enzyme, urease, that will hydrolyse urea into ammonia (NH₃), ammonium (NH₄⁺), and bicarbonate (HCO₃⁻) (Friedler et al. 2013):



Urea hydrolysis results in an increase in the pH of the urine (from 6.2 in fresh to 9.1 in hydrolysed urine). This will promote natural precipitation of different compounds, the main precipitates being struvite ($\text{MgNH}_4\text{PO}_4 \cdot 6\text{H}_2\text{O}$, also known as magnesium-ammonium phosphate, MAP), hydroxyapatite (HAP, $\text{Ca}_{10}(\text{PO}_4)_6\text{OH}_2$), and calcite (CaCO_3). (Friedler et al. 2013; Udert et al. 2006; Udert et al. 2003a; Udert et al. 2003b; Udert et al. 2003c) The precipitation of these compounds explains why the concentration of Mg and Ca is so much lower in hydrolysed urine compared to fresh one (Table 2.3.1).

Another result of the hydrolysis is that 90 % of the remaining N in urine will be present as NH_3 or its ion form NH_4^+ (also referred to as total ammonia nitrogen, $\text{TAN} = \text{NH}_3 + \text{NH}_4^+$). (Friedler et al. 2013) Since NH_3 is a weak base and NH_4^+ its counter acid, they will form an equilibrium in an aqueous solution:



The balance will shift either to the left-hand or the right-hand side depending on the overall pH of the solution, temperature, and the overall concentration of TAN (Hansen et al. 1998; Nam et al. 2010). The equilibrium pKa for $\text{NH}_4^+/\text{NH}_3$ is 9.24 in urine (Kuntke et al. 2012), which means that at this pH the amount of NH_3 and NH_4^+ is equal. If the pH is increased, the portion of NH_3 increases, and vice versa. TAN is known to inhibit microbiological processes, and more specifically NH_3 has been suggested to be responsible for ammonia inhibition (Angelidaki & Ahring 1993). Therefore, the higher the pH of a TAN containing solution, the more inhibitory it generally is for microorganisms.

With Henry's constant of $62 \text{ mol L}^{-1} \text{ atm}^{-1}$ at $25 \text{ }^\circ\text{C}$, NH_3 is very volatile. Therefore, it can be lost through volatilisation during storage and transport of urine if precautions are not taken. In addition to the loss of a valuable nutrient, volatilisation of NH_3 may result in odour and health problems. (Friedler et al. 2013; Udert & Jenni 2013)

The presence of NH_3 in urine also has its benefits. Due to its poisonous nature, NH_3 has been found to act as a sanitising agent in the urine, inactivating pathogens. Therefore, urine can be considered a low hygiene risk fertiliser and simply storing it might be an adequate sanitation step before direct use as a fertiliser. (Vinnerås et al. 2008)

However, 95 % of urine is still water (Friedler et al. 2013), which makes the transport of urine as is rather inefficient. Therefore, it is desirable to collect the key nutrients in a more concentrated form. Due to its saline nature, the direct use of urine as a fertiliser can also cause salinity in the soil. This can hinder absorption of both water and key nutrients from the soil due to osmosis and the presence of competing ions, respectively, thus affecting plant growth. Even the physical structure of the soil can be affected by the excess salts. (Mitchell et al. 2013) Therefore, different methods have been developed to more efficiently recover the key nutrients from source-separated urine.

2.3.2 Recovery of phosphorus

As can be seen from the molecular formula of struvite, it contains magnesium (Mg), N and P at a 1:1:1 molar ratio. Struvite formation has been studied intensively in regards to P and N recovery and has been found to be an attractive option since it recovers the two key plant nutrients in a solid form. (Maurer et al. 2006) It is also widely considered as the most promising option for nutrient recovery from source-separated urine (Ledezma et al. 2015). Typically, Mg is the limiting substance of struvite formation and addition of Mg in the form of MgO, Mg(OH)₂, MgCl₂, or bittern (the Mg-rich brine from table-salt production) is usually required to obtain higher precipitation rates (Maurer et al. 2006). This naturally increases the costs of the method.

90–100 % of P present in urine can be recovered through struvite formation (Maurer et al. 2006). However, N is present in urine at much higher, approximately 10-fold concentrations than P (Friedler et al. 2013), which means that up to 80–90 % of the N cannot be recovered through struvite formation due to a stoichiometric imbalance (Ledezma et al. 2015). A stoichiometric phosphate addition can result in enhanced struvite formation and an N recovery rate of more than 90 % (Maurer et al. 2006), but is not an especially sustainable solution. Therefore, other methods for N recovery have been developed.

2.3.3 Recovery of nitrogen

Ammonia stripping is currently the most commonly used process for the selective recovery of N from urine and other wastewaters (Siegrist et al. 2013). It takes advantage of the volatile nature of NH₃ under controlled vacuum conditions (Maurer et al. 2006). Ammonia stripping can be carried out either by air stripping followed by ammonia adsorption in acid or by steam stripping with ammonia recovery in the condensate. (Siegrist et al. 2013) N recovery rates as high as 80–90 % can be obtained. (Maurer et al. 2006) However, for effective ammonia stripping, most or preferably all N present should be in the form of NH₃. Even in hydrolysed urine this is not the case: at pH around 9, NH₄⁺ is still slightly the dominant species. Therefore, the pH of the urine might need to be increased even higher for efficient ammonia stripping. This requires large amounts of base due to the high buffering capacity of urine (see Chapter 3.2 for more information). (Siegrist et al. 2013)

Reverse osmosis (RO), which means permeating water under pressure through a membrane with very small pores, can also be used to concentrate N from urine. Major part of the salts and organic compounds will be retained in the concentrate due to membrane rejection. However, the retention of charged NH₄⁺ is much better than that of the uncharged NH₃, which means that the efficiency of this method is also strongly affected by solution pH. Hydrolysed urine being an alkaline solution, pH adjustment might be required to enhance N recovery with RO, after which recovery rates of 60–80 % can be

expected. Other factors that hinder the utilisation of RO are the retention of micropollutants in the membrane together with the salts, i.e. they cannot be separated from the nutrients, as well as possible membrane scaling. (Maurer et al. 2006)

Urea present in fresh urine is known to form a complex with isobutyraldehyde (IBU) which will result in the precipitation of isobutylaldehydediurea (IBDU). IBDU is a commercially available slow-release fertiliser that can be readily used in agriculture. N recovery rates of 60–80 % can be achieved. (Maurer et al. 2006) However, addition of chemicals to urine for nutrient recovery is not a sustainable solution in the long term, as already mentioned. In order to form IBDU, the treatment should also take place immediately after urine generation before urea hydrolysis, so that N would still be present as urea. From hydrolysed urine, N can be recovered through ion-exchange using zeolites with high ammonium affinity, such as clinoptilolite. After addition of the zeolite to urine solution, ammonium will attach to it and the N-loaded product can be collected. (Maurer et al. 2006) The problems related to this method are similar as to IBDU formation.

A rather simple and effective method (with >90 % N recovery) to reduce the urine volume is evaporation of the excess water. This also faces some challenges, such as possible ammonia loss due to volatilisation and large energy consumption. (Maurer et al. 2006)

A biological method for N recovery is partial nitrification, i.e. oxidation of NH_3 and NH_4^+ to nitrate, NO_3^- . This helps to stabilise the otherwise volatile and easily lost ammonia in urine. Ammonium nitrate-containing urine can then be used as a fertiliser, although the large volume due to the high water content still makes transportation costly. (Udert & Jenni 2013) To overcome this issue, biological nitrification was combined with a successive distillation process, which resulted in the formation of a nutrient-rich solid residue (Udert & Wächter 2012). However, the alkalinity of stored urine is high enough to nitrify only about half of the ammonia present. Chemical addition would therefore be needed to increase the alkalinity and thus nitrification efficiency. Acid or base dosage might also be required to prevent inhibition of nitrifying microorganisms. (Udert & Jenni 2013)

2.3.4 Decentralised wastewater treatment

Centralised WWTPs are the most common type of wastewater treatment facilities. They are used for the collection and treatment of wastewaters from a large area, usually urban or peri-urban. This naturally requires an extensive network of piping and pumps for the transport of wastewaters to a central treatment location, which usually is located near a point of a convenient surface water discharge. (Tchobanoglous & Leverenz 2013)

When urine is collected separately from other wastewater fractions, its transportation to a centralised WWTP through pipelines will cause several problems. As mentioned in Chapter 2.3.1, the naturally occurring urea hydrolysis promotes precipitation of e.g. struvite, HAP and calcite (Udert et al. 2006; Udert et al. 2003a; Udert et al. 2003b; Udert et al. 2003c), which has the potential to cause blockages in the sewer network. Transport of urine over long distances may also result in ammonia volatilisation in the sewers, causing both odour problems as well as loss of N (Udert & Jenni 2013; Udert et al. 2006). Therefore, it is reasonable to minimise the transportation distance of urine and look for decentralised treatment alternatives.

Decentralised wastewater management systems are designed to take care of the wastewaters in much smaller scale than centralised WWTPs, typically only of an individual building, a cluster of buildings or a small, often remote community. They are not connected to centralised wastewater systems through pipes but are often dependent on centralised facilities e.g. for management of process residuals, which then have to be transported to the centralised facility e.g. by trucks. (Tchobanoglous & Leverenz 2013)

The viability of a decentralised wastewater treatment system naturally depends on the amount of residues that need to be transported to other locations after the treatment. Since the utilisation of all waste fractions locally is simply not possible, especially in urban areas, the main goal of decentralised facilities is to reduce the volume and stabilise the wastewater fractions for more efficient transport to terminal utilisation sites (Larsen & Gujer 2013).

A novel approach for decentralised nitrogen recovery from urine is to turn to bioelectrochemical methods. So far, one of the major factors hindering the development of large-scale bioelectrochemical applications for wastewater treatment has been the fact that most of the existing configurations and materials cannot be scaled up to the level needed for centralised wastewater treatment plants, where the required reactor volumes would be hundreds of cubic metres (Logan et al. 2006). However, as already mentioned above, decentralised treatment facilities are meant to deal with much smaller volumes of wastewaters and therefore make the utilisation of bioelectrochemical technology possible.

3 BIOELECTROCHEMISTRY AS A NOVEL TECHNIQUE FOR NITROGEN RECOVERY FROM WASTEWATERS

3.1 Bioelectrochemical systems

Transferring electrons from an electron donor (having a lower reduction potential) to an electron acceptor (with higher reduction potential) through oxidation-reduction reactions is a natural part of microbial metabolism. The electron acceptor can be either internal or external, i.e. located inside or outside the microbial cell. (Rabaey 2010) When the electrons are transported outside the cell, the process is called extracellular electron transfer (EET) (Rabaey 2010) and the bacteria capable of doing that are called exoelectrogens or electrochemically active microorganisms (EAM) (Logan 2008).

Microorganisms always attempt to transfer electrons to the electron acceptor with the highest potential available, which will maximise their energy gain (Rabaey 2010). The energy gain available from a certain reaction can be expressed using Gibbs free energy (Logan et al. 2006):

$$\Delta G_r = \Delta G_r^{\theta} + RT \ln(\Pi), \quad (3)$$

where ΔG_r is the Gibbs free energy for the specific conditions (J), ΔG_r^{θ} is the Gibbs free energy under standard conditions (298.15 K, 1 bar pressure, 1 M concentration for all species) (J), R is the universal gas constant ($8.3145 \text{ J mol}^{-1} \text{ K}^{-1}$), T is the absolute temperature (K), and Π is the reaction quotient (unitless). Π can be calculated from the activities of the products divided by those of the reactants

$$\Pi = \frac{[C]^c [D]^d}{[A]^a [B]^b}, \quad (4)$$

where $[C]$ and $[D]$ are the concentrations of the reaction products (mol L^{-1}), $[A]$ and $[B]$ are the concentrations of the reaction reactants (mol L^{-1}), and a , b , c and d are the stoichiometric coefficients of A , B , C and D , respectively.

The electron transfer conducted by EAM can be exploited by replacing naturally occurring electron acceptors with insoluble electron acceptors, i.e. electrodes, with high potentials. (Rabaey 2010) Similarly, naturally occurring electron donors can be replaced with insoluble ones. Systems making use of microorganisms interacting with these

kinds of insoluble electrodes, where electrons that can either be removed or supplied through an electrical circuit, are called bioelectrochemical systems (BES). (Rabaey et al. 2007)

There are two types of bioelectrochemical cells: galvanic cells which generate electricity as a result of a spontaneously occurring oxidation/reduction reactions at the electrode surfaces (also known as microbial fuel cells, MFCs); and electrolytic cells which require an external power source to carry out an oxidation/reduction reaction in order to produce desired products (also known as microbial electrolysis cells, MECs) (Strathmann 2004). In order for an oxidation/reduction reaction to spontaneously take place in an MFC, the overall reaction has to be thermodynamically favourable, i.e. the Gibbs free energy change (Eq. (3)) has to be negative (Bard & Faulkner 1944; Logan et al. 2006).

For MFC systems, it is more practical to evaluate the reaction taking place in the reactor in terms of the overall cell potential, i.e. the potential difference between the electrodes. This cell potential is also known as the electromotive force (EMF) of the cell and can be calculated using the Nernst equation (Bard & Faulkner 1944; Logan et al. 2006):

$$E_{emf} = E_{emf}^{\theta} - \frac{RT}{nF} \ln(\Pi), \quad (5)$$

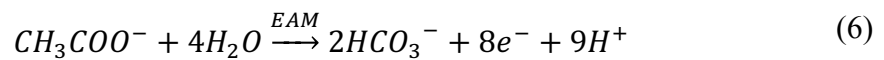
where E_{emf} is the cell potential, or EMF, for the specific conditions (V), E_{emf}^{θ} is the cell potential under standard conditions (V), n is the number of electrons per reaction mol (unitless), and F is Faraday's constant ($96,485 \text{ C mol}^{-1}$). Using Eq. (5), a favourable reaction will have a positive value. (Logan et al. 2006)

The three principle elements of any type of BES are the anode, where (biological) oxidation of a substrate takes place and electrons enter the electrical circuit; the cathode, where (biological) reduction of a terminal electron acceptor takes place and electrons leave the electrical circuit; and a separator. The function of the separator is to separate the two electrodes so that short-circuiting, i.e. direct reaction between electron donor and acceptor, is prevented. (Hamelers et al. 2010) The separator also controls ion transport between the two electrodes (Hamelers et al. 2010) and keeps the liquid containing the organic matter used by the microorganisms at the anode from reaching the cathode (Logan 2010). The separator can be a membrane or a salt-containing water layer (Hamelers et al. 2010). The most commonly used separator is a cation exchange membrane (CEM) which only allows protons (H^+) and other positively charged ions, cations, to transfer through (Logan et al. 2006). Another option is to use a proton exchange membrane (PEM) which is designed to only let protons through (Harnisch et al. 2008). Also anion exchange membranes (AEM), allowing negatively charged anions through, can be used (Logan 2010).

Multiple different BES applications have been developed and studied during the years. In the next chapter, a well-studied BES application MFC will be introduced in more detail. After that, another electrochemical application, electrodialysis (ED) is covered. ED is not a BES application but it can be combined with a BES, such as an MFC. Some examples of BES and ED combinations are introduced in Chapter 3.1.3.

3.1.1 Microbial fuel cells

The most studied form of BESs are MFCs. In MFCs, EAM oxidise an electron donor and transfer the produced electrons to an insoluble electron acceptor, the anode. A typical substrate for the EAM is acetate (CH_3COO^-) which will be oxidised to bicarbonate (HCO_3^-), producing electrons and protons:



From the anode, the transported electrons flow through an electrical circuit to another insoluble electrode, cathode, where a terminal electron acceptor is reduced (Figure 3.1.1). This creates an electrical current to the opposite direction. In other words, an MFC is a device producing net electrical power. (Logan et al. 2006; Rabaey et al. 2007)

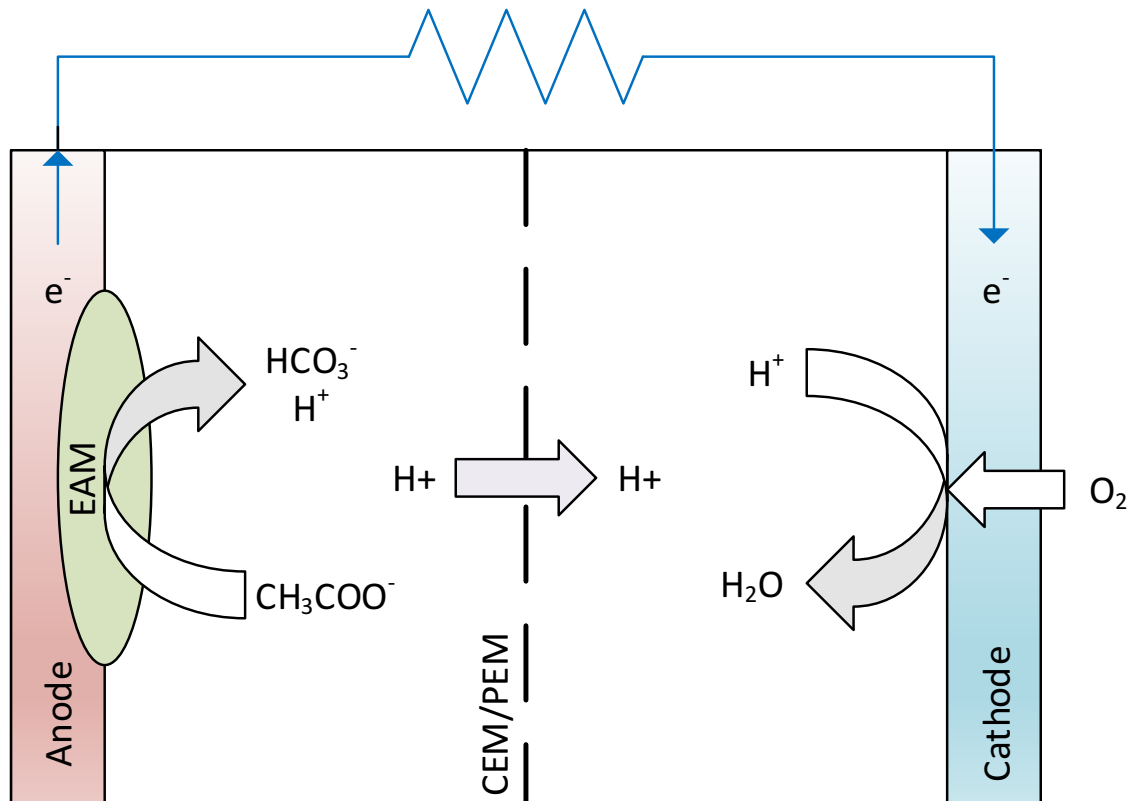
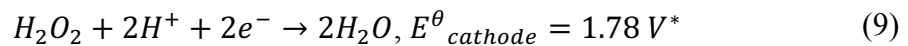


Figure 3.1.1 Operating principle of an MFC.

The flow of the electrons from one electrode to another creates an imbalance in the charge distribution, which has to be countered by an ion flow through the medium, a

salt bridge, or a charge-selective membrane. Typically, the imbalance is countered by protons (and/or other cations) migrating towards the cathode through a CEM/PEM, but also anion flow through an AEM is possible. (Logan et al. 2006; Rabaey 2010; Rabaey et al. 2007; Rabaey & Verstraete 2005; Udert et al. 2013)

It is generally accepted that oxygen is the only viable option for terminal electron acceptor in large-scale MFC applications due to its abundance in the atmosphere, which makes it a low-cost (practically free) and sustainable alternative. Oxygen reduction also results in the formation of only water and thus any chemical waste products are avoided. (Logan et al. 2006) The oxygen reduction reaction (ORR) can happen either through 1-step, 4-electron pathway directly into water (Eq. (7)), or through a 2-step, 2-electron pathway where hydrogen peroxide (H_2O_2) is produced as a reaction intermediate (Eq. (8) and (9)):



**in standard conditions (Atkins & de Paula 2014; Logan et al. 2006)*

Theoretically, ideally performing MFCs should be able to convert the entire free energy of the fuel oxidation (see Eq. (3)) into electricity. However, this would require perfect electrodes, electrochemical reactions proceeding at infinite rates, and a negligible internal resistance of the cell, which is naturally not possible in practical applications. (Schröder & Harnisch 2010) Therefore, Eq. (5) will define the upper limit for the cell voltage of an MFC, and in reality it will be lower due to various potential losses (Logan et al. 2006). These include activation polarisation, ohmic losses, concentration polarisation (also referred to as mass transfer and reaction polarisation), and reactant crossover (Schröder & Harnisch 2010). Most of these losses can be reduced to some extent by constructional and/or operational choices. Key parameters include the electrodes, membranes, electrolytes, and possible current collectors used in the reactors. Especially the electrode surface area and its ratio to the membrane surface area are of importance (Logan 2010; Schröder & Harnisch 2010)

Another issue related to MFCs is the development of a pH gradient between the anodic and cathodic compartments, also referred to as pH splitting (Rozendal et al. 2006; Schröder & Harnisch 2010; Zhao et al. 2006). As presented in Eq. (6), oxidation of an organic substrate will produce protons. This will increase the acidity of the anodic solution, i.e. decrease its pH. At the cathode, on the contrary, one proton is consumed per one electron transferred (Eq. (7)-(9)), which will produce OH^- ions and thus increase the

pH of the solution. (Freguia et al. 2008; Schröder & Harnisch 2010) pH splitting can be detrimental for the general operation of an MFC since a pH change of one unit will result in an electrode potential shift of 59 mV (assuming Nernstian behaviour). For the anode, this shift would be positive, increasing the anodic potential, and for the cathode conversely negative. (Schröder & Harnisch 2010)

CEMs/PEMs used to separate the anode and the cathode in MFCs also let through other cation species than protons, such as Na^+ , K^+ , NH_4^+ , Ca^{2+} , and Mg^{2+} . Furthermore, these other cations are typically present at up to 10^5 higher concentrations than protons. (Rozendal et al. 2006; Zhao et al. 2006) The mobility of protons in an aqueous solution is higher than that of other cations but only approximately 6-fold (Strathmann 2004), which is not enough to compensate the much higher concentrations of the other cations. Therefore, cations other than protons have been found to be mainly responsible for the transport of positive charge through the membrane, instead of protons (Rozendal et al. 2006; Zhao et al. 2006). This will further increase the pH gradient between the two electrodes. At the same time, however, the movement of other ions through the membranes during current generation provides a method for altering water chemistry that can be exploited (Cao et al. 2009).

The issue of pH splitting can be addressed e.g. by using the anodic effluent as a feed for the cathode. This concept provides the cathodic compartment with an additional flow of protons in addition to the amount that will be transferred through the CEM and has been found to effectively prevent the pH at the cathode from rising too high. (Freguia et al. 2008) Another possible approach is to increase the buffering capacity of the electrolyte. The presence of counter ions that are able to react with protons to form uncharged compounds will hinder the change in the pH, especially at the anode. (Hamelers et al. 2010) Indeed, poor buffering capacity of wastewaters has been seen as one of the major hindering factors in scaling-up of MFCs (Rozendal et al. 2006; Zhao et al. 2006), which is why waste streams with higher buffering capacity (such as urine) are preferable.

In all cases, the financial feasibility of different solutions, including costs for materials or the needed energy input, must be taken into account. (Schröder & Harnisch 2010) Indeed, the cost of the materials for MFCs can be considered the most important parameter in reactor design alongside the electrode surface areas. For practical applications of MFCs for wastewater treatment, the reactor sizes needed will be so large that extremely low cost materials are a necessity. (Logan 2010)

3.1.2 Electrodialysis

Electrodialysis (ED) is an electrochemical mass separation method relying on the use of ion-exchange membranes and the migration of charged ions towards an electrode. As mentioned earlier, there are two types of ion-exchange membranes: CEMs, which only let positive cations through, and AEMs, which only let negative anions through. This is

caused by either negatively (CEMs) or positively (AEMs) charged groups being fixed in the polymers matrix of the membrane. These fixed groups will repel ions with an identical electrical charge, called co-ions, but permit the transfer of counter-ions with an opposite electrical charge. (Strathmann 2004)

Typically, an ED cell consists of an alternating series of CEMs and AEMs arranged between an anode and a cathode (Figure 3.1.2). The applied potential difference between the two electrodes will cause the negatively charged anions and positively charged cations to migrate towards the anode and the cathode, respectively. However, the anions are only able to permeate through AEMs and cations CEMs, which will result in an ion concentrate in alternate compartments, whereas the other compartments simultaneously become depleted. (Strathmann 2004; Strathmann 2010)

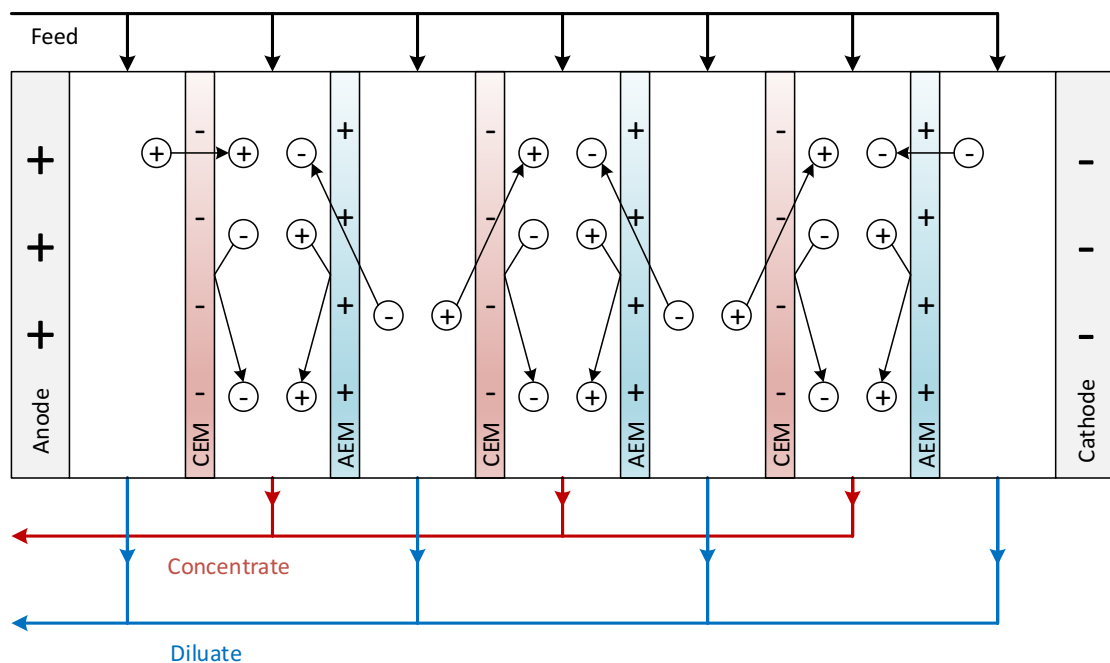


Figure 3.1.2 Operating principle of a stacked ED system.

Even though selective membranes are developed to only let certain charged ion groups through, no membranes are perfectly selective (Logan 2010; Schröder & Harnisch 2010; Strathmann 2004). The extent to which co-ions are excluded from the ion-exchange membrane matrix depends on both the properties of the membrane itself and the solution used in the system. Ideally, ion-exchange membranes should have high permselectivity, low electrical resistance, good mechanical and form stability, as well as high chemical and thermal stability. Naturally, low production costs are also favourable. (Strathmann 2004; Strathmann 2010)

Since the permselectivity of the membranes is not perfect, there are three different fluxes that need to be taken into account when studying their performance: anions, cations, and the solvent. In some cases, the transport of the solvent through the membrane due to

osmotic effects and coupling with the ion flows or the electric current can be significant. (Strathmann 2004) This will naturally result in a less concentrated product due to an increased amount of the solvent.

Due to the nature of ED cells, a concentration polarisation is naturally formed between the concentrate and the diluate compartments. This will eventually result in the salt concentration at the membrane surface facing a diluate compartment to reach zero. When this happens, a limiting current density independent of the electrical potential gradient is reached, i.e. applying a higher potential will no longer increase the current. In practical applications, it is advisable to always stay below the limiting current density in order to avoid any damage to the membrane due to water splitting and to retain energy efficiency. (Strathmann 2004; Strathmann 2010)

The main two applications of ED include desalination of salts containing solutions, typically brackish waters or industrial effluents, and concentration of electrolytes, such as table salt or certain acids and bases (Strathmann 2004; Strathmann 2010). ED has also been studied for concentration of nutrients and retention of micropollutants from human urine (Pronk et al. 2006) (see Chapter 3.2). AEMs and CEMs have the potential to retain both micropollutants and pathogens, which both occur in urine, due to their small (≤ 1 nm) pore size. (Maurer et al. 2006; Pronk & Koné 2009; Pronk et al. 2006)

Economically thinking, ED can be considered the most important separation process using ion-exchange membranes and an electrical potential driving force. (Strathmann 2004; Strathmann 2010) However, ED systems are related to relatively high energy consumptions (Cao et al. 2009; Pronk & Koné 2009), especially when solutions with high salinity are processed (Strathmann 2010). Therefore, it is feasible to compensate this energy consumption e.g. by combining ED with an electricity-producing MFC.

3.1.3 Combining MFC and ED technology

MFC and ED technology have been combined mainly for the purposes of desalination of seawater. These cells are also known as microbial desalination cells (MDCs). An MDC is typically a three-compartment cell in which the anode and the cathode are separated from an electrode-less middle chamber by AEM and CEM, respectively. The AEM and CEM prevent the migration of protons towards the cathode and hydroxide ions towards the anode, respectively. Therefore, the charge needs to be balanced by ions present in the seawater fed into the middle compartment of the cell. Cl^- ions will be transferred towards the anode and Na^+ towards the cathode. Salts are thus removed from the seawater and a diluate with low salt concentration is formed in the middle chamber. (Cao et al. 2009; Mehanna et al. 2010; Saeed et al. 2015)

In a pioneer study of MDCs, Cao et al. (2009) discovered that it was possible to reach approximately 90 % salt removal in one treatment cycle purely with the current generated by bacteria at the anode, i.e. no external power source was needed. With a salt concentration of 20 g L^{-1} and an external load of 200Ω , a maximum voltage of $\sim 600 \text{ mV}$ was produced, the power output being 2 W m^{-2} (or 3 W m^{-3}). The system was also capable of desalinating water streams with high salt contents up to 35 g L^{-1} . However, although the experiments worked as proof-of-concept, many aspects were still left to be optimised in the future. For example, ferricyanide was used as the catholyte, which would not be sustainable in long-term operation. The experiments were also only carried out in batch mode. The internal resistance of the MDC increased faster than expected by the researchers, which was assumed to result from an increased membrane/solution interface resistance due to an electrical double layer.

In a later study (Mehanna et al. 2010), the ferricyanide was replaced with an air-cathode. The maximum salt removal in a single cycle was 63 %. It was considered a relatively good results but not sufficient for drinking water production. Therefore, it was concluded that MDCs could be used for pre-treatment of saline waters before further treatment with RO. The energy required for RO depends on the salinity of the treated water, and a power-free pre-treatment step using MDC would decrease the energy consumption of the overall process.

MFC/MEC technology has also been combined with ED for nutrient recovery purposes from (synthetic) wastewaters (Chen et al. 2015; Zhang et al. 2014). Zhang et al. (2014) studied the concentrating of N and P into the catholyte of an MEC by placing the cathode inside a membrane “pocket” constructed of both a CEM and an AEM and placed in the reactor so that it was surrounded by the anode. N was driven towards the cathode due to the current generation, and P was removed through ion exchange with hydroxide ions. Without using an external power source, the removal rates were relatively low: $20.3 \pm 0.5 \%$ for N and $30.8 \pm 4.4 \%$ for P. When a voltage of 0.8 V was applied, the removal rates for N and P increased to $83.4 \pm 1.3 \%$ and $52.4 \pm 9.8 \%$, respectively. The highest concentrations reached in the catholyte were $350.0 \pm 57.7 \text{ mg L}^{-1}$ for N and $302.5 \pm 29.0 \text{ mg L}^{-1}$ for P (compared to $28.5 \pm 1.3 \text{ mg L}^{-1}$ and $5.3 \pm 0.2 \text{ mg L}^{-1}$, respectively, in the anode influent).

Chen et al. (2015) used a three-compartment configuration to study nutrient concentration in the middle chamber. The reactor was an air-cathode MFC operated with no power input and fed with synthetic wastewater. The current production of the reactor remained very low throughout the experiment (the maximum being 0.56 A m^{-2}) and the CE was only in the range of 7–15 % but despite this, rather high removal of COD ($>82 \%$), N ($>96 \%$) and P ($>64 \%$) was observed. N and P were recovered into a recovery solution, consisting mainly of NaCl, that was circulated through the middle chamber. Recovery was not especially efficient, as only 24 % of the removed N and 63 % of the P were recovered in the recovery solution. The rest of the nutrient removal was as-

sumed to be caused by several different factors, including biomass uptake, physical adsorption, chemical precipitation, and membrane fouling.

3.1.4 Enhanced oxygen reduction at the air-cathode

Cathode can be considered the most challenging part of an MFC design (Logan 2010) that will have the greatest effect on MFC performance. While a lot of research efforts have been put into understanding and improving the anode performance, cathodic reactions were almost neglected for several years (Harnisch & Schröder 2010).

As oxygen is considered the most viable terminal electron acceptor in MFCs (see Chapter 3.1.1), air-cathodes are commonly used in MFCs. Constructing an effective air-cathode can be challenging since it needs to facilitate a three-phase interaction between oxygen from the outside air, protons from water inside the reactor, and electrons from the electrical circuit to obtain efficient ORR (Figure 3.1.1 and Figure 3.1.3). In fuel cell processes, the 4-electron pathway for ORR (Eq. (7), Figure 3.1.3(B)) is much preferred over the 2-electron pathway (Eq. (8) and (9), Figure 3.1.3(A)) due to its higher energy-efficiency as well as the avoidance of an unwanted intermediate product formation. The ORR mechanism depends on the electrode material, possible catalyst(s) used as well as the nature of the electrolyte. (Song & Zhang 2008)

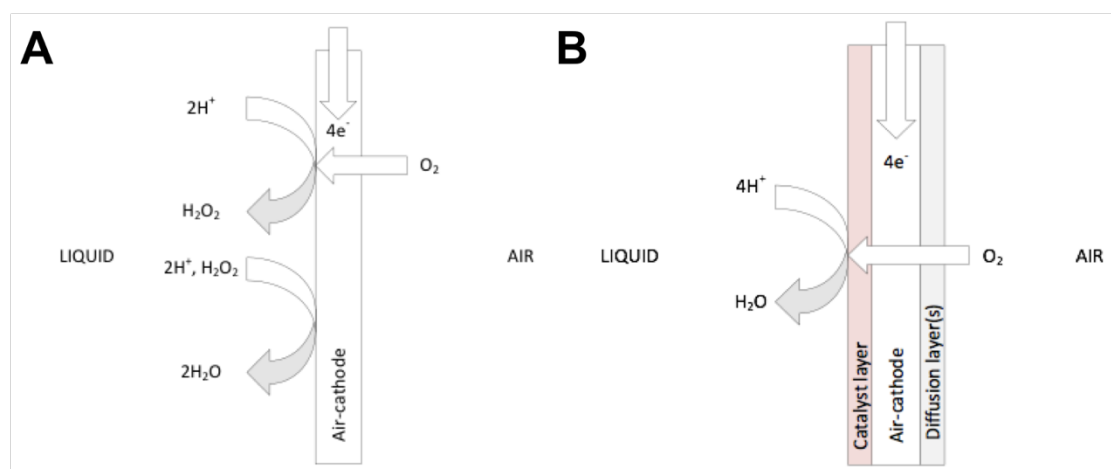


Figure 3.1.3 ORR at the air-cathode (A) via the 2-electron pathway and (B) via the 4-electron pathway, facilitated by a catalyst layer on the water-facing side and diffusion layer(s) on the air-facing side.

Similar materials are usually used for both anodes and cathodes but cathodes often also contain catalyst materials to increase the rate and reduce the overpotentials of the ORR at the cathode. This catalyst material is typically applied on the water-facing side of the cathode where the reduction reaction takes place (Figure 3.1.3(B)). (Logan 2010; Logan et al. 2006) Applying a catalyst material on the cathode tends to decrease the onset potential, i.e. make it happen earlier (at a more positive voltage), and increase the reduction current for ORR (see also Chapter 3.1.5) (Song & Zhang 2008). The application of

a catalyst layer(s) also provides the cathode with additional surface area which usually results in increased power generation (Logan 2010). So far, the most studied and commonly used catalyst material for cathodes has been platinum (Pt) (Song & Zhang 2008). However, Pt is a rather scarce and expensive material, which makes it unsuitable for large-scale application of MFC technologies. Therefore, there is an increasing interest in finding alternative, non-noble electrocatalysts for MFC cathodes. (Kundu et al. 2009)

Lately, different kinds of carbon-based nanomaterials have been gaining an increasing interest as substitutes for Pt as catalyst materials, since carbon is an abundant and therefore inexpensive material (Terrones 2004). These nanomaterials include e.g. graphite, glassy carbon, activated carbon, and carbon nanotubes. The catalytic ORR activity and mechanism vary significantly depending on the carbon material and the preparation method used. (Song & Zhang 2008) For example, carbon nanotubes can be produced through different ways, such as arc discharge, pyrolysis of hydrocarbons over catalysts, laser and solar vaporisation, and electrolysis (Terrones 2004).

It is also possible to dope carbon materials with heteroatoms, such as N, in order to further enhance their catalyst activity toward ORR. In an N-doped carbon material, the carbon atoms adjacent to the N atom act as the active sites. (Song & Zhang 2008) At least N-doped carbon nanotubes (NCNTs) (Feng et al. 2011a; Gong et al. 2009; Kundu et al. 2009), N-doped graphene (NG) (Feng et al. 2013; Feng et al. 2011b), and N-doped carbon powder (NCP) (Shi et al. 2012) have been studied as catalyst materials in air-cathode-MFCs. It has been assumed that the presence of the N-atoms increases the ability of e.g. graphene sheets to donate more electrons which accelerates the ORR. N in NCNTs can also be present in several different forms, such as pyridinic-like, pyrrole-like, imine-like or graphitic N, which have been found to affect NCNT performance in different ways. (Kundu et al. 2009) Pyridinic-like N is generally considered to be responsible for increased onset potential for ORR, whereas graphitic N has been found to increase limiting current density (Kundu et al. 2009; Lai et al. 2012). The NCNT synthesis conditions, such as temperature, feed gas composition and N precursor, have a large impact on the amount of each N species present (Kundu et al. 2009).

In addition to catalyst layers, ORR can be enhanced by applying diffusion layers (DLs) on the air-facing side of the cathode to increase oxygen diffusion through the electrode into the liquid electrolyte (Figure 3.1.3(B)). A widely used method is to apply successive polytetrafluoroethylene (PTFE) layers on a carbon/PTFE base layer on the air-facing side of the cathode. (Cheng et al. 2006a) PTFE is known to have good oxygen transfer properties. It is also highly hydrophobic, which will help limit water leakage through the air-cathode. (Cheng et al. 2006b) This technique has been found to improve the coulombic efficiency, i.e. the ratio between the amount of electrons actually being transferred and the theoretical amount of electrons delivered by the substrate (Logan et al. 2006; Rabaey & Verstraete 2005), and maximum power density of an MFC as well as reduce water leakage through the air-cathode. (Cheng et al. 2006a)

3.1.5 Cyclic voltammetry for analysing BES performance

Cyclic voltammetry (CV) is a simple and rapid method for evaluating the kinetics and redox behaviour of a compound, a biological matter, or an electrode surface that has been used for decades (Kissinger & Heineman 1983; Nicholson 1965). A CV test is conducted by changing the potential of the working electrode (anode or cathode) from a chosen start potential to a chosen end potential at a constant rate so that the scan is carried out in both directions, i.e. it will end at the same potential it started from (Logan et al. 2006). Typical scanning rates vary from 1 to 1000 mV s^{-1} (Qi 2008). The potential of the studied working electrode is varied against a reference electrode which is typically a silver/silver chloride (Ag/AgCl) electrode. The current generated at the electrode by the varying potential is measured and plotted versus the potential to form a voltammogram (Figure 3.1.4). (Kissinger & Heineman 1983) A voltammetry measurement can also be run only in one direction and is then referred to as a linear sweep voltammetry (LSV) (Logan et al. 2006).

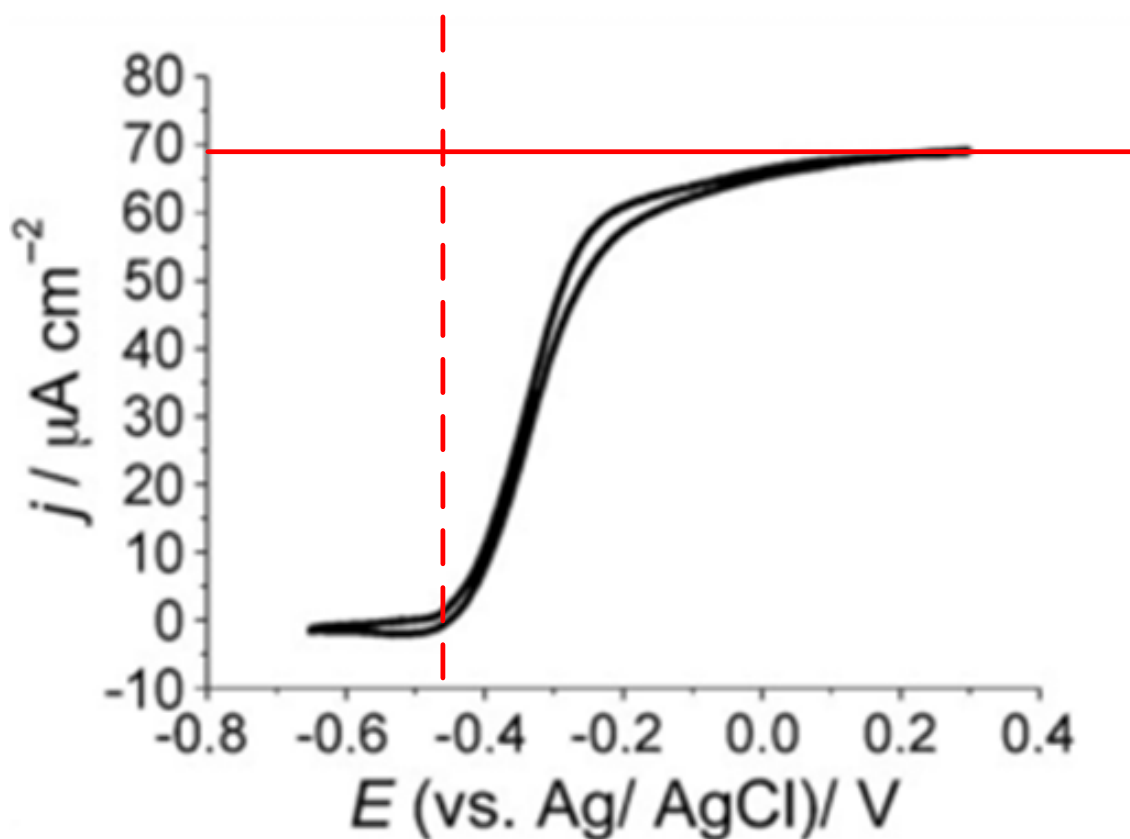


Figure 3.1.4 Typical shape of a turnover (i.e. all proteins involved in the pathway are oxidized and reduced multiple times (LaBelle & Bond 2010)) CV with scan rate 1 mV s^{-1} (Harnisch & Freguia 2012). Onset potential for the oxidation reaction (dashed line) and peak anodic current (solid line) are marked with red.

The increase in the current in the voltammogram (Figure 3.1.4) is caused by the oxidation reaction at the anode. After reaching the peak anodic current (red solid line in Figure 3.1.4), the current starts to decrease again. (Harnisch & Freguia 2012) The potential

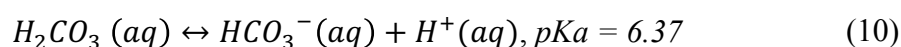
at which either a reduction or oxidation reaction starts to proceed, is called its onset potential (onset potential for anodic oxidation presented with a red dashed line in Figure 3.1.4).

CV technique is also suitable for analysing the performance of different catalyst materials adsorbed on electrode surfaces. CV provides information e.g. on the catalytic activity of a catalyst with respect to an electrochemical reaction. Important parameters in demonstrating the catalytic activity of a catalyst are the onset potential and peak current. (Song & Zhang 2008)

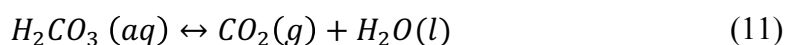
3.2 Bioelectrochemical methods for nitrogen recovery from urine

The greatest potential of MFC technology can be considered to be in wastewater treatment. Using wastewater as the feed for an MFC, a double benefit of waste treatment combined with energy recovery can be obtained. (Harnisch & Schröder 2010) When also valuable nutrients are simultaneously recovered, the technique is even more beneficial. However, when using different kinds of BESs for wastewater treatment, the performance of the BES is often restricted by the low electric conductivity (EC) (typically around 1–2 mS cm⁻¹) and low buffering capacity (typically around 5–10 mM) of wastewaters (Ledezma et al. 2015).

Urine, on the other hand, has a higher EC (approximately 19 mS cm⁻¹) and buffering capacity (on average 22 mM) due to high urea concentration of 21 g L⁻¹ (Friedler et al. 2013; Udert et al. 2006). When urine has gone through urea hydrolysis prior to treatment, its buffering capacity increases up to 490 mM, NH₃ and HCO₃⁻ being the main buffering compounds (Udert et al. 2006). In addition, acetate (CH₃COO⁻) can also act as a buffer at acidic pH. Like NH₃ and NH₄⁺ (Eq. (2)), HCO₃⁻ and its counter acid carbonic acid, H₂CO₃, form an equilibrium in aqueous solutions:

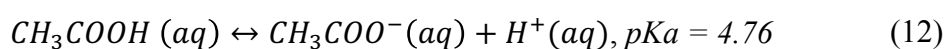


Furthermore, carbonic acid readily decomposes to carbon dioxide, CO₂, and water:



CO₂ gas can then be lost from the liquid phase into the gas phase.

Similarly, acetate and acetic acid, CH₃COOH, form an equilibrium in water:



It should be noted that the above-mentioned pK_a values are true for aqueous solutions but due its saline nature, in urine they might be substantially different, i.e. lower. The

high buffering capacity of hydrolysed urine makes it an attractive choice for BES feed. Urine also contains a large amount of organic material (expressed as chemical oxygen demand, COD; see Table 2.3.1). Since the EAM in BESs need COD for their metabolism, this is another reason why urine is suitable for BES feed.

Most N recovery methods described in Chapter 2.3.3 require the addition of chemicals to the urine solution in order to facilitate efficient recovery. In large-scale, this is not sustainable. BESs offer a chemical-free alternative for N recovery that, in the best case, can actually generate positive net energy instead of requiring energy input when using MFC technology.

N recovery from urine coupled with electricity production in an MFC (Kuntke et al. 2012; Kuntke et al. 2011) as well as hydrogen production in an MEC (Kuntke et al. 2014) have been studied lately. Kuntke et al. (2011) studied the effect of an increasing ammonium concentration on the cell potential and current density of a two-chamber MFC as well as the concentration of cations at the cathode for possible ammonium recovery. Synthetic wastewater was used as the anolyte and ferricyanide as the catholyte. pH at the anode was kept constant at 7. This resulted in even high ammonium concentrations in the feed (up to 4 g L^{-1}) having no negative effect on the MFC performance due to the low portion of free NH_3 . Average current densities of approximately 0.32 A m^{-2} were observed and from a polarisation curve, a maximum current density of 6 A m^{-2} was obtained. NH_4^+ -N was concentrated by a factor of 5–7 at the cathode, migrational and diffusional fluxes being the main transport routes. Thus, the studied method was found suitable for N concentration and recovery. However, concentrating ammonium in ferricyanide still requires an extra final step to separate the ammonium, e.g. through ammonia stripping.

In a following study, Kuntke et al. (2012) further studied the effect of an increasing ammonium concentration on a two-chamber MFC performance. This time, N recovery was obtained through ammonia stripping. Ferricyanide was replaced with a more sustainable air-cathode and real urine was studied in addition to synthetic urine in order to obtain more realistic conditions. The pH of the anolyte was not regulated. Increase in ammonium concentration at the anode was found to have little effect on the MFC performance which was in contrast to earlier findings in a single-chamber MFC (Nam et al. 2010). Average current densities were found to be considerably lower than in the previous study (0.059 A m^{-2}) which was explained by the less efficient cathode construction. Ammonium transport to the cathode was found to happen through similar pathways as reported by Kuntke et al. (2011), and at the cathode ammonia stripping took place at the liquid-gas boundary due to localised high pH and aeration of the gas diffusion cathode. However, only 31 % of the produced electrons were found to participate in ammonium transport.

Ammonium recovery was coupled with hydrogen production in an MEC (Kuntke et al. 2014). A constant voltage of 1.0 V was applied and both synthetic and 5 times diluted real urine were studied. Higher current densities were obtained with real urine (up to 23 A m^{-2}) than with the synthetic medium (8 A m^{-2}) but the diffusion of ammonium from cathode to anode led to changes in pH and thus short stable operation periods. In the different experiments, an average ammonium removal efficiency of 30 % was discovered. Ammonium concentrations at the cathode were found to be up to 10 times higher than those at the anode but the applied MEC design was not suitable for ammonia stripping. Applying an effective stripping process would be essential for final recovery of ammonium from the cathode medium as well as to prevent ammonium diffusion back to the anode, thus lengthening the stable operation period of the system. Another drawback of the proposed technique was the need for urine dilution, which adds to the operational costs.

The inability of BESs to completely remove TAN from the wastewater and recover it in the acid or as a gas has been noted and the effect of load ratio (defined as the ratio of the applied current and TAN loading rate) on the BES performance in regards to TAN recovery was very recently studied (Rodriguez Arredondo et al. 2017). The load ratio was found to be an essential parameter in assessing the TAN removal efficiency and energy input of the process. It was found that the load ratio should be higher than one to achieve complete TAN removal since some of the ammonia is still diffused back to the anode from the cathode. However, load ratios higher than the “limiting” one did not provide an advantage due to an increased energy consumption with only a marginal increase in removal efficiency.

As a summary, ammonia stripping integrated to other methods is in common use also in BESs. However, the technique still struggles to obtain high recovery rates. It also tends to require addition of chemicals (e.g. acids for ammonia adsorption) as well as large volumes of stripping gases, which can result in a high energy demand (Kuntke et al. 2016).

Kuntke et al. (2016) studied the possibility to lower the high energy demand related to the high gas volumes of ammonia stripping by integrating a transmembrane chemisorption module to the cathode of an MEC for ammonia recovery. Similarly to the previous studies, TAN was transported as NH_4^+ through diffusion and migration from the anode to the cathode, where it was turned into NH_3 due to the high pH. The catholyte was then circulated over a hydrophobic tubular membrane unit which permeated the volatile NH_3 gas and captured it into sulfuric acid placed inside the membrane. The use of the membrane reduced the need for carrier gases and thus the energy demand of the system. An average ammonia removal rate of $42 \pm 6 \%$ was obtained, of which approximately 95 % could be recovered from the catholyte. The maximum recovery on an individual day of operation was 49 %. However, the current density produced by the MEC was relatively low ($1.7 \pm 0.21 \text{ A m}^{-2}$). The set-up also did not remove the need for the use of an acid,

which will also have to be replaced from time to time to ensure sufficient absorption capacity.

3.3 The UGold project

The UGold project (ARC Linkage Project, LP150100402) was initiated and is led by Dr. Stefano Freguia and Dr. Pablo Ledezma at the Advanced Water Management Centre of the University of Queensland, Brisbane, Australia. The aim of the project is to develop a novel technique for decentralised nitrogen recovery from source-separated urine using a three-compartment BES combining MFC and ED technology. The structure of the UGold cell is similar to an MDC (see Chapter 3.1.3) but the operating principle is reversed: instead of aiming at removal of ions from the middle chamber, the target is to concentrate key nutrients in the middle compartment (Figure 3.3.1). The first scientific paper about UGold, presenting the proof-of-concept of the system, was published in January 2017 (Ledezma et al. 2017).

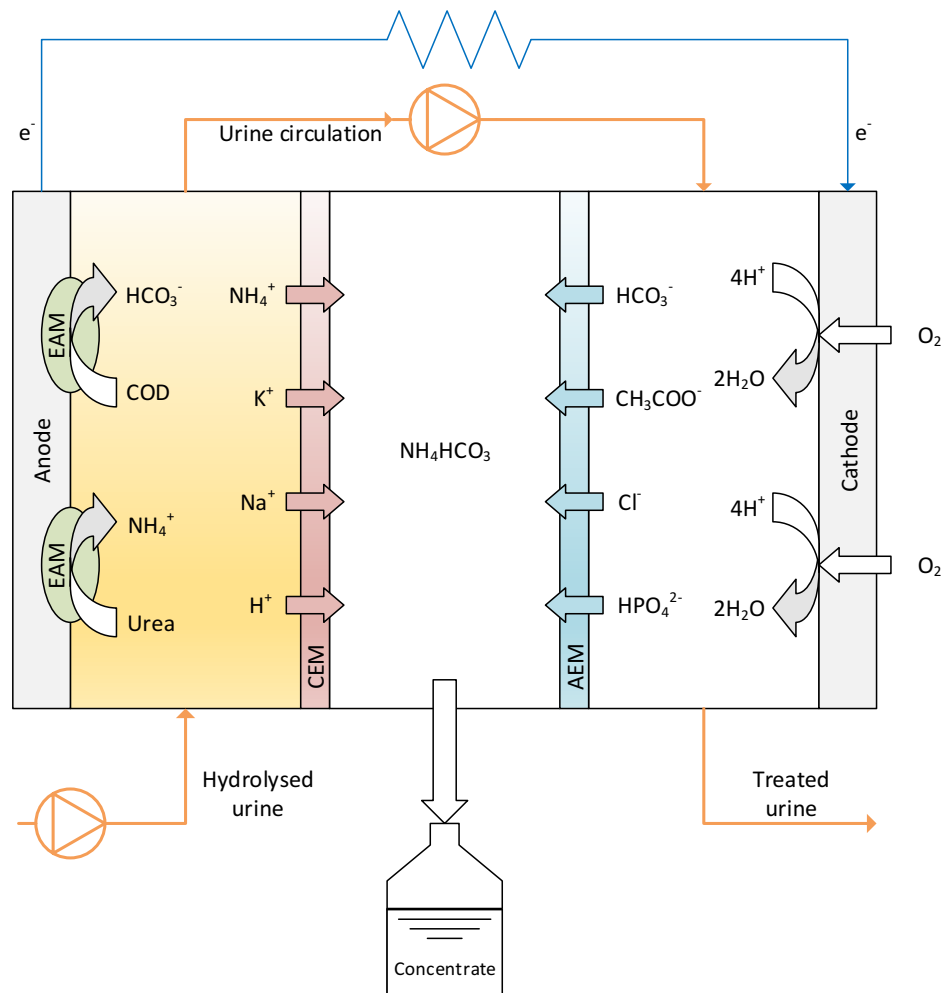


Figure 3.3.1 Operating principle of the UGold reactor. The flow of urine is presented in orange and the flow of electrons in blue.

In the UGold process, hydrolysed urine is fed to the anodic compartment of the cell, which contains a biologically active anode that has been adapted to the organic matter in the urine (Figure 3.3.1). The biological degradation of the organic matter releases electrons to the anode and carbonate to the medium. The EAM at the anode also degrades the possible remains of urea in the urine to NH_4^+ . The electrons are transported from the anode to the air-cathode through a resistor. Urine is also circulated from the anodic chamber to the cathode, providing it with a stream containing salts, leftover COD and CO_2 . At the cathode, oxygen is reduced to water, which closes the electron loop and produces a current.

The anodic and cathodic chambers are separated from the electrode-less middle compartment by a CEM and an AEM, respectively. The utilisation of both CEM and AEM creates an ED cell in which both cations and anions are trapped and thus concentrated. Simultaneously to the electron transfer, cations present in the urine migrate towards the cathode, i.e. through the CEM to the middle chamber to reciprocate the electron flow. NH_4^+ is usually found at the highest concentration in urine but also sodium (Na^+) and potassium (K^+) are present (see Table 2.3.1). From the cathodic side, anions similarly migrate through the AEM to the middle chamber. HCO_3^- is present at the highest concentration due to the previously happened hydrolysis of urine (Eq. (1)) as well as the degradation of organic matter at the anode. Other cations present in the urine are acetate (CH_3COO^-), phosphate (HPO_4^{2-}), and chloride (Cl^-). A concentrate with ammonium bicarbonate (NH_4HCO_3) present at the highest concentration is created in the middle chamber.

The UGold process takes advantage of the fact that ion-exchange membranes also transport other charged ions in addition to protons and hydroxide ions (see Chapter 3.1.3). In fact, in the UGold process conditions, the transport of protons and hydroxide ions is negligible compared to the other ions. When there are more than one salt present in a solution, as is the case for source-separated urine, the desalination effect is generally rather different for different salts. The actual transport rates of different ions through the membranes are proportional to their permeability, which is determined by their concentration and mobility in the membrane matrix. (Strathmann 2004)

As mentioned before, due to the use of membranes, ED is an effective method in preventing micropollutants and pathogens entering the nutrient concentrate. Therefore, the concentrate can be expected to contain no or very little micropollutants and pathogens. This aspect makes the concentrate well suited for further use as fertiliser. The product cannot be used for fertilising purposes directly in the form of NH_4HCO_3 but since the N obtained through the Haber-Bosch process is also in the form of NH_4^+ , the fertilising industry already has the needed means to further process it. Transport of the concentrated product is more feasible than that of untreated urine.

3.4 Research objectives

The goal of this work was to separately focus on improving the anode and cathode performances of the UGold reactor towards power-free operation. Thus, the objectives can be divided into three different research questions: (1) optimisation of anode performance; (2) optimisation of cathode performance; and (3) power-free operation of the UGold reactor.

The first objective was to enrich an electroactive consortium for the anode that would be able to grow and operate under neutral or slightly acidic conditions but still tolerating the high TAN concentrations of the hydrolysed urine. A lower pH in the range of 5.5–7.5 would increase the fraction of TAN present as NH_4^+ and therefore enhance the concentration of N through the CEM in the middle compartment. Correspondingly, the amount of toxic and inhibitory NH_3 would be lower. A lower pH would also facilitate a more complete utilisation of the buffer capacity of the hydrolysed urine. The hypothesis was that the lower the pH at the anode, the more active the biomass would be.

The second objective was to design a powerful air-cathode using carbon cloth as the electrode material, carbon-based nanoparticles as catalysts, and PTFE as DLs. The hypothesis was that the catalyst material would be able to both shift the onset potential of the oxygen reduction to the positive direction and increase the current density obtainable.

After carrying out the separate anodic and cathodic experiments, the results obtained were used to build a power-free UGold reactor, which was the third research objective. This was carried out in two three-compartment UGold reactors constructed utilising the best-performing cathode design as well as the biomass from the enrichment experiments as the biological anode. The original hypothesis was to be able to operate the reactors power-free, i.e. utilising only the energy produced by the microbes at the bioanode. Based on preliminary test results, however, this was concluded not possible. Thus, the reactor was run with little external power input to create a low-energy, chemical-free N recovery system.

4 MATERIALS AND METHODS

The experimental part of this thesis was divided into three main research questions: (1) enrichment of a neutrophilic electroactive consortium to further enhance the performance of the UGold reactor; (2) construction and optimisation of an air-cathode using carbon nanomaterials as catalysts and commercial PTFE sprays as diffusion layers; and (3) operation of UGold reactor using air-cathode and low energy input in order to obtain a low-power, chemical-free N recovery system. These three experimental set-ups are described in more detail in the following sections. All experiments were carried out at room temperature (22.0 ± 2.5 °C).

4.1 Enrichment of a neutrophilic electroactive consortium

In experiments conducted for the UGold project at AWMC, research fellow Pablo Ledezma has successfully cultivated a microbial consortium capable of growing at the high pH and toxic conditions (due to the high NH_3 concentration) of hydrolysed urine (Ledezma et al. 2017). However, in order to further enhance the performance of the fuel cell and accelerate the concentration of the desired ions in the middle chamber, it is desirable to acclimatise the microbial consortium to lower pH. This was carried out in triplicate reactor experiments.

4.1.1 Reactor configuration and start-up

Enrichment of neutrophilic electroactive consortia was carried out in triplicate single-chamber, membrane-less 400 mL glass reactors with eight or nine outlet ports. Working electrodes (anodes) were constructed as follows: 4 x 8 cm pieces of titanium mesh (Advent Research Materials, United Kingdom) were folded into a basket shape (with dimensions of 4.5 cm x 1.5 cm x 1.0 cm, resulting in a total volume of 6.75 cm^3) that was tightly packed with 4 g of graphite granules (EC-100, Graphite Sales, USA). The granules were pre-treated by soaking successively in 1.0 M HCl and 1.0 M NaOH overnight in each and rinsing thoroughly with distilled water until neutral pH was obtained. A smaller (2 x 4 cm) piece of titanium mesh was used to seal the open end of the basket and titanium wire was wrapped tightly around the basket (Figure 4.1.1 (A)). A Fluke 179 True RMS digital multimeter (Fluke, USA) was used to make sure that the anodes were conductive throughout. Two working electrodes were placed in each of the reactors to work as duplicates; this resulted in altogether six working electrodes. The projected surface area of the anodes was assumed to be 6.75 cm^2 per anode, which meant

13.5 cm² per reactor. Both anodes in one reactor were connected to the working electrode of one potentiostat channel (Figure 4.1.2).

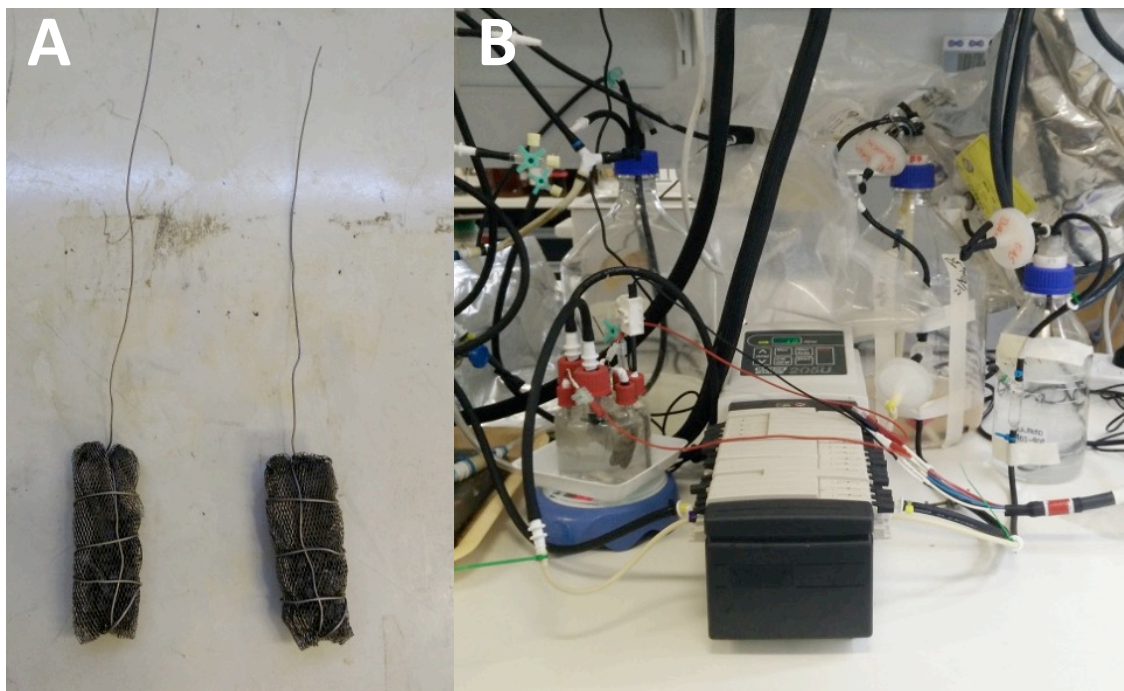


Figure 4.1.1 Photos of (A) the anodes constructed for the enrichment reactors, and (B) the experimental set-up when operating the enrichment reactors in continuous mode.

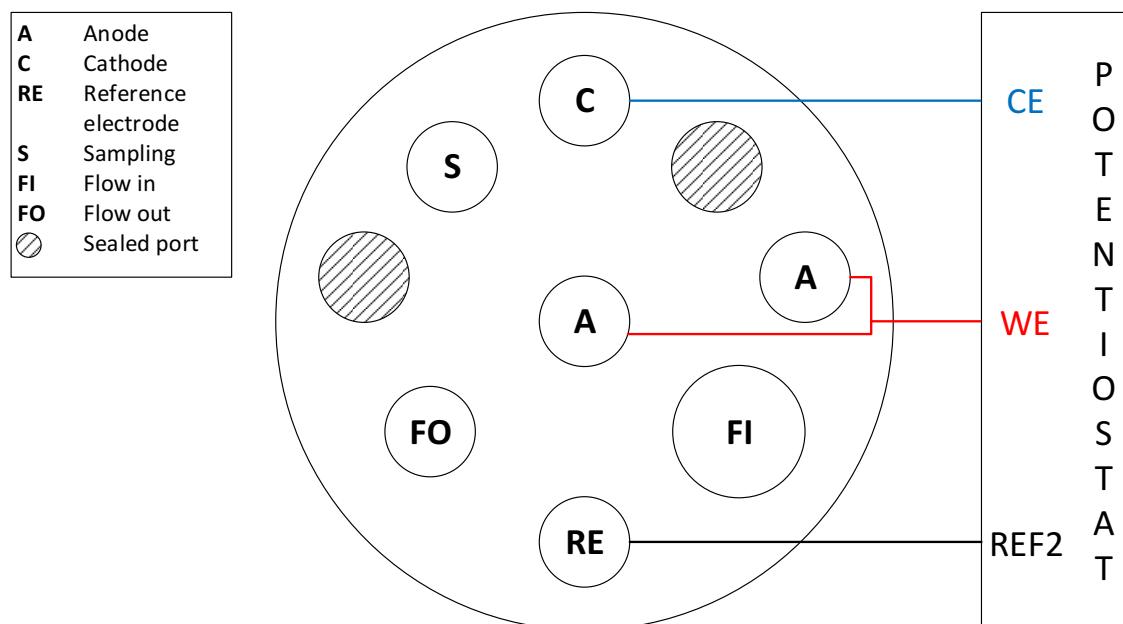


Figure 4.1.2 Schematic picture of the reactor configuration (from above) used in the enrichment experiments. In batch mode, the ports for flow in and out were also sealed.

Counter electrodes (cathodes) were graphite rod with 5 mm diameter (Element14, Australia). Self-constructed Ag/AgCl electrodes in saturated KCl and commercial BASi Ag/AgCl electrodes in 3 M NaCl (Bioanalytical Systems, USA) were used as reference

electrodes. Sampling ports were set up and the rest of the ports were sealed with rubber stoppers or screw tops to ensure anaerobic conditions.

Reactors were inoculated with an electroactive consortium collected from the effluent or directly from the anodic chamber of a UGold reactor operated for one year on synthetic hydrolysed urine (Ledezma et al. 2017). Synthetic hydrolysed urine was used as the medium (Table 4.1.1). All reactors were first operated in batch mode and the microbial community was adjusted to increasing ammonium concentrations by changing the medium composition according to Table 4.1.1. Reactors were run with the start-up medium (having a concentration of approximately 0.4 g TAN L⁻¹) at pH 7.5 until the measured current produced by the microorganisms reached a maximum value and started to decrease, indicating that the COD in the medium had depleted. Then, the medium was changed step by step every few days until an ammonium concentration representing 40 % of real urine strength was obtained. This ammonium concentration (equivalent to approximately 5 g TAN L⁻¹) was chosen because it realistically represented the concentration that would be found at the anode in a real MFC. All feed media were prepared in distilled water that was bubbled with N₂ to remove any oxygen before adding the components according to Table 4.1.1.

Table 4.1.1 Compositions of the synthetic hydrolysed urine feeds. Green, red and blue values represent changes made to the feed compositions during the experiments.

Constituent	Concentration (mM)					
	Start-up	10 % urine strength	20 % urine strength	40 % urine strength	40 % urine strength without HCO ₃ ⁻	60 % urine strength
CaCl ₂	3.4 (0.5)	3.4 (0.5)	3.4 (0.5)	3.4 (0.5)	3.4 (0.5)	3.4
KCl	3.9	3.9	3.9	3.9	3.9	3.9
K ₂ HPO ₄	23.7	23.7	23.7	23.7	34.0	23.7
KH ₂ PO ₄	-	-	-	-	67.8 (214.5)	-
MgCl ₂ ·6H ₂ O	4.2 (0.5)	4.2 (0.5)	4.2 (0.5)	4.2 (0.5)	4.2 (0.5)	4.2
NaCH ₃ COO	139.9	-	-	-	-	-
NaCl	82.6	48.1 (83.1)	30.0 (100.0)	0.0 (83.8)	83.8	-
NaOH	-	35.0 (0.0)	70.0 (0.0)	84.0 (0.0)	-	168.0
Na ₂ SO ₄	16.7	16.7	16.7	16.7	16.7	16.7
NH ₄ CH ₃ COO	139.9	35.0	70.0	140.0	140.0	140.0
NH ₄ Cl	23.0	-	-	-	140.0	-
NH ₄ HCO ₃	-	35.0	70.0	140.0	-	280.0
Trace elements ¹	1 mL L ⁻¹	1 mL L ⁻¹	1 mL L ⁻¹	1 mL L ⁻¹	1 mL L ⁻¹	1 mL L ⁻¹

¹ Recipe of trace elements in Appendix A

Originally, the pH of the feed was increased to ≥ 9 (imitating real hydrolysed urine) when changing the start-up medium to the following media with higher TAN concentrations. This, however, resulted in the inhibition of growth of the biomass. Therefore, the synthetic hydrolysed urine recipe was modified by replacing NaOH with an equal concentration of NaCl (values in red between brackets in Table 4.1.1), which resulted in a pH of 7.6–7.7 of the medium. It was also observed that struvite was precipitating at the cathode in the reactor (see photo in Appendix B), confirmed by a Raman analysis at the School of Chemical Engineering, University of Queensland (data not shown here), which is why the concentration of both $\text{MgCl}_2 \cdot 6\text{H}_2\text{O}$ and CaCl_2 was reduced from the original after switching the reactors to continuous mode (values in green between brackets in Table 4.1.1).

Reactors were constantly stirred with Big Squid and Color Squid magnetic stirrers (IKA, Germany), starting with 150 rpm and quickly increasing the speed to 300 rpm. The reactors were run in chronoamperometric (CA) mode with the WE at a potential E_{we} of 0 V vs. SHE (corresponding to -0.197 V vs. Ag/AgCl) and the produced current was measured every 60 s with a VSP potentiostat driven by EC-Lab software (Bio-Logic Science Instruments, France).

4.1.2 Continuous operation and pH adjustment

After the desired ammonium concentration was reached, the three reactors were switched to continuous mode using the synthetic 40 % urea strength medium as the feed. A Watson Marlow 205U multi-channel peristaltic pump (Watson-Marlow Fluid Technology Group, United Kingdom) was used for pumping the feed at a rate of 0.24 mL min^{-1} (Figure 4.1.1(B)), resulting in a hydraulic retention time (HRT) of 1.15 d. When all reactors had reached their target pH, the feed rate was increased to 0.48 mL min^{-1} (resulting in HRT of 0.57 d). As in batch mode, all reactors were constantly stirred at 300 rpm using magnetic stirrers.

Three target pH values were chosen: pH 5.5 (reactor A5.5), pH 6.5 (reactor A6.5), and pH 7.5 (reactor A7.5). All reactors were first run at pH 7.5, after which the pH was lowered by 0.5 steps until the target pH was reached. The pH adjustment was carried out with 5 M HCl. However, it was observed that at lower pH, HCO_3^- in the feed medium started to convert to CO_2 and escape from the solution into the gas phase. This also resulted in a continuous increase of pH in the feed medium. Therefore, HCO_3^- was replaced with a non-volatile phosphate buffer using K_2HPO_4 and KH_2PO_4 when operating at $\text{pH} \leq 6.5$. This naturally changed the composition of the feed but it still retained the high salinity and EC typical for hydrolysed urine. The amount of phosphate buffer needed was calculated based on the amount of electrons produced at the average current production:

$$c_{e^-} = \frac{I}{F}, \quad (13)$$

where c_{e^-} is the concentration of electrons produced (mol s^{-1}) and F is Faraday constant ($96,485 \text{ C mol}^{-1}$). An average current density of 10 A m^{-2} was used based on earlier results. The calculated amount of electrons was equal to the number of protons needed to neutralise the pH, i.e. the basic form of the phosphate buffer (K_2HPO_4). The amount of the acidic form, KH_2PO_4 was calculated using the Henderson–Hasselbalch equation aiming at the target pH:

$$\text{pH} = \text{p}K_a + \log \frac{[\text{base}]}{[\text{acid}]}, \quad (14)$$

where $\text{p}K_a$ is the logarithmic acid dissociation constant (6.8 for $\text{HPO}_4^-/\text{H}_2\text{PO}_4^{2-}$). Concentrations used for pH 6.5 and pH 6.0 in continuous mode operation are presented in black and blue, respectively, in Table 4.1.1. Since other ions in the medium contributed to the overall pH of the solution, the calculated phosphate buffer amounts did not result in the target pH and 5 M KOH was used to adjust the pH to the desired value.

The current production practically stopped in reactor A5.5 already at pH 6.0. Despite of this, pH 5.5 was tested but this was again carried out in batch mode (with K_2HPO_4 and KH_2PO_4 concentrations of 16.0 mM and 100.8 mM, respectively).

4.1.3 Sampling

Samples for pH measurements were collected directly from the reactors (during operation in batch mode) or from the effluent tube (during operation in continuous mode) using three-way valves as sampling ports. In addition, pH of the feed was measured each time new feed was prepared.

Samples for DNA sequencing and analysis were collected two times during the experiments to evaluate changes in microbial community over time and changes in conditions. The sample of the original biomass was collected after 45 d of operation (15 d after all reactors had been re-started) from the suspended biomass in the reactor media. The media of all three reactors were mixed and a Centurion Scientific K3 Series benchtop centrifuge (United Kingdom) at 4,000 rpm for 30 min was used to separate the suspended biomass from the liquid. The sample was stored in phosphate buffer at $6 \text{ }^\circ\text{C}$ over weekend before being sent for analysis. For the latter microbial community analysis, graphite granules used as the anodes and colonised by the active biomass were collected from the reactors and sent for analyses. The granular samples were also stored in phosphate buffer at $6 \text{ }^\circ\text{C}$ before being sent for analysis.

4.1.4 Microbial community analysis using DNA pyrosequencing

The DNA pyrosequencing for the microbial communities of the enrichment reactors was carried out at the Australian Centre for Ecogenomics (ACE), University of Queensland, Brisbane, Australia. Illumina SSU 16S ribosomal RNA gene (rRNA) amplicon analysis with SSU 926F-1392WR as the primer pair was used. As a quality control, all files were trimmed with Trimmomatic software (Bolger et al. 2014) and any reads with less than 250 bases were excluded from further processing. The amplicon clustering was carried out with QIIME (Caporaso et al. 2010) and taxonomy assignment on representative OTU sequences using BLAST (National Center for Biotechnology Information, USA) against a reference database (Greengenes version 2013/5) (DeSantis et al. 2006).

4.2 Development of an efficient air-cathode

The second research objective of this thesis was to design a powerful air-cathode for enhanced ORR. Three different carbon nanomaterials were tested as the catalyst layer on the water-facing side and three different commercial PTFE sprays as diffusion layers on the air-facing side of the cathode.

4.2.1 Cathode preparation

Plain carbon cloth (Fuel Cell Earth, USA) was used as the air-cathode. N-doped carbon nanotubes (NCNTs) and N-doped graphene nanoparticles (NG), prepared as previously described (Feng et al. 2011a and Feng et al. 2011b, respectively) and provided by the Tongji University in China, were studied as catalyst materials to enhance ORR at the cathode. Their performance was compared with a commercial powdered activated carbon (PAC) (Norit XS Plus, Cabot, USA). Two different dispersion techniques with and without a pre-treatment step with acid were compared: (1) direct dispersion in Milli-Q water; (2) dispersion in Milli-Q water after a pre-treatment step with acid; (3) direct dispersion in a mixture of polyvinylidene fluoride (PVDF) and acetonitrile; and (4) dispersion in a mixture of PVDF and acetonitrile after a pre-treatment step with acid (Table 4.2.1). Attachment of the nanoparticles on the electrode surface was carried out by electrophoretic deposition (EPD). The reason for NG being studied less than the other two materials was simply the smaller amount of it being available (and since its performance did not seem better compared to the other two, a more comprehensive study was thought not worth it).

Table 4.2.1 Tested catalyst materials and different parameters used

Catalyst material	Pre-treatment with acid	Dispersion medium	Deposition voltage	Deposition time	Sample ID
NCNT	-	Milli-Q	30 V	15 min	NCNT
NCNT	yes	Milli-Q	30 V	15 min	Acid-NCNT
NCNT	-	PVDF and acetonitrile	50 V	5 min	PVDF-NCNT
NCNT	yes	PVDF and acetonitrile	50 V	5 min	Acid-PVDF-NCNT
NG	-	Milli-Q	30 V	15 min	NG
NG	-	PVDF and acetonitrile	50 V	5 min	PVDF-NG
PAC	-	Milli-Q	30 V	15 min	PAC
PAC	yes	Milli-Q	50 V	5 min	Acid-PAC
PAC	-	PVDF and acetonitrile	30 V	15 min	PVDF-PAC
PAC	yes	PVDF and acetonitrile	50 V	5 min	Acid-PVDF-PAC

The pre-treatment in acid for each cathode was carried out as follows: 3 M HNO₃ and 3 M H₂SO₄ were mixed at a 1:1 ratio to a total volume of 200 mL. 300 mg of nanoparticles were added and the solution was mixed for 2 h using a Branson Sonifier 450 tip sonicator (Branson Ultrasonics, USA) with the output control at 7. The particles were then separated from the acidic liquid by centrifugation at 4,000 rpm for 30 min (Centurion Scientific K3 Series benchtop centrifuge, United Kingdom) and washed four times with Milli-Q water. It was assumed that approximately 50 % of the original nanoparticles were recovered after the washing steps (Thomas et al. 2005). The nanoparticles were used for EPD immediately after washing without a drying step as this was reported to dramatically increase the dispersion quality compared to dry nanoparticles (Boccaccini et al. 2006).

Plain or acid-pre-treated nanoparticles were dispersed in either Milli-Q water or a mixture of PVDF and acetonitrile at a ratio of 0.5 mg mL⁻¹. For dispersion in Milli-Q, 150 mg nanoparticles were mixed with 300 mL Milli-Q for 1 h using the tip sonicator at output 7. For dispersion in PVDF and acetonitrile, 1.08 g of PVDF in N-Methyl-2-Pyrrolidone (NMP) solution was first mixed with 300 mL of acetonitrile for 20 min with the tip sonicator at output 5. Then, 150 mg nanoparticles were added and the mixture was mixed for another 20 min with the sonicator. EPD was carried out immediately after dispersion of nanoparticles into the liquid to avoid settling of the particles at the bottom of the beaker.

Prior to EPD, a 3 cm x 10 cm carbon cloth was pre-treated by plasma cleaning with either nitrogen or atmospheric gas for 20 min using a Harrick Plasma plasma cleaner connected to a Plasmaflo PDC-FMG flow meter (Harrick Plasma, USA). For nanoparticles in Milli-Q, EPD was carried out with 30 V for 15 min using an ISO-TECH IPS 2303 Laboratory DC power supply (RS Components Ltd, UK). For nanoparticles in PVDF-acetonitrile, EPD was carried out with 50 V for 5 min using an Aim TTi PLH250 DC power supply (Aim & Thurlby Thandar Instruments, UK). The higher voltage made it

possible to use a shorter deposition time but due to the poorer EC of the Milli-Q solution, it was not possible to go over 30 V and thus a longer deposition time was used (Table 4.2.1). Titanium mesh was used as the counter electrode in the EPD. The electrode being coated was connected to the positive and the counter electrode to the negative end of the power supply.

After comparing the performance of the different catalyst materials, two with the best performance were chosen for further experiments with diffusion layers on the air-facing side of the cathode. Three different commercial PTFE sprays were chosen for comparison: Ezy Glide Dry Non-Oily Lubricant (Selleys, Australia), WD-40 Specialist Anti Friction Dry PTFE Lubricant (WD-40 Company, USA), and 3-in-one Professional Garage Door Lubricant (WD-40 Company, USA). Different amounts of PTFE layers were applied on the cathodes to find the optimal number of layers. The spraying was carried out so that the cathode was attached to the frame of the small test reactor (see Chapter 4.2.2) and PTFE was sprayed from approximately 10 cm distance, according to the product instructions. One layer of spray meant spraying the whole projected surface area of the cathode one time. After each layer, the spray was left to dry for at least 5 min or until the cathode surface looked dry. The speed at which the spray was moved across the cathode surface area was tried to keep as even as possible between all layers but naturally there was a human error to it since it was carried out by hand.

4.2.2 Cathode performance analyses

The effect of both the catalyst materials and the PTFE diffusion layers were studied by conducting CV measurements (VSP potentiostat driven by EC-Lab software, Bio-Logic Science Instruments, France). The tests were carried out in small-scale air-cathode reactors with surface area of the working electrode being 8 cm² (Figure 4.2.1). Titanium wire was attached to the carbon cloth cathodes by threading through the cloth to act as current collector. Either titanium mesh or platinum wire connected to titanium mesh was used as the counter electrode and self-constructed Ag/AgCl electrodes in saturated KCl as reference electrodes. The first CV tests using plain NCNT and NG as the catalyst layers were carried out in air-saturated 0.1 M phosphate buffer at pH 7±0.2 and 1.0 M ammonia buffer at pH 9±0.5 scanning from +0.700 V to 0 V vs. SHE. For the other catalyst layers, the ammonia buffer was diluted to 0.1 M and the scan range was from +0.600 V to -0.600 V vs. SHE. CV scan rate was 1 mV s⁻¹ and the scan was repeated three times. For the DL experiments, a CV scan rate of 5 mV s⁻¹ was used. In addition to the CVs, the performance of the DLs was also evaluated based on sensory perceptions on how well they prevented water from leaking through the cathode.

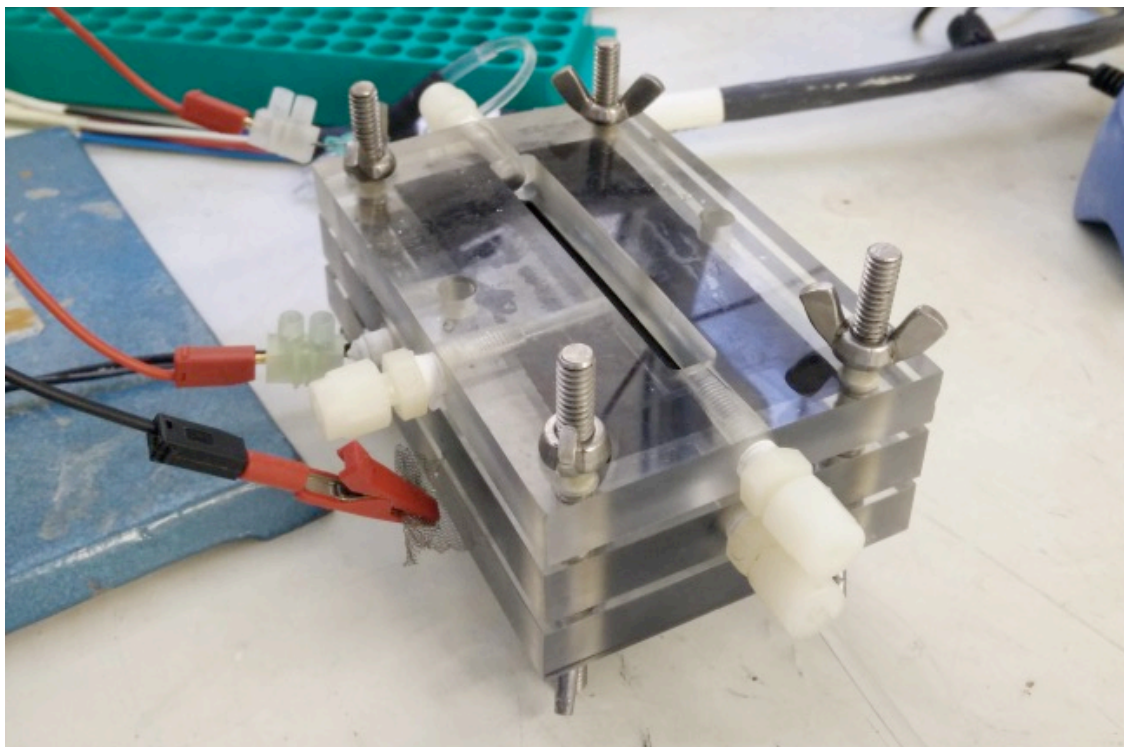


Figure 4.2.1 The small-scale air-cathode reactor used in the preliminary tests for different cathode catalyst and PTFE materials.

4.3 Operation of UGold reactors with air-cathodes

The ultimate goal of the UGold project is to launch a bioelectrochemistry-based decentralised wastewater treatment application that will be completely self-sufficient energy-wise, i.e. it will produce as much (or even more) electricity as it consumes for the N recovery process. The third and final experimental part of this thesis focused on operating the UGold reactor using the biomass enriched in the first part and the air-cathode designed in the second part of the experiments. Duplicate reactors were run with as little external power input as possible to see how high current densities were obtainable.

4.3.1 Reactor configuration and start-up

Duplicate three-compartment BESs were used for the experiments (referred to as UGold1 and UGold2). The reactors were constructed of rectangular plastic plates screwed together with bolts. Anodic and cathodic compartments were separated from the middle chamber with a CEM (CMI-7000, Membranes International, USA) and an AEM (AMI-7001, Membranes International, USA), respectively, to allow ion transport to the middle compartment from both sides. The projected surface area of both membranes was $7\text{ cm} \times 5\text{ cm} = 35\text{ cm}^2$.

Graphite granules pre-treated by soaking in acid and base (see Chapter 4.1.1) were used as the anode. The reactors were inoculated by carefully mixing 4 g (wet weight) of

graphite granules from Reactor 3 of the enrichment experiments, colonised with an active electroactive biomass, with 25 g of non-colonised dry graphite granules. The anodic chamber (7 cm x 5 cm x 1 cm, resulting in chamber volume of 35 cm³) was filled with the granules and two graphite rods (\varnothing 5 mm) were inserted into the granule bed to act as current collectors. During the start-up period which aimed at biomass enrichment, stainless steel mesh was used as the cathodes in closed cathodic compartments. Self-constructed Ag/AgCl electrodes in saturated KCl were used as reference electrodes in the anodic chambers.

The anodic and cathodic compartments were filled with the start-up feed (Table 4.1.1) and the middle compartment with a similar solution except without ammonium and acetate compounds before starting the reactors. The hydraulic volumes of the anode, cathode and middle chamber were approximately 20 mL, 35 mL and 35 mL, respectively. Enrichment of the biomass was carried out similarly to the anode enrichment experiments (see Chapter 4.1.1) by gradually increasing the feed ammonia concentration from start-up to 40 % strength medium using the synthetic urine feeds presented in Table 4.1.1 (at pH 7.6–7.7 and with lower concentrations of Ca and Mg). The lower amount of Ca and Mg compounds resulted in higher pH (up to >8), which is why 5 M HCl had to be used to adjust pH to 7.5 ± 0.2 . During pH adjustment, the feed was mixed thoroughly and HCl added slowly drop by drop to prevent HCO_3^- from turning into CO_2 and volatilising due to a low local pH.

The enrichment was carried out in continuous mode and started with a feed rate of 0.12 mL min^{-1} (meaning HRTs of approximately 0.1 and 0.2 d for anode and cathode, respectively). Anodic effluent was used as a feed for the cathode at the same rate. The feed rate was gradually increased up to 1.21 mL min^{-1} on day 10 (resulting in a decrease of the HRTs to 0.01 and 0.02 d for anode and cathode, respectively), at which rate it was mainly kept for the rest of the enriching. After reaching the 40 % urine strength medium at pH 7.5, the pH of the feed was increased to 9 ± 0.1 according to the original recipe (Table 4.1.1) in order to adjust the biomass to a higher feed pH which was going to be used when operating with the air-cathodes. When feeding at higher pH was started, the feed rate was lowered back to 0.12 mL min^{-1} so that the biomass had time to adjust to it.

During the enrichment, the reactor was operated as an MEC in CA mode by applying a constant E_{we} of 0 V vs. SHE.

4.3.2 Operation with air-cathode

For the final part of the experiments, the stainless steel cathodes were replaced with air-cathodes, constructed according to the results from the preliminary experiments with catalyst materials and diffusion layers as follows: 600 mg of NCNTs were mixed with 400 mL of 3 M HNO_3 /3 M H_2SO_4 mixture for 2 h by ultrasonication at output 7. After

being separated from the acid and washed four times with Milli-Q, the remaining NCNTs (approximately 300 mg) were mixed with 600 mL of Milli-Q by ultrasonication for 1 h at output 7. A 8 cm x 10 cm piece of plain carbon cloth (Fuel Cell Earth, USA) was cleaned with plasma for 20 min using atmospheric air and then coated with the acid-pre-treated NCNTs by EPD (30 V, 15 min). The cloths were dried vertically for 20 min, after which they were rinsed with distilled water to remove excess nanoparticles. Then, the cathodes were dried vertically overnight in a fume hood. After this, four layers of WD-40 PTFE spray were applied on the air-facing side to act as diffusion layers. Each layer was dried for 5 min before application of the next one, and after spraying all four layers, the spray was left to dry overnight in a fume hood. As this amount proved not to be waterproof enough, four more layers of the PTFE spray were applied the following day, after which the cathodes were dried in an oven at 100 °C for 1 h. The projected surface area of the cathodes was 7 cm x 5 cm = 35 cm². Titanium wire was used as the current collector similarly to the preliminary cathode tests.

With the air-cathodes, the reactors were turned from a vertical to a horizontal position with the cathodes on top to minimise any catholyte leakage through them (Figure 4.3.1 and Figure 4.3.2). Reactors were also slightly tilted to ensure more efficient removal of possible air present in the system with the effluent.

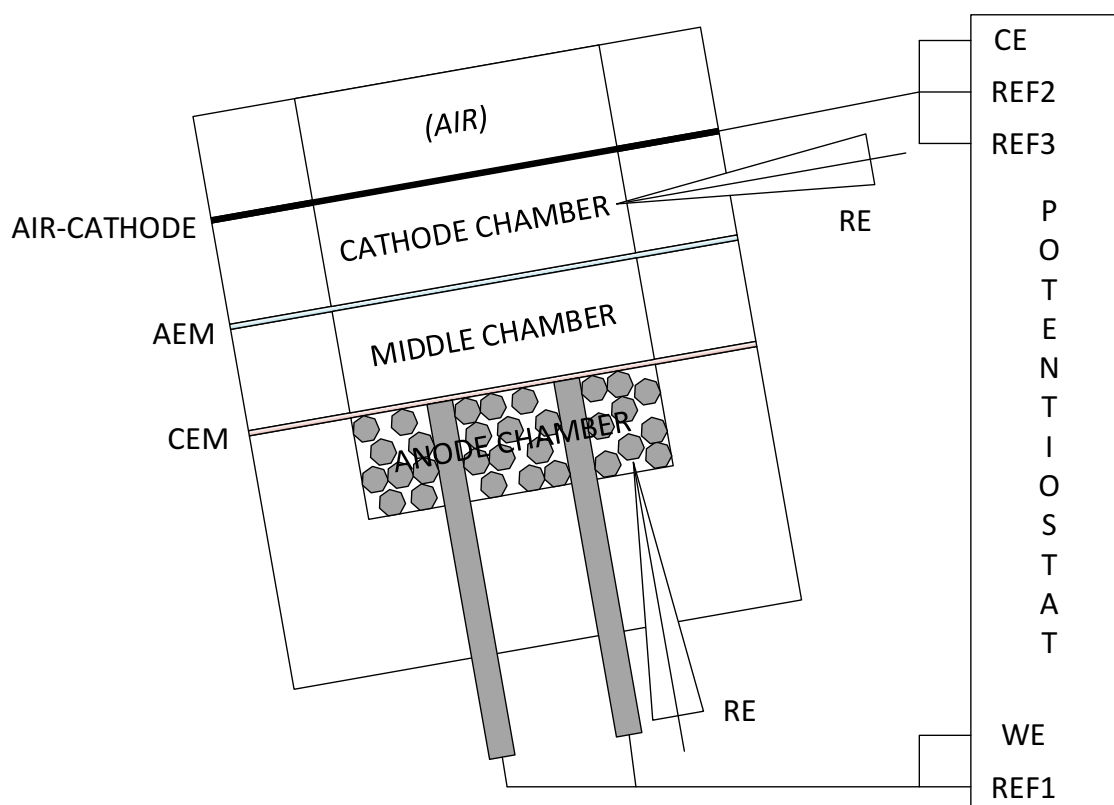


Figure 4.3.1 Schematic picture of the reactor configuration when operating UGold reactors with air-cathodes.

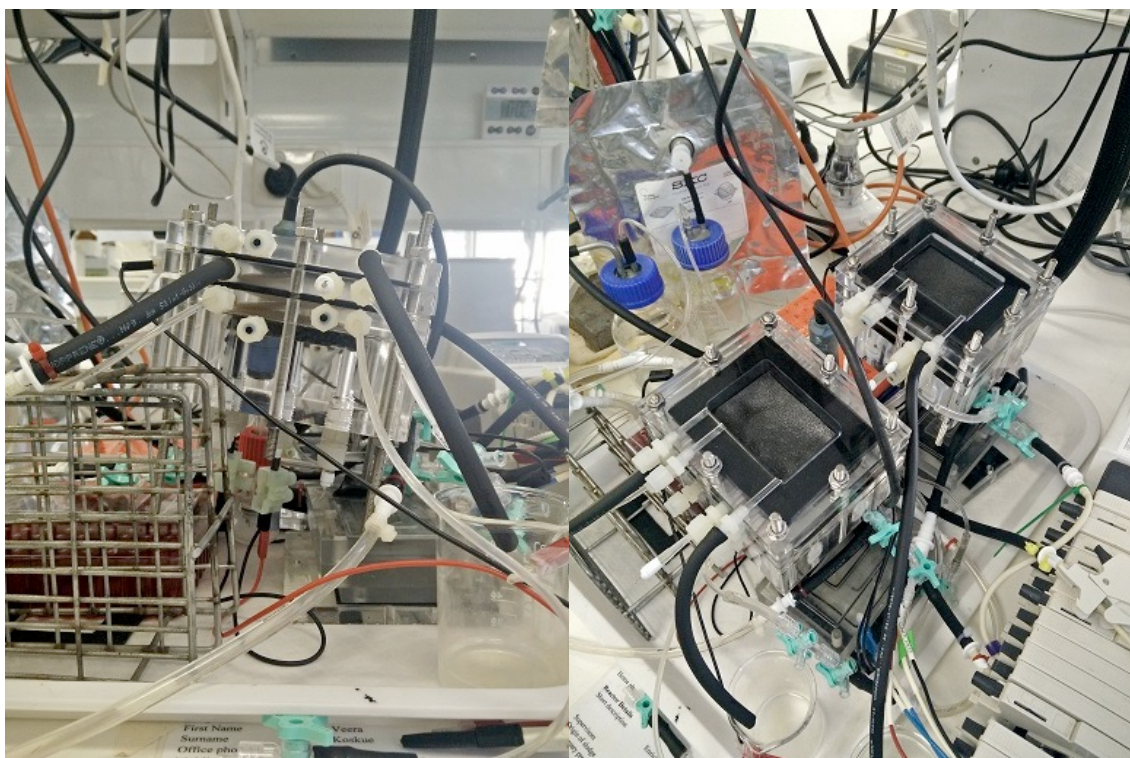


Figure 4.3.2 Photos of the UGold reactors operated with air-cathodes.

The positioning of the reactors was not enough to prevent leakage through the cathodes, which is why some more PTFE was sprayed on problematic parts in a precision manner when the reactors were already in operation. This, however, was still not enough to stop the leaking completely, and there were some leaking problems throughout the experiment. Air could also not be removed completely from the system and there was a constant air bubble inside the cathodic compartment, reducing the area of the cathode that actually was in contact with the catholyte.

Anodic chambers were first filled with the old anolyte recovered after the enrichment. Middle chambers were filled with a similar start-up medium as earlier (see Chapter 4.3.1) and cathode chambers with the feed used in the experiments. 60 % synthetic hydrolysed urine (with original amounts of Mg and Ca, Table 4.1.1) with pH 9.2 ± 0.1 and EC $34 \pm 1 \text{ mS cm}^{-1}$ was used as the feed at rate 0.12 mL min^{-1} (Watson Marlow 205U multi-channel peristaltic pump). The feed rate was kept low to prevent leakage through the air-cathodes. As in the previous construction, the anodic effluent was used as the feed for the cathode (Figure 4.3.3). A concentrate was collected as the overflow from the middle chamber.

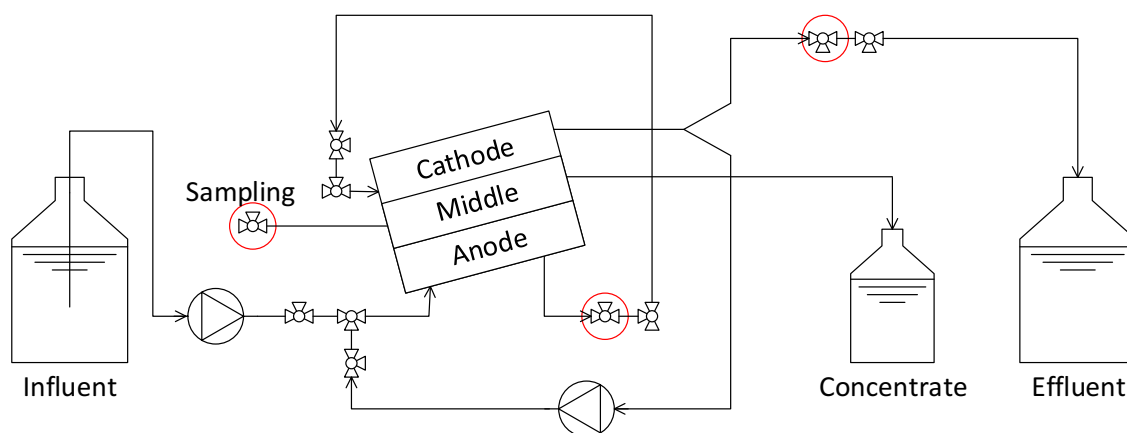


Figure 4.3.3 Schematic picture of the experimental set-up when operating UGold reactors with air-cathodes. pH sampling points are marked with red.

In the beginning of the experiments, the recirculation from the cathode back to the anode (Figure 4.3.3) was not used. Later in the experiments, the effect of the recirculation on the power output was tested for two days. A Watson Marlow Sci-Q 323 peristaltic pump (Watson-Marlow Fluid Technology Group, United Kingdom) at flow rate 1.4 mL min^{-1} was used for the recirculation. When the recirculation was in operation, the feed rate of the fresh feed to the anode was also increased to 0.73 mL min^{-1} because this seemed to reduce leaking through the cathodes.

The original goal was to operate the reactors as MFCs without any power input but based on the results from the preliminary cathode tests, it was concluded that small voltage would have to be applied in order to facilitate current production. I.e., the reactors were operated as MECs but the use of air-cathodes eliminated the production of hydrogen at the cathode and replaced it with oxygen reduction to water. In order to control the overall cell voltage, E_{cell} , the anode of the reactor was connected to the WE and REF1 and the cathode to CE, REF2 and REF3 of one potentiostat channel (VSP potentiostat driven by EC-Lab software, Bio-Logic Science Instruments, France) (Figure 4.3.1). The potentiostat applied the E_{cell} as the difference between REF1 and REF2, i.e. the difference between the WE and the CE:

$$E_{\text{cell}} = E_{\text{we}} - E_{\text{CE}} \quad (15)$$

The reactors were in CA mode, starting by applying an E_{cell} of 0 V and then increasing it step-wise up to 1.0 V, after which it was lowered again. Self-constructed Ag/AgCl reference electrodes in saturated KCl were inserted in both the anode and the cathode chamber for monitoring the electrode potentials and conducting CV measurements.

4.3.3 Sampling

Samples for pH measurements were collected through three-way valves or a sampling port (middle chamber) from three points in the system: anodic effluent, cathodic efflu-

ent, and the middle chamber (marked with red in Figure 4.3.3). The pH of the feed was also measured each time a new one was prepared.

4.4 Analyses and calculations

The pH was measured using LAQUAtwin Compact pH Meter pH 22 (Horiba Scientific, Japan) and InLab Expert Pro pH meter (Mettler Toledo, Germany). LAQUAtwin Compact Conductivity Meter EC22 (Horiba Scientific, Japan) was used for EC measurements.

CV measurements (VSP potentiostat and EC-Lab software, Bio-Logic Science Instruments, France) were used to evaluate the performance of the anodes in the enrichment experiments. A scan rate of 1 mV s^{-1} was used and the scan was repeated three times from $+0.600 \text{ V}$ to -0.200 (or later to -0.400 to determine the onset potential) V vs. SHE.

Visual MINTEQ software (version 3.1) was used to determinate the speciation of different ionic compounds at different pH values in the enrichment experiments in order to study changes in buffer capacity. The concentrations of ion compounds present in different 40 % media used in the continuous mode experiments were fed into the software and the pH was fixed at the desired value. The buffer capacities of different media could then be calculated by summing up the concentrations of main buffer compounds, also taking into account how many protons each species was able to absorb. Based on the calculated buffering capacities, theoretically obtainable current densities were calculated using the following formula (assuming the amount of protons and electrons produced in the system to be equal):

$$I_{buffer} = Q * c_{buffer} * F, \quad (16)$$

where Q is the feed flow rate (L s^{-1}) and c_{buffer} is the estimated concentration of the buffer expressed in how many moles of protons the feed is able to neutralise ($\text{mol H}^+_{\text{absorbed}} \text{ L}^{-1}$).

For the UGold reactors with air-cathodes, cathode and anode potentials were measured regularly with a Fluke 179 True RMS multimeter (Fluke, USA). Originally, the goal was to also measure COD removal in the reactor and the concentration of the target nutrients and other ions in the middle chamber concentrate. However, the power production of the reactors remained so low that this was concluded unnecessary since the possible changes were assumed to be so minor that they could not be detected within the error of the analyses.

CVs were conducted separately for the anodes and the cathodes of the air-cathode reactors towards the end of the experiments. The scan rate was 1 mV s^{-1} . For the anodes, the scan range was the previously used $+0.600 \text{ V}$ to -0.400 V vs. SHE and for the cathodes, $+0.600 \text{ V}$ to -0.700 V vs. SHE based on the cathode potential measurements.

5 RESULTS

5.1 Enrichment of neutrophilic electroactive consortia

Throughout the enrichment experiments, the joint current production of the two anodes in the reactors was monitored. This data was complemented with individual CVs conducted for all anodes. Both the microbial communities and the buffer capacities at different pH values were analysed and calculated, respectively, in order to find explanations for the bioelectrochemical results.

5.1.1 Electrochemical measurements

The enrichment experiments were first started with two reactors (A5.5 and A6.5), and a third reactor (A7.5) was added after 22 days. A6.5 suffered from serious electrical connection problems in the beginning of the study, which is why it was restarted after 10 days of operation and the results from these 10 first days are not presented. These reasons resulted in different total operation times for all reactors: 126, 116 and 103 d for A5.5, A6.5 and A7.5, respectively. The most important changes in operation conditions and when they were conducted for all three reactors are collected in Table 5.1.1.

Table 5.1.1 Changes made to operation conditions in the three enrichment reactors during the experiments

Change	Time after start-up (d)		
	A5.5	A6.5	A7.5
Addition of second anode	15	5	-
Re-start	22, 30	20	8
Change to 10 % medium (pH 9)	44	34	23
Change to 20 % medium (pH 9)	50	40	28
Change back to 10 % medium (pH 9)	55	-	33
pH adjustment to 8.2–8.3	58	48	36
Change to 20 % medium (pH 7.5)	65	-	50
Change to 40 % medium (pH 7.5)	69	73	-
Re-start	-	75	63
Change to 10 % medium (pH 7.5)	-	81	72
Change to 20 % medium (pH 7.5)	-	84	76
Change to 40 % medium (pH 7.5)	-	88	78
Switch to continuous mode	73	90	80
pH adjustment to 7.0	86	96	-
pH adjustment to 6.5	92, 104	103	-
pH adjustment to 6.0	99	-	-
pH adjustment to 5.5	113	-	-

Current densities produced by A5.5, A6.5 and A7.5 are presented in Figure 5.1.1, Figure 5.1.2 and Figure 5.1.3, respectively. Before continuous operation and pH adjustment, all reactors were run in batch mode and the TAN concentration of the reactor media was increased from 0.4 to 5 g L⁻¹, representing approximately 40 % of real hydrolysed urine. Electricity generation with the start-up feed (at pH 7.5) was observed much faster in reactor A6.5 (days 0–20 in Figure 5.1.2) than in the other two reactors (Figure 5.1.1 and Figure 5.1.3), which is why the anodes of A6.5 were switched with one anode from A5.5 and one from A7.5 and all reactors re-started according to Table 5.1.1. After this, current generation rapidly started in all reactors. It was observed in all reactors that the initial increase in feed pH to >9 after the start-up medium lead to inhibition and significant drop in the current generation. This is why the pH of all reactors was first adjusted to 8.2–8.3 and then kept at 7.6–7.7 when changing feed according to Table 5.1.1. After lowering the feed pH, reactors A5.5 and A7.5 recovered quite quickly but the current production of A6.5 remained at a clearly lower stage. Therefore, both anodes of A6.5 were discarded on day 75 and replaced with one active anode from A7.5 and one completely new one. A new anode was also added to A7.5 to replace the anode moved to A6.5 and both reactors were re-started (day 63 of operation for A7.5). After this, the increase in TAN concentration of the feed could be carried out in 15–17 d. The highest current densities obtained in batch mode during the TAN concentration increase were in the range of 15–18 A m⁻², A6.5 and A7.5 performing slightly better than A5.5

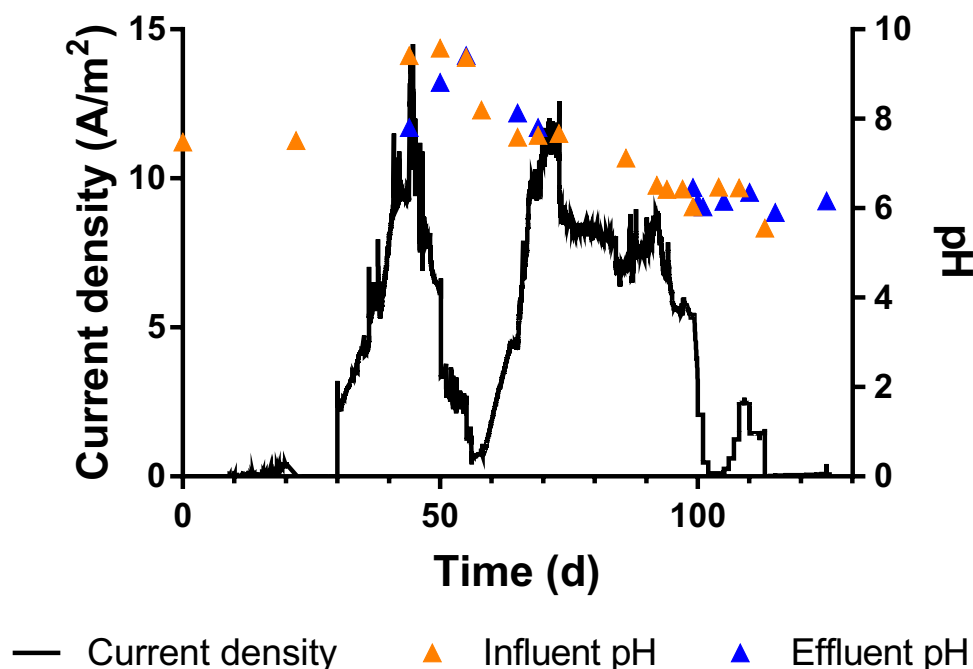


Figure 5.1.1 Current density and influent and effluent pH of A5.5 during enrichment experiments.

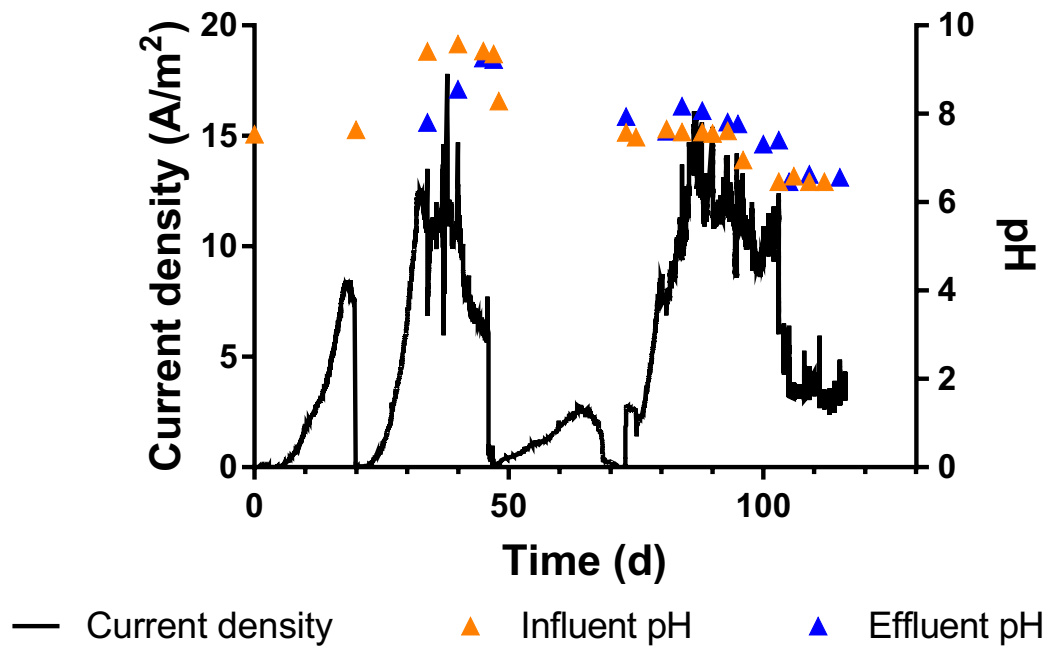


Figure 5.1.2 Current density and influent and effluent pH of A6.5 during enrichment experiments.

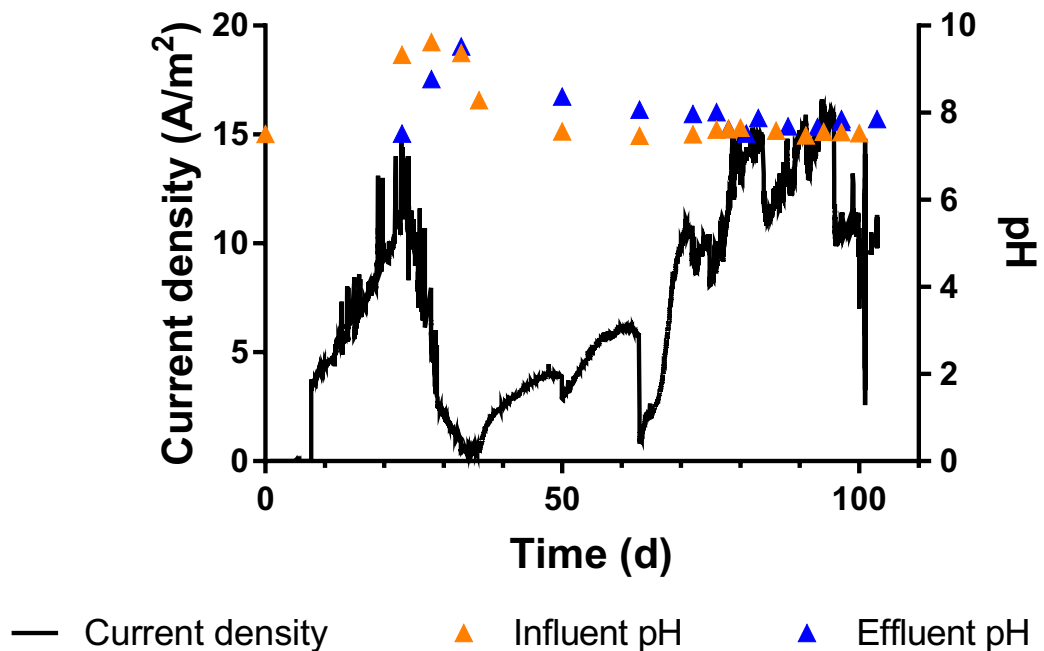


Figure 5.1.3 Current density and influent and effluent pH of A7.5 during enrichment experiments.

After switching to continuous mode (on days 73, 90 and 80 for A5.5, A6.5 and A7.5, respectively; Table 5.1.1), all reactors were first run at pH 7.5, after which the feed pH

of A5.5 and A6.5 was lowered in 0.5 steps. Lowering the feed pH to 7.0 (days 86 and 96 for A5.5 and A6.5, respectively; Figure 5.1.1 and Figure 5.1.2) did not have a notable effect on the current generation but a further decrease to 6.5 resulted in a clear drop in current density from approximately 10 to 6 and from 12 to 4 A m⁻² in A5.5 and A6.5, respectively. When pH was further lowered to 6.0 in A5.5 (Figure 5.1.1), current production practically stopped but some of the biomass recovered after the pH was increased back to 6.5 on day 104. This indicated that the low pH inhibited the bacteria present in the reactor, rather than permanently damaged them. Even though the current generation was almost 0 already at pH 6.0, A5.5 was switched back to batch mode at pH 5.5 on day 113 out of curiosity, but practically no activity was observed within the 13 d of operation at pH 5.5.

Reactor A7.5 (Figure 5.1.3), on the other hand, performed much better compared to the other two, reaching a new maximum current density of 16 A m⁻² in continuous mode operation at pH 7.5 even though its performance was rather unstable. The larger drop and variation in current production during days 95–106 was at least partially due to an unstable reference electrode. The results clearly indicate that of the pH values studied, 7.5 was the most suitable pH for the enriched culture.

In all three reactors (Figure 5.1.1, Figure 5.1.2 and Figure 5.1.3), the effluent pH was lower than the feed pH during the first part of the experiment (feed pH at ≥ 9), indicating that more protons were produced in the reactor than consumed. However, the inhibition caused by the high feed pH led to decreased activity and increased effluent pH. When the feed pH was lowered, the effluent pH was almost identical or slightly higher than the influent pH in all reactors.

The performance of the two anodes in each enrichment reactor was individually evaluated using CV measurements (Figure 5.1.4, Figure 5.1.5 and Figure 5.1.6 for A5.5, A6.5 and A7.5, respectively). Values in brackets in the legend represent days (from the beginning of the experiment) when measurements were conducted. Most of the voltammograms did not show signs of plateauing within the voltage range used, indicating that mass transfer of neither a substrate nor a buffer was the limiting factor in the current generation. Even though the electrodes were supposed to be identical in size, the new anodes (Anode 2) in A6.5 and A7.5 (Figure 5.1.5(B) and Figure 5.1.6(B)) seemed to have a larger surface area than the old anodes (Anode 1) (Figure 5.1.5(A) and Figure 5.1.6(A)) based on the higher capacitance seen in the graphs. This might be due to the fact that the new anodes were entirely colonised by active biomass, whereas the old anodes had suffered from the high pH in the early stage of the experiments. The high pH might have killed some of the biomass already growing on the electrode surface, but the biomass was not removed and thus remained taking space from more active biomass. It also seems that the new anodes were capable of higher current production at same voltages than the old anodes, which is most likely due to the higher capacitance.

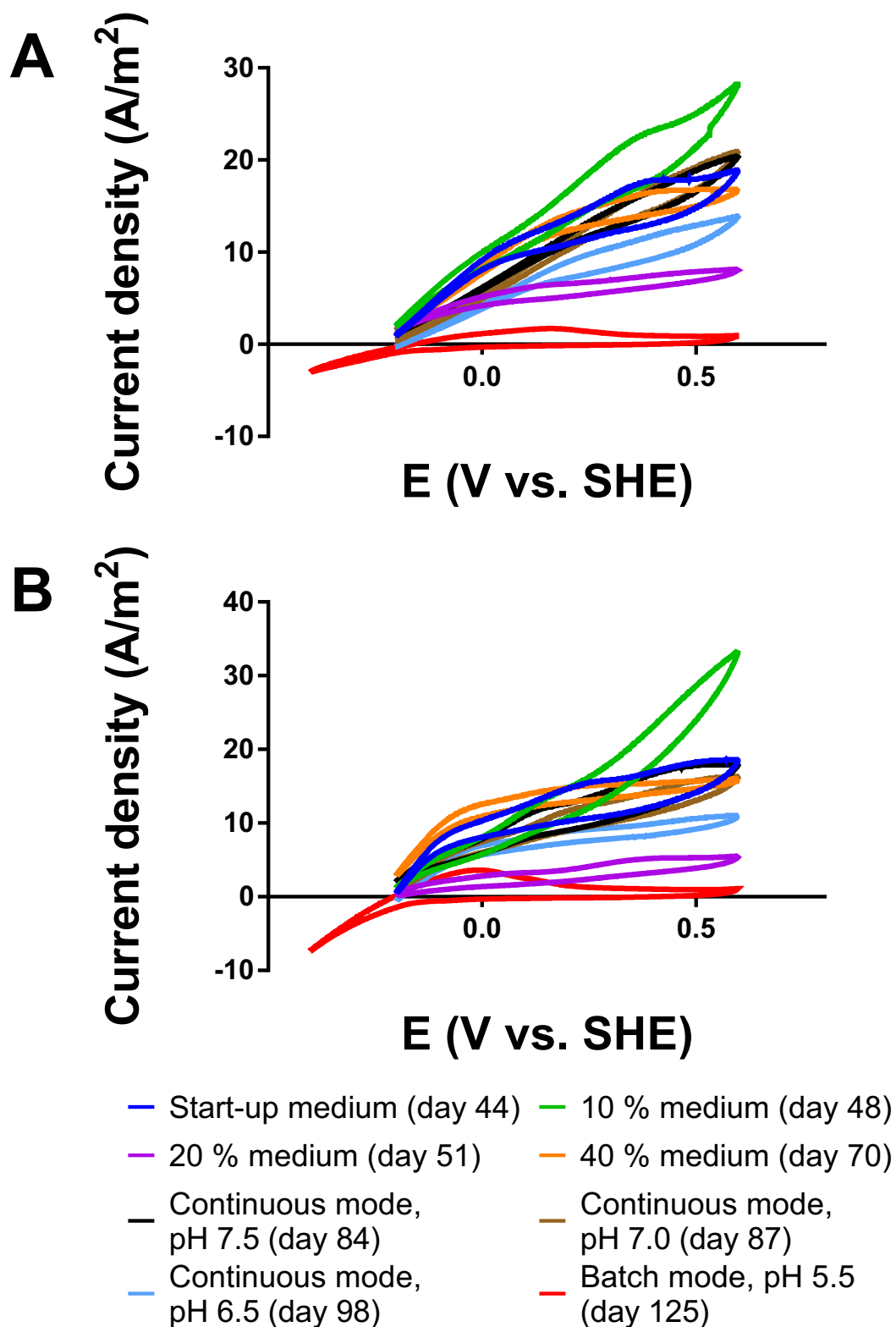


Figure 5.1.4 CVs conducted individually to the two anodes in A5.5 after re-start on day 30: (A) Anode 1, meaning the anode moved from A6.5, and (B) Anode 2, meaning the anode originally in the reactor. Days when measurements were conducted are presented in brackets.

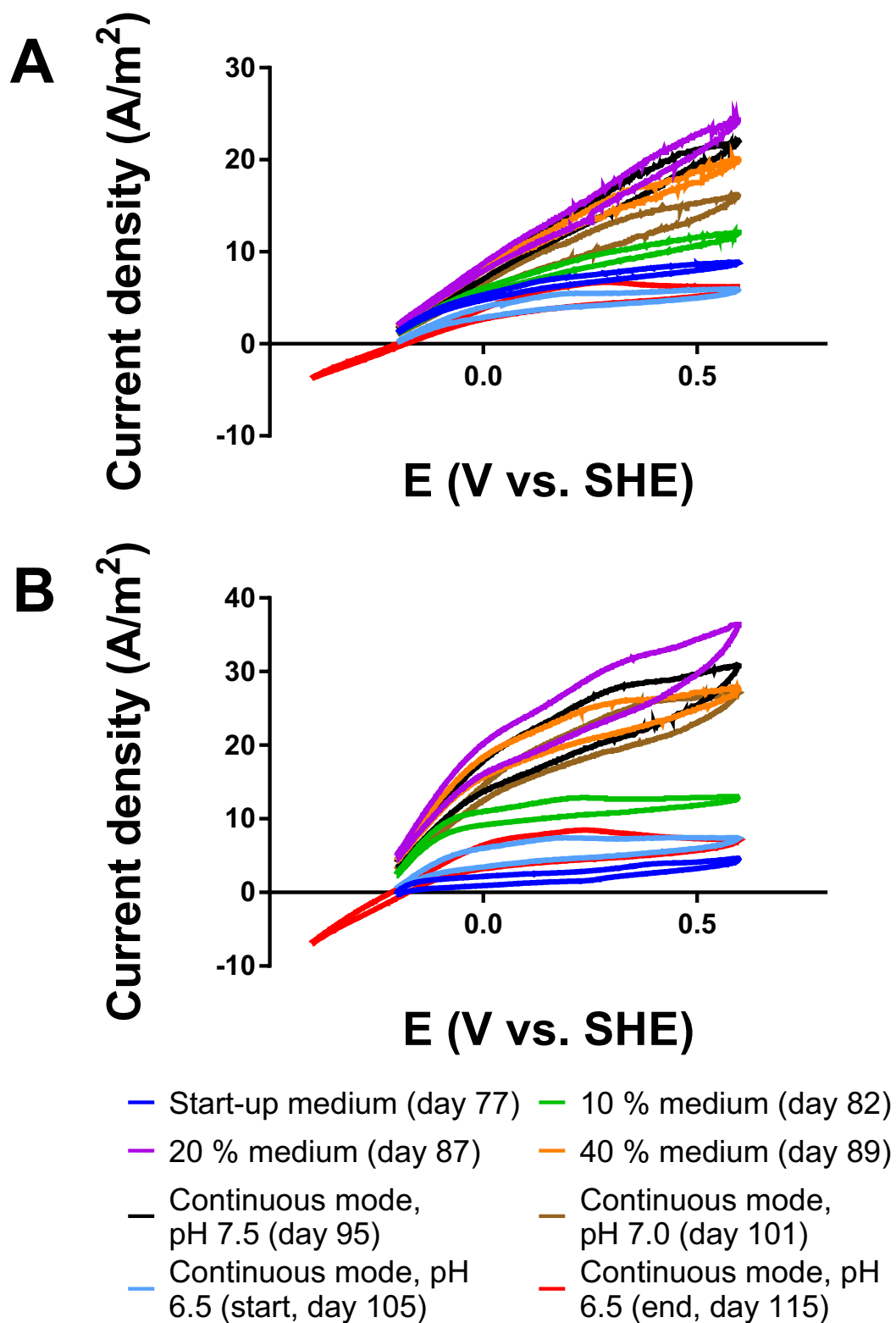


Figure 5.1.5 CVs conducted individually to the two anodes in A6.5 after the re-start on day 75: (A) Anode 1, meaning the anode moved from A7.5, and (B) Anode 2, meaning the completely new one. Days when measurements were conducted are presented in brackets.

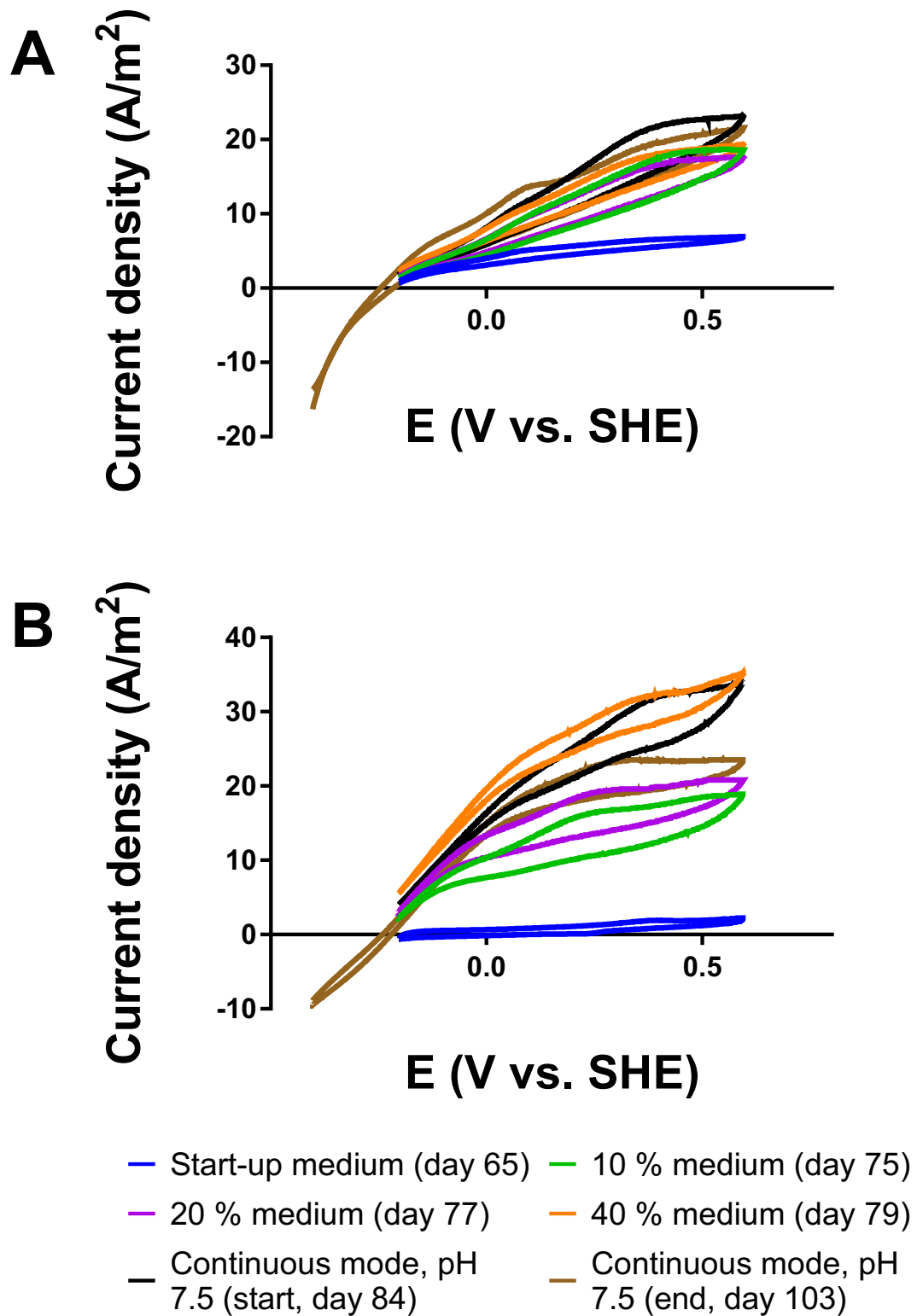


Figure 5.1.6 CVs conducted individually to the two anodes in A7.5 after the re-start on day 63: (A) Anode 1, meaning the original anode in the reactor, and (B) Anode 2, meaning the completely new one. Days when measurements were conducted are presented in brackets.

The fact that the voltammograms measured in pH 6.5 after 2 days and after 12 days of the pH change are identical (Figure 5.1.5) suggests that there were no changes in the microbial activity during this time. In reactor A7.5, on the other hand, there seems to be a decrease in the current generation ability at least for Anode 2 (Figure 5.1.6(B)) during the 27 days of continuous operation at pH 7.5.

5.1.2 Microbial community analyses

Samples for microbial community analyses were collected twice during the enrichment experiments: an original sample representing the community in the start, collected 45 d after starting the first reactors (15 d after all reactors had been re-started) as a combined sample from all reactors, and separate samples from each three reactors at the end of the enrichment after 103–126 d of operation. A heat map presenting species present at $\geq 2\%$ in at least one of the samples is presented in Figure 5.1.7.

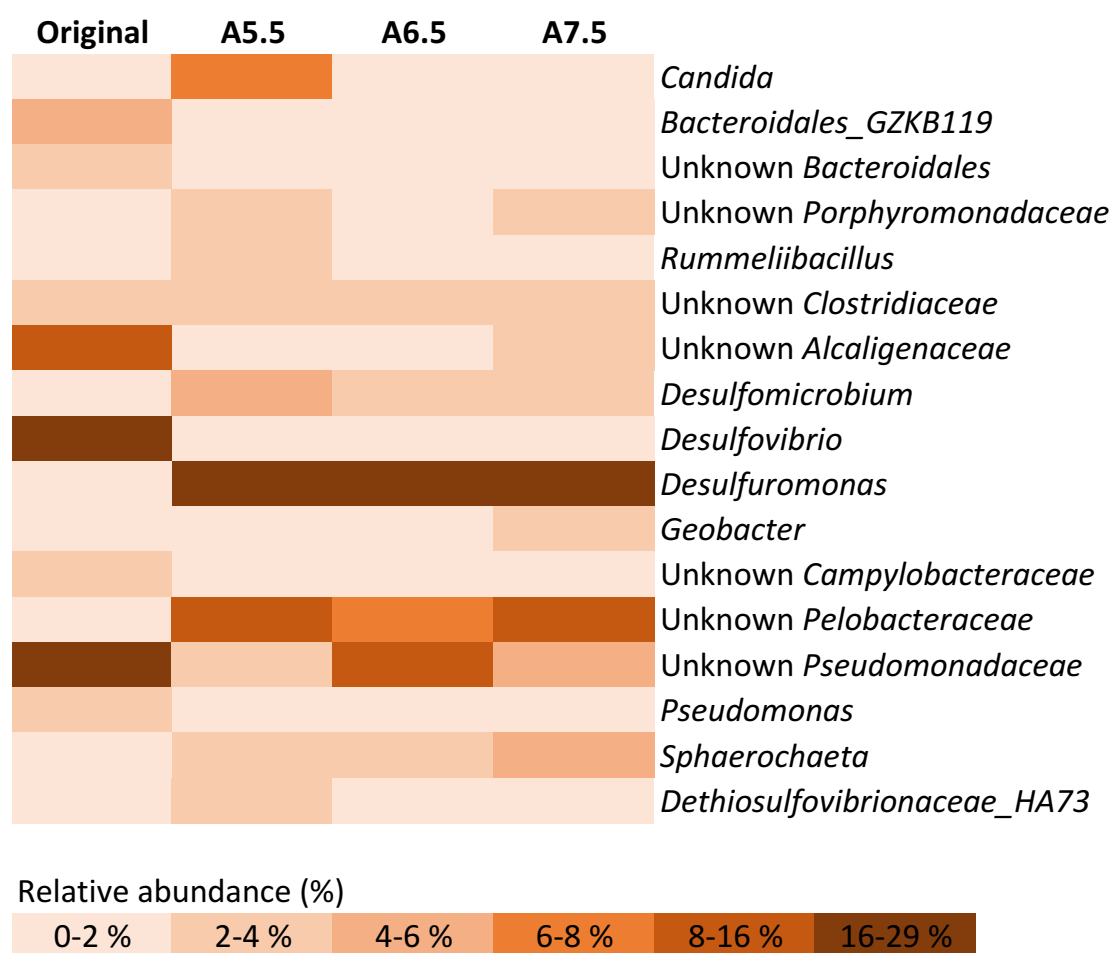


Figure 5.1.7 Heat map summarising the relative abundancies of different bacteria in the biomass samples. For clarity, only bacteria present at $\geq 2\%$ in at least one of the samples are presented.

All four biomass samples were dominated by sulfate-reducing bacteria (Figure 5.1.7). In the original sample, the dominating species was *Desulfovibrio* (18.7%), whereas it had

been replaced by *Desulfuromonas* at all studied pH values after the enrichment, the relative abundancies being 17.5 % for A5.5, 28.1 % for A6.5, and 18.1 % for A7.5. Correspondingly, the amount of *Desulfuromonas* in the original sample as well as that of *Desulfovibrio* after the enrichment were below 2 %. In the samples taken after enrichment, the relative abundance of another sulfate-reducing bacteria, *Desulfomicrobium*, had also slightly increased compared to the original culture (increase from 0.6 % in original sample to 4.4 %, 2.8 % and 2.8 % in A5.5, A6.5 and A7.5, respectively). This is an interesting result considering that all these sulfate-reducing bacteria are reported to prefer a pH range of 6.6–7.5 (or 6.8–7.5 for *Desulfuromonas*) (Holt et al. 1994).

In the original biomass sample, two other bacterial families were also present at high concentrations: unknown *Pseudomonadaceae* (16.9 %) and unknown *Alcaligenaceae* (14.3 %). This is also interesting since both these bacterial families have been reported to be strictly aerobic and have a respiratory type of metabolism with oxygen as the terminal electron acceptor (Brenner et al. 2005; Holt et al. 1994). The unknown *Pseudomonadaceae* was also the second largest (11.0 %) bacterial group in A6.5.

In the three reactors after enrichment, unknown *Pelobacteraceae* was present at rather high concentrations: 12.3 % in A5.5, 6.9 % in A6.5 and 12.7 % in A7.5, whereas it was almost completely lacking from the original biomass (0.1 %). On the other hand, *Geobacter*, which is generally present at neutral conditions, was almost completely lacking from all three enrichment reactors based on the results. However, *Geobacter* is so close to the properties of *Pelobacter*, a member of the *Pelobacteraceae* family, that it could be misidentified as *Pelobacter* in the community analysis, which could explain the rather high amounts of the unknown *Pelobacteraceae*. On the other hand, if the number of *Geobacter* in all samples is as low as indicated by the results, it might be one explanation for the overall low electricity generation. (Based on a discussion with Stefano Freguia and Bernardino Viridis)

A5.5 had also been contaminated by a yeast *Candida Palmioleophila* (7.0 %). Yeast being a eukaryote, it is difficult to quantitatively compare it to the bacterial species present. Since the analysis was not meant for eukaryotes, this result is also somewhat uncertain.

Based on the quality control (QC) data provided by the ACE (Figure 5.1.8), most of the original biomass sample (approximately 70 %) failed the QC, i.e. the reads had less than 250 bases and were excluded from further processing, and therefore remained unknown. In fact, the fraction that was included in the final results, i.e. OTUs ≥ 0.05 %, was only slightly over 20 %. For the samples taken after the enrichment, the fraction that completely failed the QC was much lower (≤ 20 %). The amount of biomass that was included in the results was ≥ 60 % for all three reactors. Thus, the results for A5.5–A7.5 can be assumed to be more reliable than for the original biomass sample.

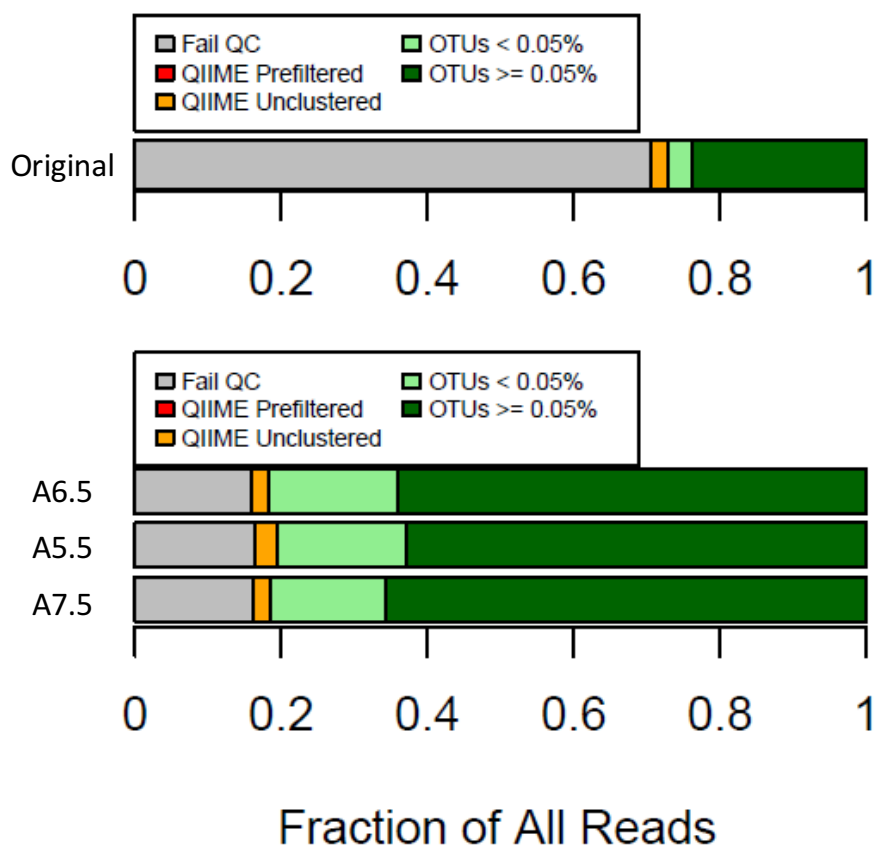


Figure 5.1.8 Quality control (QC) statistics of the four different runs.

5.1.3 Buffer capacity

Even though the reactors used in the enrichment experiments were single-cell and membrane-less, meaning that the overall proton production (at the anode) and consumption (at the cathode) should even each other out eventually, the buffer capacity of the reactor medium plays a role near the surface of the anode. Here, protons are produced as a result of the oxidation reaction (Eq. (6)), which might result in a low local pH if the medium is not able to neutralise these protons. Therefore, the buffer capacities of the media at different pH values were studied to see if lack of buffer capacity might be a reason for low current generation.

The ion speciation of the main buffering compounds present in the different 40 % hydrolysed urine media used at different pH obtained using Visual MINTEQ, is presented in Table 5.1.2 (complete table including the speciation of all the compounds present in the media can be found in Appendix C). The values in the table are a rough estimation of the species distribution and should only be used as a guideline. It is also important to note the nature of the buffering compounds, not just their amount. For example, CH_3COO^- only acts as a buffer at acidic pH (Eq. (12)) and NH_4^+ at slightly basic pH (Eq. (2)), which is why they are of little importance at the studied pH values.

Table 5.1.2 Ion species distribution of main buffering compounds at different pH

Compound	Species	Distribution (%)		
		pH 5.5	pH 6.5	pH 7.5
NH₄⁺	NH ₄ ⁺	97.8	97.6	96.4
	NH ₄ SO ₄ ⁻	2.2	2.2	2.4
	NH ₃ (aq)	0.0	0.1	1.1
	CaNH ₃ ²⁺	0.0	0.0	0.0
CH₃COO⁻	CH ₃ COO ⁻	83.8	92.2	95.1
	CH ₃ COONa (aq)	2.9	3.1	3.5
	CH ₃ COOK (aq)	3.2	3.5	1.1
	CH ₃ COOH (aq)	9.9	1.1	0.1
	CH ₃ COOMg	0.1	0.1	0.1
	CH ₃ COOCa	0.1	0.1	0.1
PO₄³⁻	PO ₄ ³⁻	0.0	0.0	0.0
	HPO ₄ ²⁻	3.8	24.1	59.3
	H ₂ PO ₄ ⁻	75.5	47.8	11.5
	H ₃ PO ₄	0.0	0.0	0.0
	MgPO ₄ ⁻	0.0	0.0	0.0
	MgHPO ₄ (aq)	0.0	0.2	0.5
	CaHPO ₄ (aq)	0.0	0.1	0.3
	CaPO ₄ ⁻	0.0	0.0	0.0
	CaH ₂ PO ₄ ⁺	0.1	0.1	0.0
	NaHPO ₄ ⁻	1.3	7.7	19.8
	KHPO ₄ ⁻	1.3	7.8	5.9
	K ₂ HPO ₄ (aq)	0.2	1.0	0.2
	KH ₂ PO ₄ (aq)	10.8	6.7	0.5
	KPO ₄ ²⁻	0.0	0.0	0.0
	Na ₂ HPO ₄ (aq)	0.0	0.3	0.7
	Na ₂ PO ₄ ⁻	0.0	0.0	0.0
	NaH ₂ PO ₄ (aq)	7.0	4.3	1.1
	NaPO ₄ ²⁻	0.0	0.0	0.0
	CO₃²⁻	CO ₃ ²⁻	0.0	0.0
HCO ₃ ⁻		0.0	0.0	92.8
H ₂ CO ₃ * (aq)		0.0	0.0	4.4
MgCO ₃ (aq)		0.0	0.0	0.0
MgHCO ₃ ⁺		0.0	0.0	0.0
CaHCO ₃ ⁺		0.0	0.0	0.1
CaCO ₃ (aq)		0.0	0.0	0.0
NaCO ₃ ⁻		0.0	0.0	0.2
NaHCO ₃ (aq)		0.0	0.0	2.2

In reactor A7.5, both phosphate and carbonate compounds could be considered to be acting as buffers, whereas in reactors A5.5 and A6.5, lacking completely the carbonate buffer, phosphate buffer acted as the main buffer compound. For A7.5, the total concentration of phosphate and carbonate buffers would be 114 mM (Table 4.1.1) When considering the speciation of the buffers presented in Table 5.1.2 and a flow rate of 0.48 mL min^{-1} (corresponding to $8 \cdot 10^{-6} \text{ L s}^{-1}$), a theoretical current generation of 130 mA should be possible based on Eq. (16). The total concentration of phosphate buffer in reactor A6.5 was 102 mM, resulting in a theoretical current of 88 mA. These values would mean current densities in the range of $65\text{--}96 \text{ A m}^{-2}$. For reactor A5.5 the situation is slightly different since it was operated in batch mode. Naturally, these are merely rough estimations but clearly indicate that the lack of buffering capacity is not the growth limiting factor at low pH, but rather the composition of the microbial community.

5.2 Enhanced ORR at the air-cathode

The cathode coating experiments were started with the different catalyst materials. After this, two of the best performing catalyst materials were chosen for the DL tests with different PTFE sprays. These results are presented in the following chapters.

5.2.1 Catalyst coating

The catalyst coating experiments were first started with NCNT and NG with no pre-treatment step and simply dispersing the nanoparticles in Milli-Q for the EPD. The effect of the coating was tested immediately after the deposition at least in one of the two buffers used and also the following day to see if there was a difference. As a comparison, results obtained with plain carbon cloth with no coating in both phosphate and ammonia (0.1 M) buffers are included.

The first results with NCNT showed better performance in phosphate buffer than in ammonia buffer immediately after the deposition (Figure 5.2.1), which could be expected based on the increased theoretical reduction potential at lower pH (see Chapter 3.1.1). However, when the cathode was tested in ammonia buffer the following day, its performance was notably better than in either of the buffers immediately after the deposition. This was most likely due to the effect of the overnight drying step, which has also been reported to be used in the literature (An et al. 2010; Thomas et al. 2005). At this point, the molarity of the ammonia buffer was (accidentally) 10-fold compared to that of the phosphate buffer, and hence its EC was also notably higher. This is another factor that might have contributed to the unexpectedly good performance in the ammonia buffer.

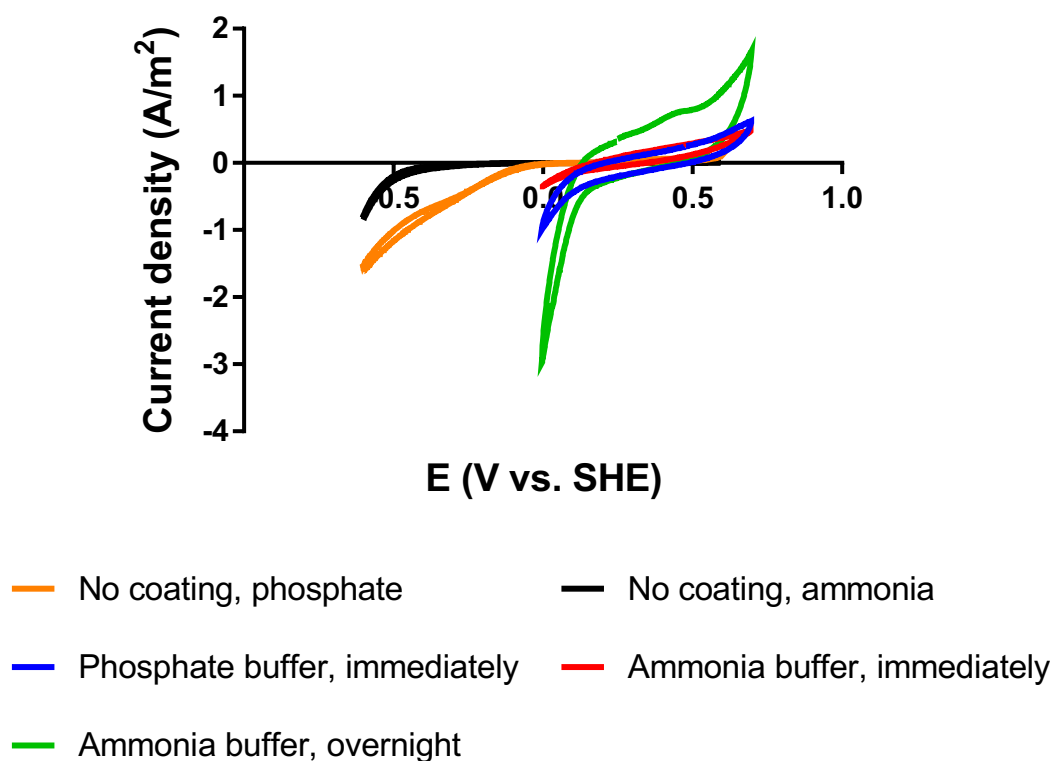


Figure 5.2.1 CVs conducted for the NCNT-coated cathode in two different buffers immediately after the deposition and in ammonia buffer the following day (marked “overnight”). CVs conducted for plain carbon cloth in both buffers are included for comparison.

The NG-coated cathode was tested immediately after the deposition in the ammonia buffer (1.0 M) and in both buffers the following day (Figure 5.2.2). Here, the performance in the ammonia buffer seemed to outrun the performance in phosphate buffer, which was unexpected. However, this was expected to again be due to the higher EC of the ammonia buffer. This was also supported by the result in a diluted ammonia buffer (0.1 M) after 21 days of the deposition. This time, the CV scan range was larger and in total higher current densities were obtained, but the current densities at similar voltages were not as high as in 1.0 M ammonia buffer.

The positive effect of the drying step was not as clear with NG. Despite this, an overnight drying step in a fume hood was used for the rest of the catalyst material experiments. The ammonia buffer was also diluted to the same molarity as the phosphate buffer (0.1 M), which decreased its EC (from 57.9 mS cm⁻¹ to 7.88 mS cm⁻¹, compared to 15.24 mS cm⁻¹ of the phosphate buffer). For the rest of tests, the CV scan range was also increased to be from +0.600 V to -0.600 V vs. SHE.

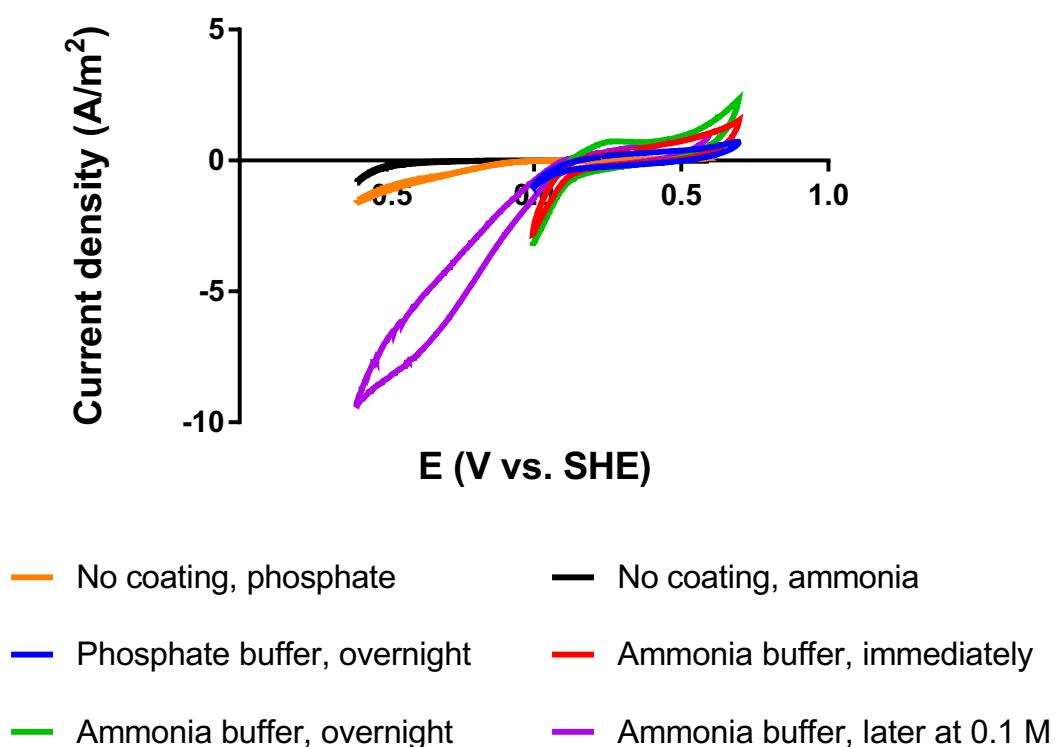


Figure 5.2.2 CVs conducted for the NG-coated cathodes in ammonia buffer immediately after the deposition, in both buffers the following day, and in a more dilute ammonia buffer 21 days after the deposition (also tested with a larger range). CVs conducted for plain carbon cloth in both buffers are included for comparison.

The voltammograms obtained with the rest of the tested catalyst materials in phosphate buffer are presented in Figure 5.2.3. In general, there was relatively large variation in the results of the different materials in phosphate buffer. The best performing coating was PVDF-PAC, reaching a current density of 34 A m^{-2} at -0.600 V vs. SHE . However, the voltammogram of e.g. Acid-NCNT clearly plateaus around 10 A m^{-2} at voltages lower than -0.200 V vs. SHE , which indicates a mass transfer limit. This was supported by the observation of water formation on the cathode during the test, significantly reducing oxygen diffusion through the cathode into the catholyte.

In the neutral conditions of the phosphate buffer, the effect of all the catalyst materials on the onset potential of the reduction reaction was rather small. For the cathode with no catalyst coating, the onset potential for ORR was approximately 0 V vs. SHE , whereas the catalysts were only able to increase it to approximately $+0.1 \text{ V vs. SHE}$ (Figure 5.2.3).

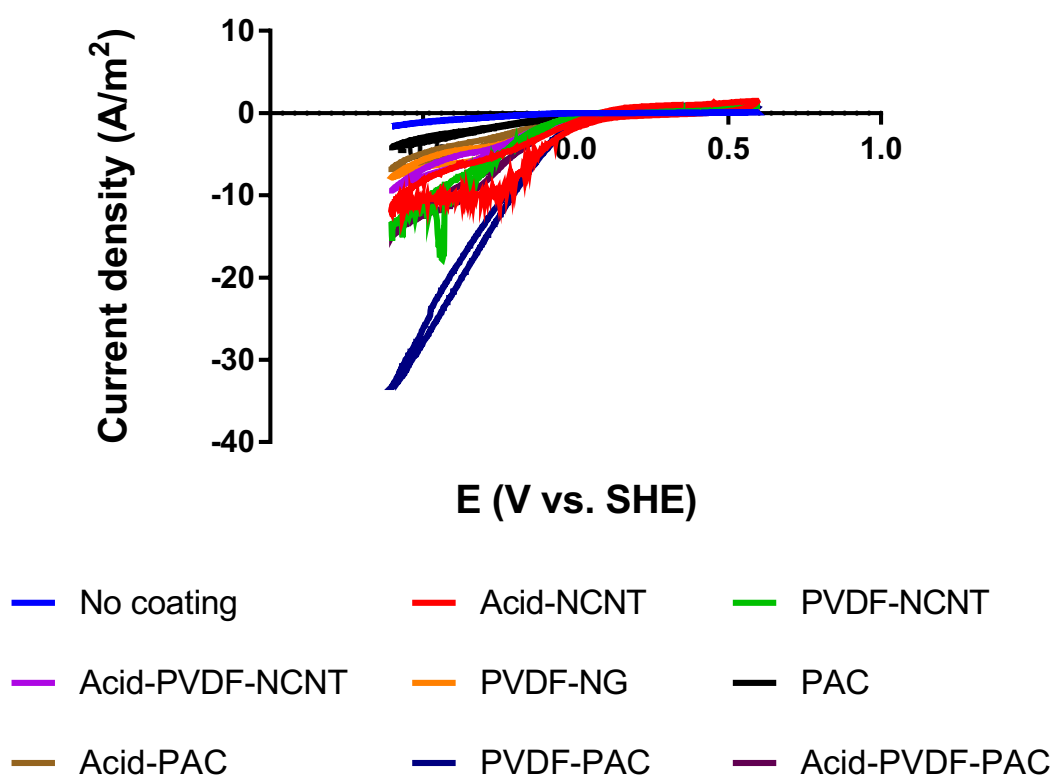


Figure 5.2.3 A summary of the CVs in phosphate buffer for the rest of the catalyst materials tested. All CVs were conducted after an overnight drying period. CVs conducted for plain carbon cloth in both buffers are included for comparison.

Corresponding voltammograms with the same catalyst materials in basic ammonia buffer are presented in Figure 5.2.4. In these tests, conducted with buffers with identical molarity, a better performance in phosphate buffer (Figure 5.2.3) compared to that in ammonia buffer could be seen more clearly. An exception was Acid-NCNT which was clearly the best performing cathode in the alkaline conditions of the ammonia buffer, reaching current densities over 20 A m⁻² at -0.600 V vs. SHE. The maximum current density reached in neutral conditions with this cathode was only approximately half of this. However, as mentioned above, Acid-NCNT seemed to be affected by mass transfer limitation in phosphate buffer, which decreased its performance. The best-performing catalyst in phosphate buffer, PVDF-PAC, had a much more modest performance in ammonia buffer, the maximum current density remaining under 10 A m⁻².

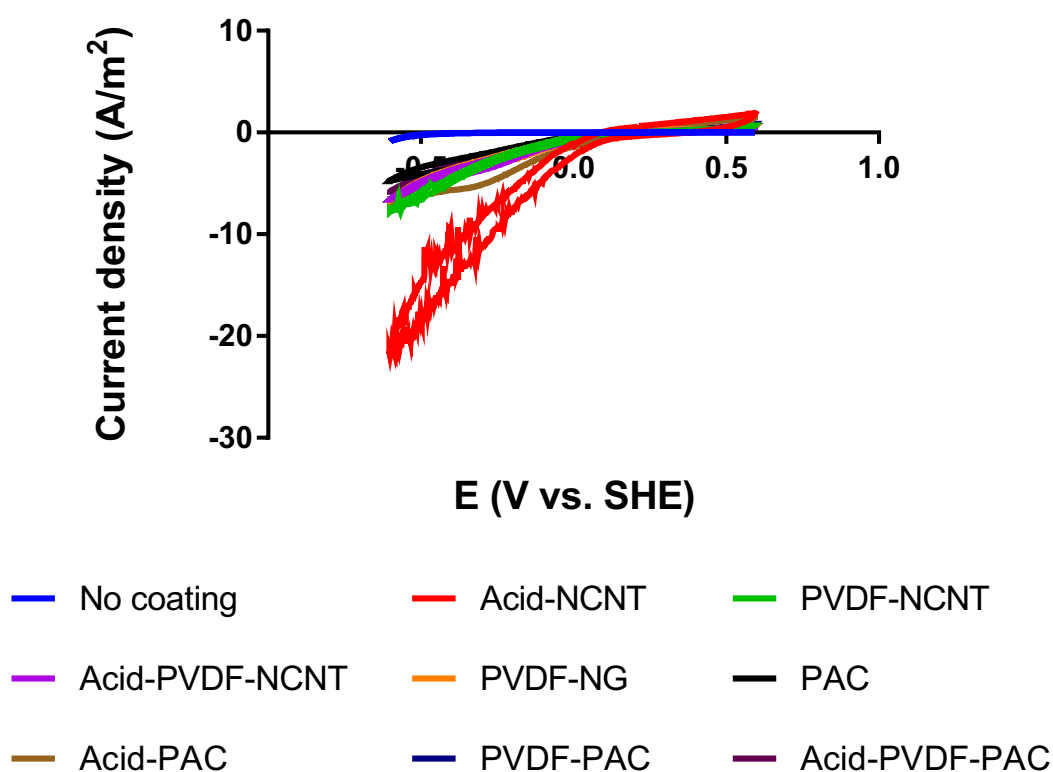


Figure 5.2.4 A summary of the CVs in ammonia buffer for the rest of the catalyst materials tested. All CVs were conducted after an overnight drying period. CVs conducted for plain carbon cloth in both buffers are included for comparison.

In ammonia buffer, the effect of the catalysts on the onset potential of ORR was more clear than in phosphate buffer. However, this was not because the onset potential with catalysts would have been higher in ammonia than in phosphate buffer; it was actually almost identical compared to the results in phosphate buffer, +0.1 V vs. SHE. The onset potential without a catalyst, however, was much lower in ammonia than in phosphate buffer, being approximately -0.5 V vs. SHE. All in all, the effect of the catalyst materials on the onset potential for ORR was not as large as hoped for, and the onset potential remained lower than intended.

PVDF-PAC and Acid-NCNT that were the best performing catalysts in phosphate and ammonia buffers, respectively, were chosen for the further experiments with the PTFE sprays.

5.2.2 PTFE coating

PTFE coating was provided as a diffusion layer on the air-facing side of the cathode. The first PTFE spray tested with Acid-NCNT and PVDF-PAC cathodes was Ezy Glide (Figure 5.2.5). In the literature, a commonly used method is applying four PTFE layers by painting (Cheng et al. 2006a), which is why four spraying layers was chosen as the

starting point, even though a clear correlation between these two techniques cannot be made. A control with no catalyst layer (with 4 layers of WD-40 spray) is added for comparison. It shows that the catalyst layer is mostly responsible for the increased current production and that the diffusion layers alone are not enough.

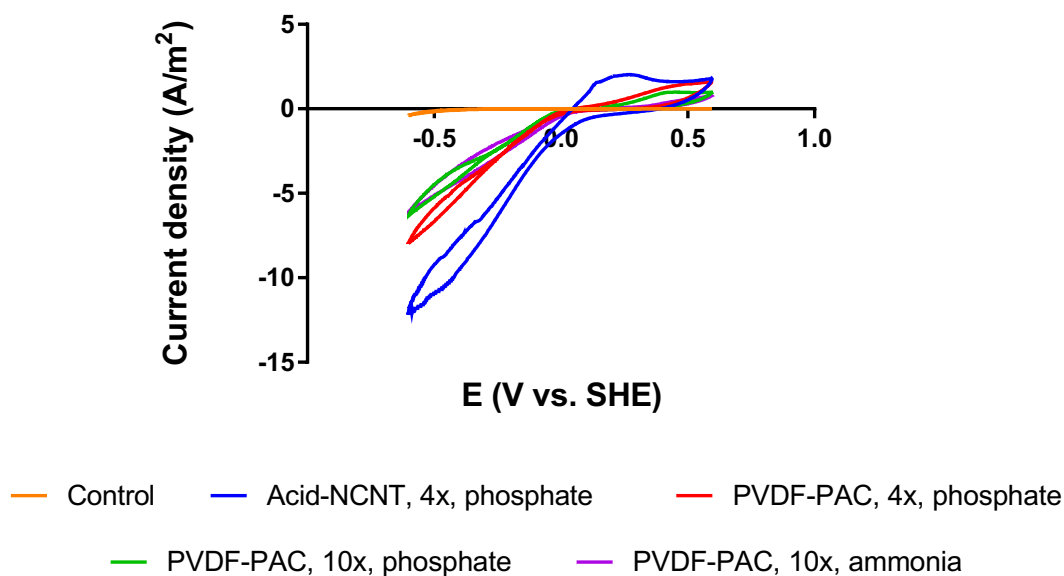


Figure 5.2.5 CVs conducted for Acid-NCNT and PVDF-PAC with different amounts of Ezy Glide PTFE spray in phosphate or ammonia buffer. Control means a cathode with no catalyst coating and 4 layers of WD-40 PTFE spray, measured in 0.1 M ammonia buffer..

Both Acid-NCNT and PVDF-PAC with four layers of Ezy Glide spray were first tested in phosphate buffer. Acid-NCNT outperformed PVDF-PAC clearly but the results were not nearly as good as without the PTFE coating. Furthermore, four layers was not enough to make the cathodes waterproof and leakage through the carbon cloths was observed. Therefore, more layers were applied on PVDF-PAC, resulting in a total of ten layers. This was then tested in both buffers. Ten layers were enough to make the cathode waterproof but unfortunately the current density was further reduced, indicating that the PTFE was blocking the effective surface area of the cathode to some extent and reducing oxygen diffusion. Therefore, the focus was moved to another spray, WD-40.

With WD-40, the testing was carried out by applying one layer at a time and conducting CV testing before adding the next layer to better find out the optimal number of layers. For clarity, not all the results are included in Figure 5.2.6, but only enough to see the pattern being formed. For WD-40, all CV tests were carried out in ammonia buffer which resembled the actual cathode conditions more realistically.

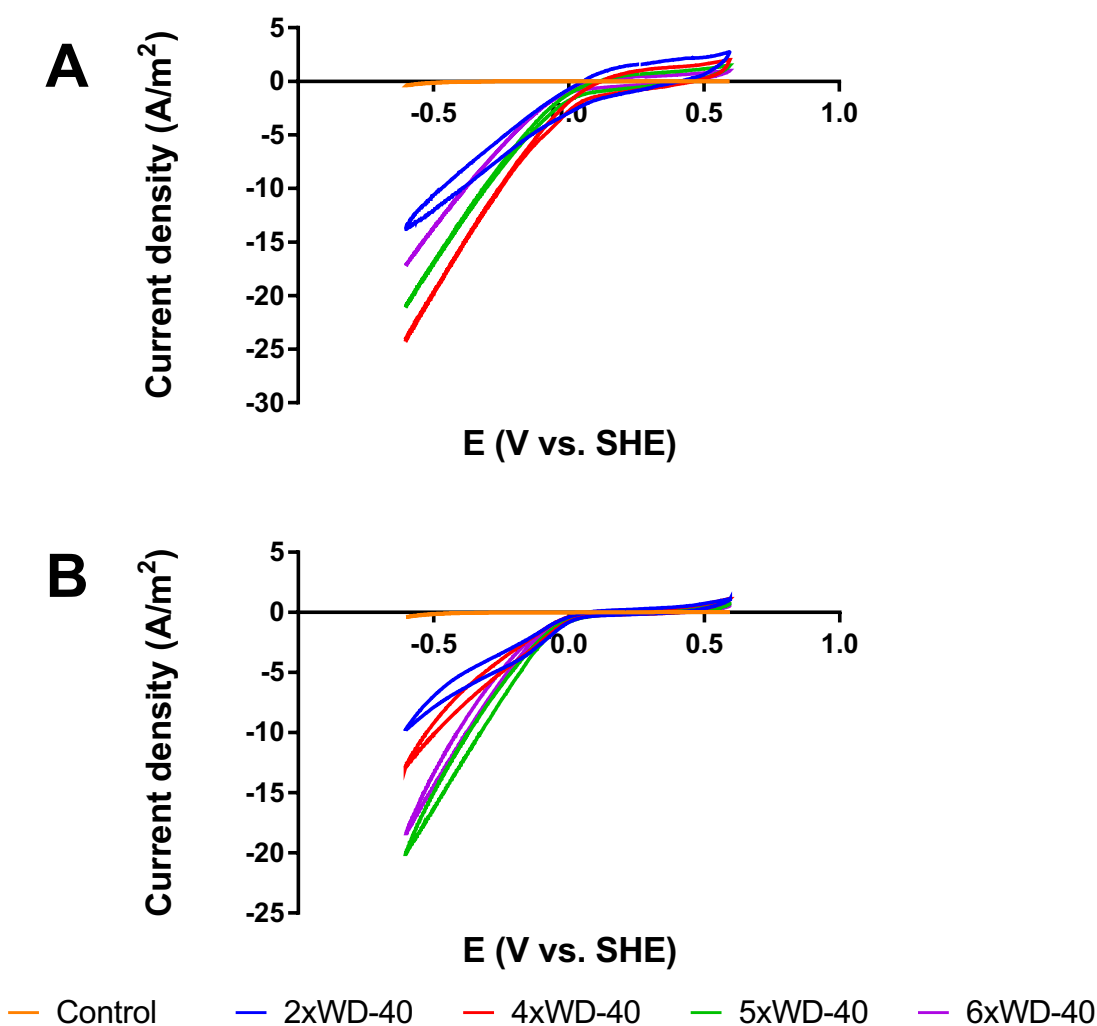


Figure 5.2.6 CVs conducted in ammonia buffer for (A) Acid-NCNT and (B) PVDF-PAC with varying numbers of layers of WD-40 PTFE spray. Control means a cathode with no catalyst coating and 4 layers of WD-40 PTFE spray, measured in 0.1 M ammonia buffer..

The tests with WD-40 were started with Acid-NCNT (Figure 5.2.6(A)). The first three layers were only allowed to dry for approximately 5 min (according to the instructions on the package, the spray would dry within seconds) before conducting a CV. The fourth layer, however, was allowed to dry overnight and this immediately resulted in a better result. The current densities obtained with 4xWD-40 (up to 24 A m⁻²) were in fact even higher than the performance of Acid-NCNT without any PTFE (Figure 5.2.4). After this, applying more PTFE layers again resulted in reduced current production, which is why four layers was concluded to be the best amount of WD-40 to be applied.

For PVDF-PAC (Figure 5.2.6(B)), each layer of WD-40 was allowed to dry overnight from the beginning. The trend of the increasing number of layers followed the pattern already seen with Acid-NCNT: applying more layers increased the current production to a certain point, after which it started to decrease again. For PVDF-PAC, five layers was

found to be the optimal number. A maximum current density of 20 A m^{-2} was obtained with this amount, which was more than reached with PVDF-PAC without PTFE in ammonia buffer (Figure 5.2.4). However, this was lower than what was reached with Acid-NCNT.

The third PTFE spray, 3-in-one, was briefly tested using the third best catalyst material, PVDF-NCNT, but it failed to make the cathode waterproof. Due to this and the excellent performance of WD-40, further testing with 3-in-one was concluded unnecessary and the data is therefore not shown here.

The cathodes that had been prepared using the PVDF method seemed to be more waterproof than cathodes coated using Milli-Q as the dispersion medium to begin with. This was most likely due to the fact that PVDF is a fluoropolymer like PTFE and thus already contributed to the waterproofing. However, since the current production performance of Acid-NCNT was better than that of PVDF-PAC and it was also made waterproof using WD-40, Acid-NCNT with four layers of WD-40 was chosen as the cathode construction for the UGold reactors.

5.3 Operation of UGold reactor with air-cathodes

The actual UGold reactors were started with enrichment of the anodic biomass. At this point, the air-cathodes were not yet used. After the enrichment, stainless steel cathodes were replaced with the air-cathodes. The results of these experiments are presented in the following chapters.

5.3.1 Enrichment of anodic biomass

In the enrichment of the anodic biomass in the UGold reactors, it was again observed that growth started quickly after inoculation with a solid electrode material already colonised by an active biomass. Even when the fraction of the colonised granules was only 13.8 % of the complete mass of granules used as the anodes, the enrichment could be completed in 18 d. Towards the end of the enrichment, the CA data became rather noisy (possibly due to a bad reference electrode connection and/or air bubbles in the system), which is why the values presented in Figure 5.3.1 are calculated as the averages of nine consecutive data points (including four before and four after the data point in question, measured every 60 s). The current density is expressed against the membrane surface area (35 cm^2).

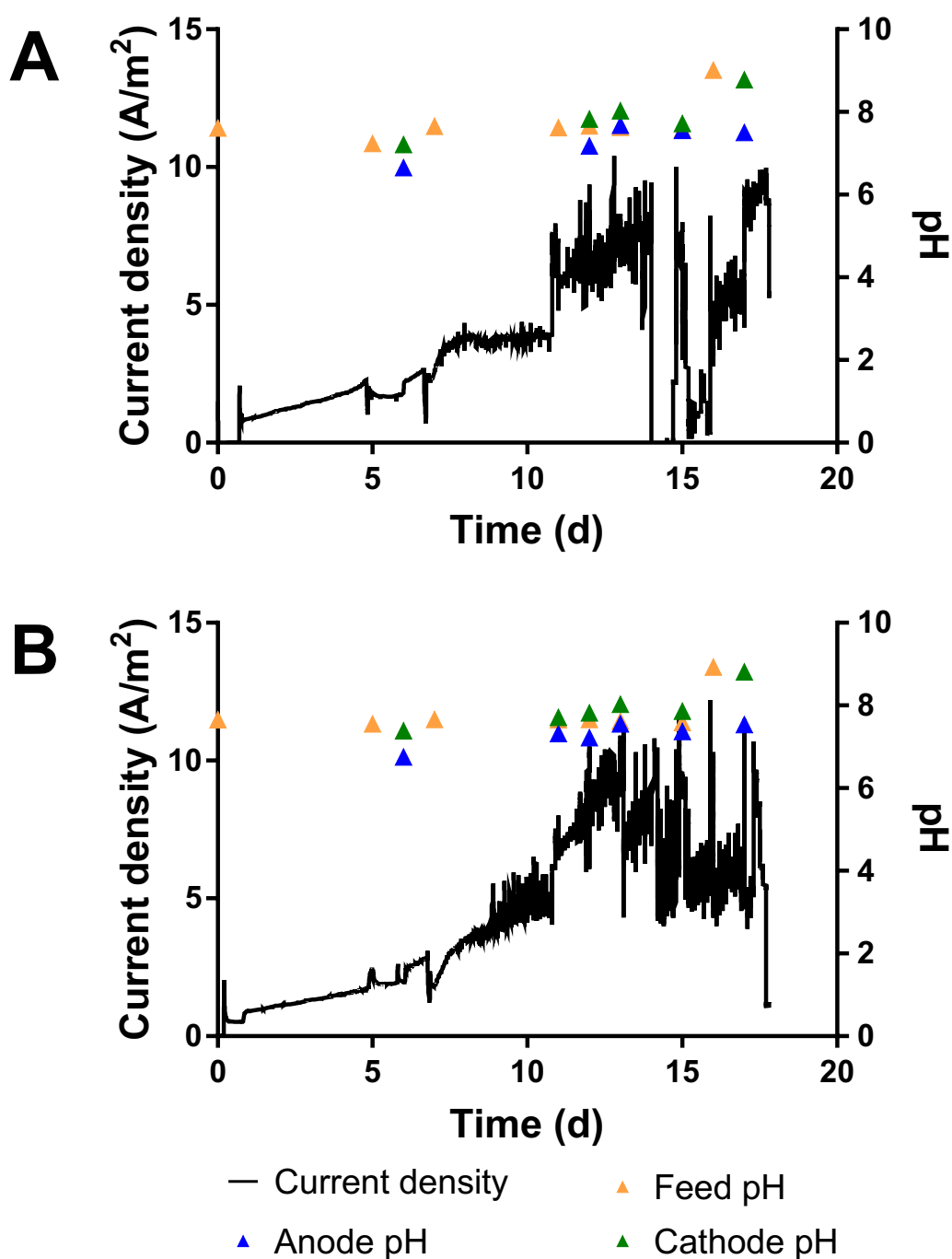


Figure 5.3.1 Current density (calculated as the averages of nine consecutive data points) and feed, anode and cathode pH of (A) UGold1 and (B) UGold2 during the enrichment of biomass at the anode.

The current production was constantly increasing in UGold1 during the ammonia concentration increase, reaching maximum values of approximately 10 A m^{-2} with the 40 % medium (Figure 5.3.1(A)). The sudden drop in the current production on day 14 was due to a misconnected reference electrode. After having recovered back to its former level, the current dropped again, this time due to a depletion of the medium in the feed

bottle. After this, however, the current production increased back to its original level even though the feed pH was increased shortly after the collapse.

The current production of UGold 2 (Figure 5.3.1(B)) developed in a similar manner to UGold1 and the maximum current densities obtained were in the same range. UGold2 did not suffer similar kinds of sudden drops in the current as UGold1 but the current production in general decreased slightly (from approximately 8 to 6 A m⁻²) when the reactor was run with the 40 % medium and remained at this level also after the increase in feed pH. There was also a larger drop in the current density at the very end of the enrichment, which was due to a blockage somewhere in the tubing that caused the anode chamber to collapse.

In the UGold reactors, the anode and cathode chambers were separated from each other using membranes, which facilitated the formation of a pH gradient between the two electrodes. This was observed even though the anodic effluent was used as the feed for the cathode (Figure 5.3.1). Overall, the pH at the anode was slightly lower and the pH at the cathode slightly higher than the feed pH throughout the ammonia concentration increase in both reactors, which could be expected. The anode pH of UGold1 started from 6.7 on day 6, then increasing slightly to 7.2 on day 12 and finally stabilising around 7.6±0.1. Even after the pH of the feed was increased from 7.5 to 9 on day 16, the pH at the anode remained at 7.6±0.1, proving that the microbial culture was stable and able to neutralise the alkaline pH. The anode pH of UGold2, however, stabilised to a slightly lower level of 7.3±0.2 compared to UGold1. The feed pH being practically identical indicates that the biomass of UGold2 was slightly more active and able to produce more protons.

Similarly to the anode pH, the cathode pH of UGold1 was rather low (7.2) in the beginning, then increasing and stabilising around 7.8±0.2 (Figure 5.3.1(A)). After the increase in the feed pH, the cathode pH also increased almost to the same level with the feed pH, the measured pH being 8.8. The cathode pH of UGold2 was almost identical to that in UGold1.

In addition to the CA data, the performance of the two anodes was evaluated by conducting a CV both in the beginning and at the end of the enrichment (Figure 5.3.2). Unfortunately, the CVs obtained after the enrichment were rather noisy, most likely again due to a poor reference electrode connection. Interestingly, the CVs both at the beginning and the end of the enrichment seem to differ between the two reactors. At the beginning, the voltammogram of the anode in UGold2 was almost a flat line, whereas the anode of UGold1 showed larger capacitance and capability of higher current production. After the enrichment, however, the situation was the opposite: the anode of UGold2 showed capability of higher current production at similar voltages. This is consistent with the lower pH measured at UGold2 anode.

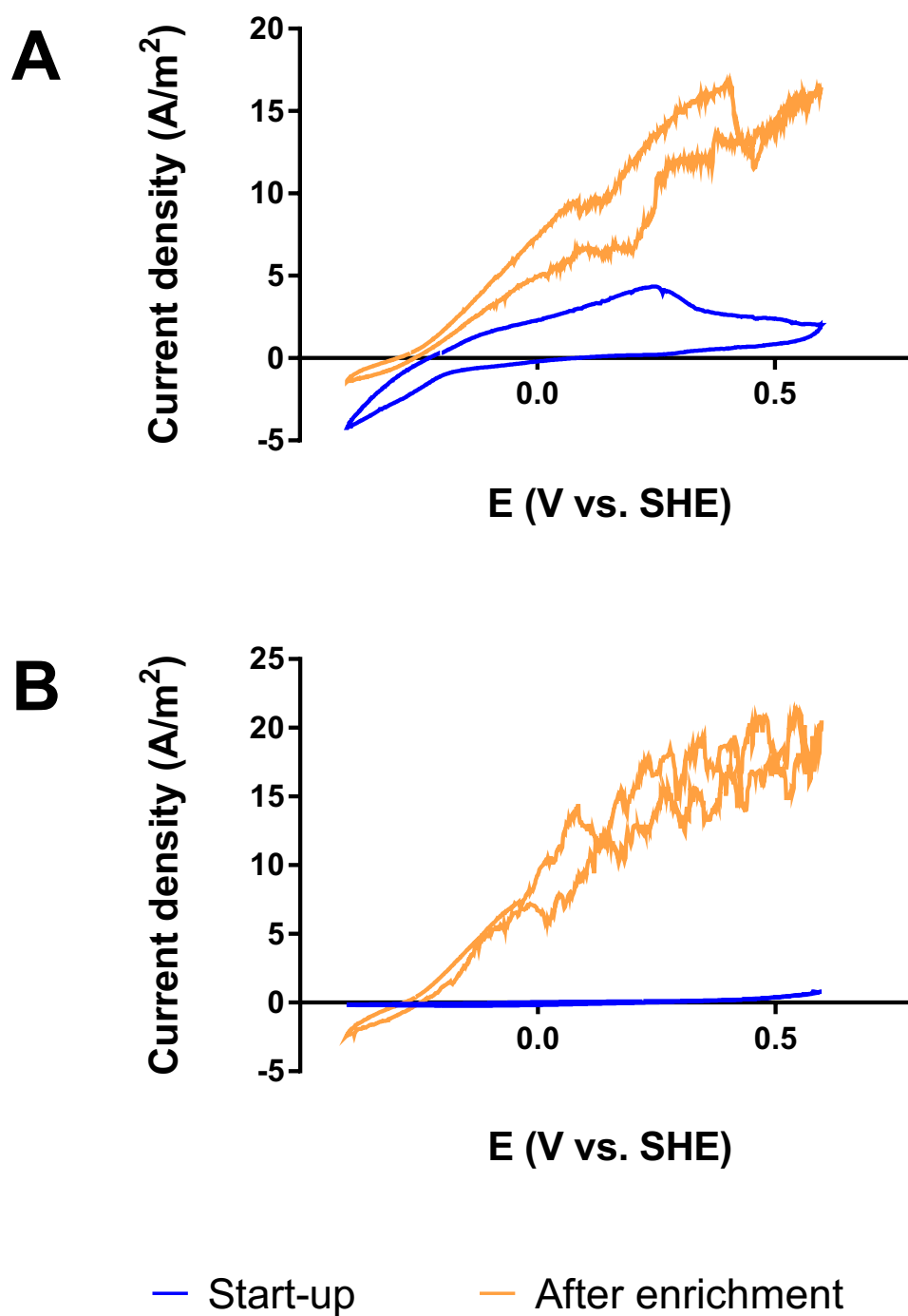


Figure 5.3.2 CVs conducted at the start-up and after the enrichment for the anodes in (A) UGold1 and (B) UGold 2.

5.3.2 Operation with air-cathodes

As the final part of the experiments, UGold1 and UGold2 were operated with air-cathodes for 14 days (longer operation was not possible within the timeframe of the project). As mentioned in Chapter 4.3.2, the PTFE treatment on the air-cathodes was not

enough to make the cathodes waterproof, which resulted in repetitive leakages and thus unstable current production throughout the experiments (Figure 5.3.3 and Figure 5.3.4). The cathode of UGold1 was leaking more in the beginning of the experiments, which is why more extra PTFE was also applied on it compared to the cathode of UGold2. After a couple of days, it was concluded that constantly adding more PTFE would most likely end up blocking the cathodes completely, which is why no more PTFE was added and small leaking was accepted.

UGold1 was first run for two days at $E_{\text{cell}} = 0 \text{ V}$, after which the E_{cell} was increased to 0.1 V and briefly to 0.2 V before going to 0.5 V. At voltages below 0.5 V, there was no clear change in current production in relation to increasing voltage; it remained relatively stable around 1 A m^{-2} . At $E_{\text{cell}} = 0.5 \text{ V}$, current production doubled to 2 A m^{-2} . When the E_{cell} was increased further to 0.8 V and 1.0 V, there was an instant peak in the current production to 3.6 and 3.9 A m^{-2} , respectively, but after that the current density decreased back to around the same level that was observed at 0.5 V.

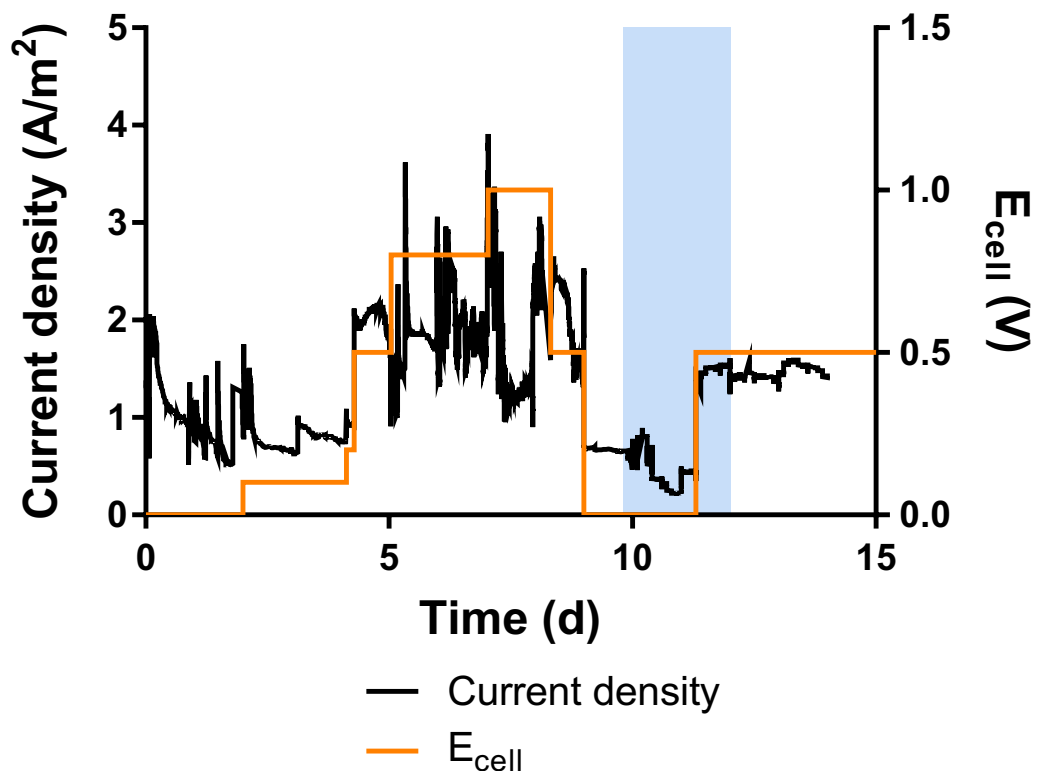


Figure 5.3.3 Current density produced by UGold1 at different applied cell voltages when operated with air-cathode. Blue area represents the time period when recirculation from cathode to anode was used.

Current production in UGold2 (Figure 5.3.4) again followed the same trend as in UGold1 expect for being slightly higher for reasons discussed above. Here, the current density remained just below 2 A m^{-2} at E_{cell} range of 0–0.2 V, and at 0.5 V, it increased

to almost 4 A m^{-2} , being approximately twice as high as the current density of UGold1. Higher E_{cell} values of 0.8 and 1.0 V again resulted in instant peaks in current density (reaching 6.9 A m^{-2} at best) but similarly to UGold1, current production then rapidly decreased back to around 4 A m^{-2} .

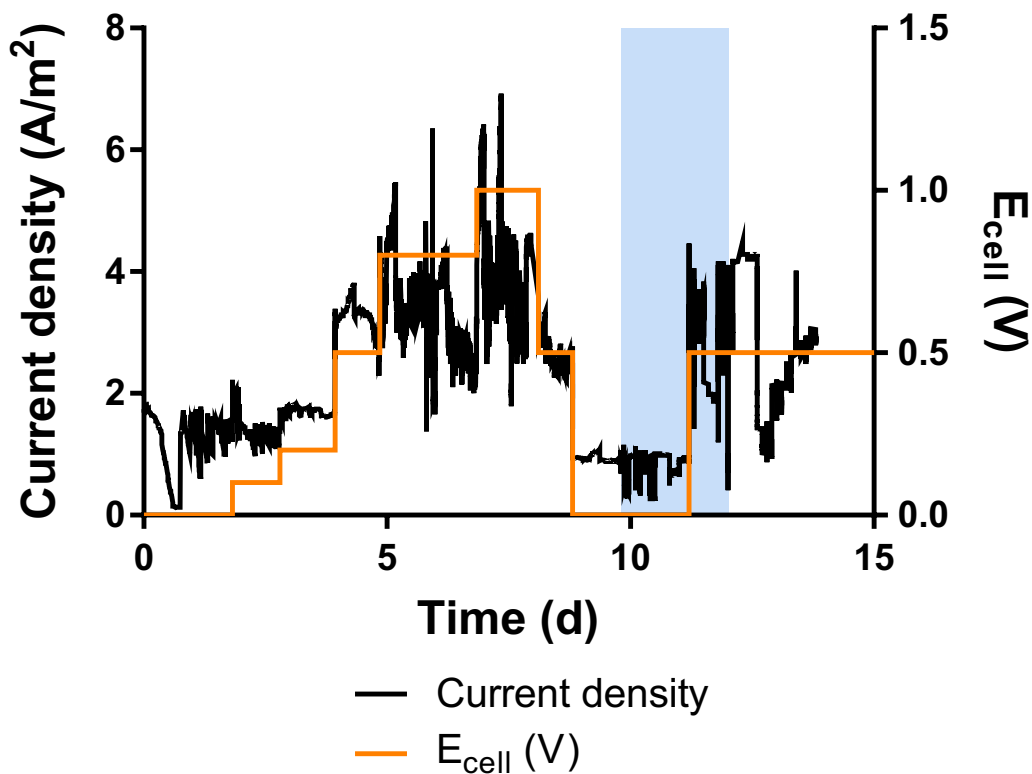


Figure 5.3.4 Current density produced by UGold2 at different applied cell voltages when operated with air-cathode. Blue area represents the time period when recirculation from cathode to anode was used.

Interestingly, the current production of both reactors was slightly lower when going back to the lower E_{cell} values (0 and 0.5 V) compared to the performance in the beginning at these voltages. The current production of UGold2 at $E_{\text{cell}} = 0.5 \text{ V}$ does not quite follow this trend, but at this point the reactor was suffering from increased leaking, which resulted in unstable current output. One explanation for the reduced performance could be the clear formation of biomass on the air-facing side of the cathodes, which might have blocked parts of the cathode and thus reduced oxygen diffusion into the cathode and catholyte. An example of the biomass growth on the cathode of UGold2 at the end of the experiments is presented in Figure 5.3.5. The biomass on the cathode was not analysed in more detail within this study.

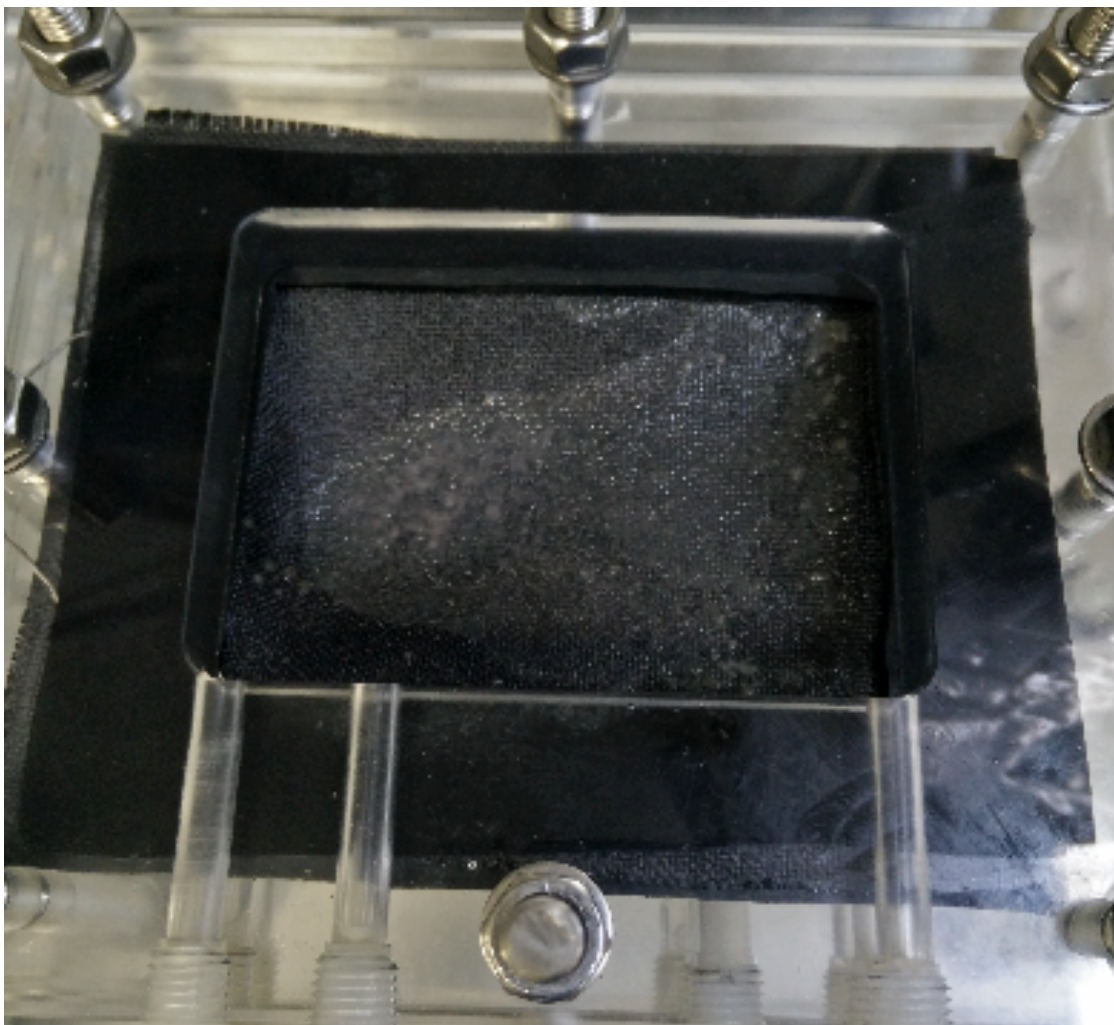


Figure 5.3.5 Biomass growing on the cathode of UGold2 at the end of the air-cathode experiments.

The effect of recirculating the cathodic effluent back to the anode was tested between days 10–12 at E_{cell} 0 V and 0.5 V (Figure 5.3.3 and Figure 5.3.4). The recirculation did not have a notable effect on the current density, apart from causing it to have slightly more variation. The aim of the recirculation was to decrease the pH gradient formed between the two electrodes (see Chapter 3.1.1), and the small effect of the recirculation on the power output here can be explained by the fact that the pH differences between the anode and the cathode were very small to begin with (Figure 5.3.6). The recirculation also provides the anode with an extra source of buffer but clearly the buffering capacity of the anolyte was not a limiting factor here since the recirculation did not result in an increase in current density produced.

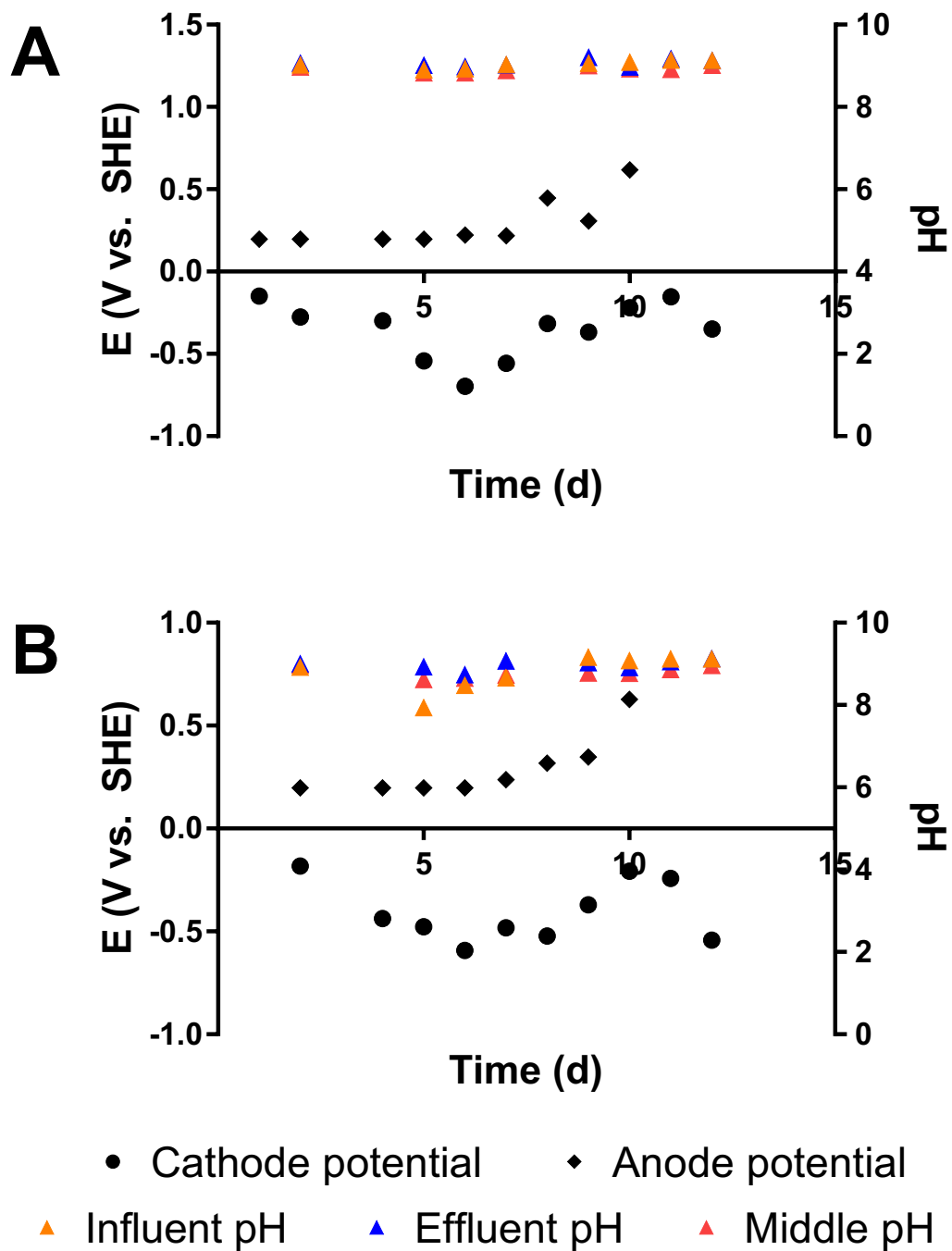


Figure 5.3.6 Measured cathode and anode potentials and influent, effluent and middle chamber pH of (A) UGold1 and (B) UGold2 during the operation with air-cathodes.

As already mentioned, there were no large differences in the pH of the different compartments in the UGold reactors (Figure 5.3.6). For UGold1 (Figure 5.3.6(A)), the anode, cathode, and middle compartment pH remained very stable at 9.0 ± 0.1 , 9.1 ± 0.1 and 8.9 ± 0.1 , respectively. In UGold2 (Figure 5.3.6(B)), there was an initial decrease in anode pH to 7.9 on day 5, but after that it steadily increased and stabilised around 9.1. At times, the cathode pH was actually lower than the anode pH (on day 10), and the overall

average for the cathode pH was 8.9 ± 0.2 . The middle compartment pH remained at 8.8 ± 0.2 .

The measured cathode potentials varied from -0.1 to -0.7 V for UGold1 (Figure 5.3.6(A)) and -0.2 to -0.6 V vs. SHE for UGold2 (Figure 5.3.6(B)), the cathode potentials decreasing with increasing E_{cell} . The measured anode potentials remained relatively stable around $+0.2$ V vs. SHE in both reactors during the first 7 days of operation. After this, the anode potential in both reactors increased, reaching $+0.6$ V vs. SHE on day 10. For the rest of the experiments, the anode potentials could no longer be measured due to problems with reference electrodes in anode chambers.

The individual voltammograms of the anodes and cathodes of the two reactors are presented in Figure 5.3.7. The voltammogram of Acid-NCNT with four layers of WD-40 obtained in the preliminary cathode experiments is also included for comparison. It can be seen that neither of the UGold cathodes quite comes up to the performance of the preliminary test cathode. The cathode of UGold2 (Figure 5.3.7(B)) also seems to be able to reach slightly higher current densities as the cathode of UGold1 (Figure 5.3.7(A)), which was already seen in the CA data. This is also true for the anodes. When comparing the measured cathode and anode potentials to the voltammograms, the current production of both UGold reactors could be expected to be much higher than measured. For example on day 6, when the E_{cell} was at 0.8 V, the measured cathode potentials were -0.7 and -0.6 V and anode potentials $+0.2$ and $+0.2$ V vs. SHE for UGold1 and UGold2, respectively. For UGold1, this would mean current densities around 10 A m^{-2} and for UGold2, current densities higher than 20 A m^{-2} . In reality, the measured current densities were closer to 2 and 4 A m^{-2} , respectively. This suggests that the reactor configuration and operation could still be optimised in order to obtain higher current densities.

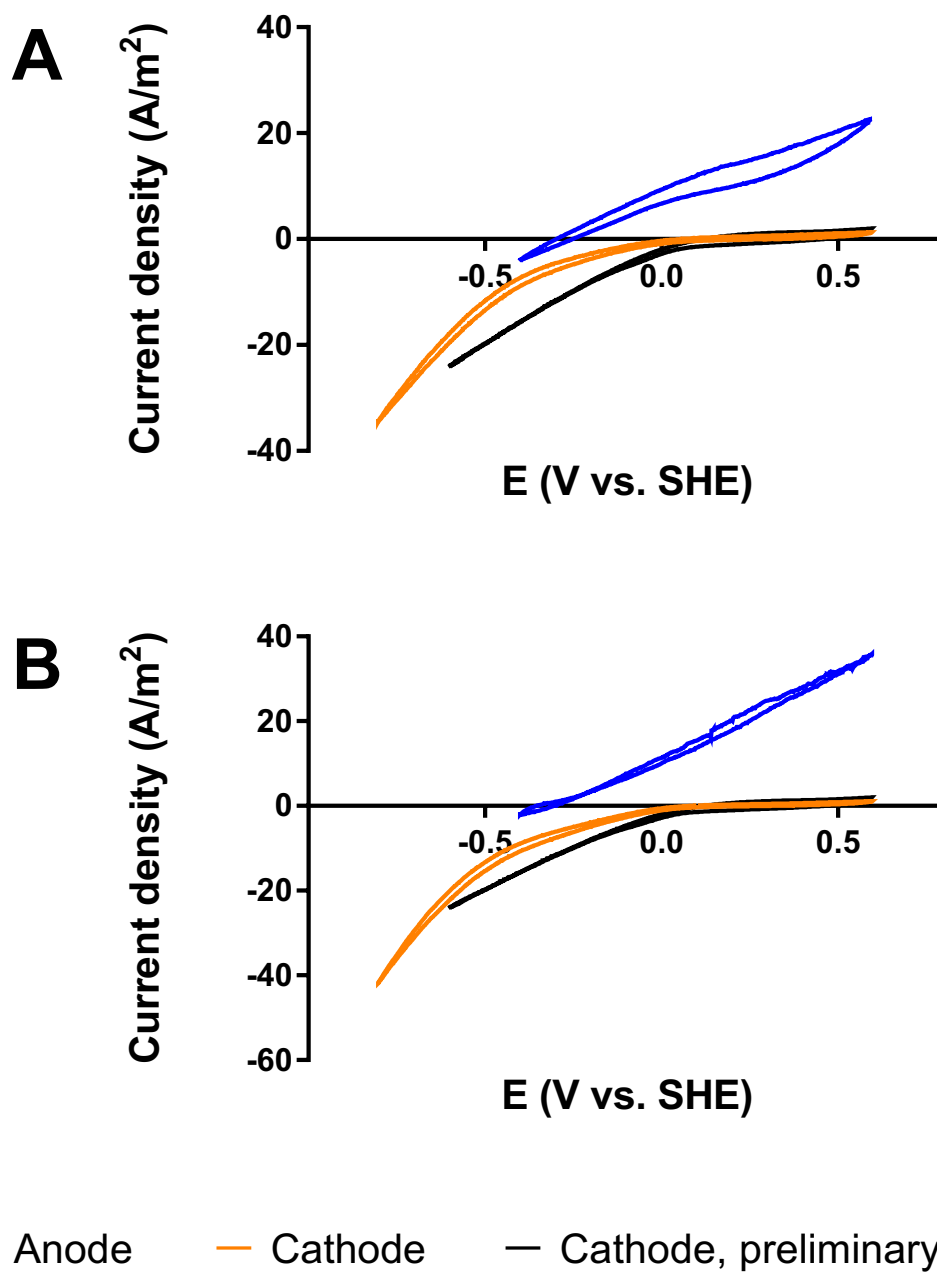


Figure 5.3.7 CVs conducted for the anodes and the cathodes in (A) UGold1 and (B) UGold2. The voltammogram of Acid-NCNT with 4xWD-40 in the preliminary experiments is included for comparison.

6 DISCUSSION

The preliminary experiments conducted separately to the anodic and cathodic side of the UGold reactor provided information and understanding of the performance of the cell. To a certain extent, the results were also promising towards a low-energy nutrient recovery system, even though reaching power-free operation still needs further research.

6.1 Enrichment of the neutrophilic consortium

Feed pH 7.5 was found to be most suitable for the enriched electroactive consortium, compared to the other two pH values studied, 6.5 and 5.5. Indeed, the current production by the anodic biomass decreased with decreasing feed pH. In a previously studied three-compartment UGold reactor, fed with synthetic hydrolysed urine at $\text{pH } 9.2 \pm 0.2$, the anodic pH stabilised to 6.8 during steady-state operation and power densities up to 37.6 A m^{-2} were obtained (Ledezma et al. 2017). I.e., the best performance in this study was obtained at a pH higher than the working pH in the earlier study, whereas the highest current densities obtained here (around 15 A m^{-2}) were less than half of what was reached before. Thus, this study was not able to provide results that would help optimise the anode performance in the UGold reactor.

In another Master's thesis (Winkler 2009), the effect of increasing TAN concentration followed by increasing pH on anode biomass performance in an MFC was studied. The tests were carried out in two-compartment MFCs using graphite electrodes, inoculated with a mixture of different activated sludge samples. The TAN concentration change was carried out in continuous mode, increasing the concentration from <1 up to 6.35 g N L^{-1} at the anode. Even the highest TAN concentrations were not found to inhibit the power production, although it decreased slightly towards the end of the experiments (which was assumed to mostly be due to other factors, such as technical problems with pumping and increased feed discharge). After completing the TAN concentration increase, the pH of the anode was also increased from 7 to 9 in 0.5 daily steps. Each increase in anode pH actually led to an increase in power production, resulting in a total change from 1.3 to 8.2 mW m^{-2} . No inhibition was detected, even though the concentration of inhibitory NH_3 was already around 3 g N L^{-1} at pH 9. These results seem to be in accordance to what was seen in this study, i.e. the higher the pH, the higher the power output. This is interesting considering the increasing concentration of NH_3 with increasing pH, and the commonly accepted inhibitory effect of NH_3 .

As the rough buffer capacity analysis showed, the buffer capacity of the feed did not seem to be the activity limiting factor even at a low pH in the enrichment experiments. However, even if the buffer capacity of the reactor medium is enough to neutralise the protons produced at the anode, protons might be accumulating within the anode biofilm if they are not transported to the medium fast enough. This might lead to the pH of the anode biofilm being up to one pH unit lower than in the surrounding medium. A pH decrease from 7 to 6 in the reactor medium was found to inhibit current production by *Geobacter sulfurreducens*, an organism closely related to bacteria often found on MFC anodes and capable of producing high current densities. When pH was increased back to 6.8, the biofilm recovered, indicating that the damage by low pH was not permanent. (Franks et al. 2009) Similar trend was observed in this study when the pH of the reactor feed was first lowered from 6.5 to 6.0, resulting in a current density drop from approximately 6 to 0 A m⁻², but then recovering back to approximately 2.5 A m⁻² when the pH was returned to 6.5. Overcoming this limitation might require changes to the structure and/or materials used in MFCs in order to better facilitate proton migration out of the anode biomass. Another option would be to engineer the microbes themselves to form more porous biofilms or tolerate lower pH values better. (Franks et al. 2009)

However, the CVs conducted for the anodes in the enrichment experiments did not show clear signs of plateauing, i.e. the mass transfer of neither a substrate nor a buffer seemed to be the limiting factor in the current generation. Thus, it seems more likely that the reason for poor performance at low pH was related to the composition of the microbial communities themselves. Even though the microbial community analysis showed that there were some changes and shifts in the communities at different pH values, the main limiting factor might be in the choice of the original inoculum. The reactors were inoculated with a community that had been adjusted to a feed pH of 9.2±0.2 for a long time and was therefore highly specialised in growing under such conditions (Ledezma et al. 2017). In order to achieve better results at lower pH, it might be more reasonable to choose a wider start-up community that is not specialised to certain conditions. A successful enrichment with this approach might, however, take notably more time, and would not have been possible within the time frame of this project.

The microbial community analysis conducted within this project was also a rather rough one and only provided information on the species present in the microbial community. In order to fully understand the roles of the different bacteria in the system and how they were developed, a detailed metagenomics analysis would be required. This was beyond the scope of this thesis, but will be carried out in the near future as part of the UGold project to further understand the system.

An interesting observation during the experiments was that when a reactor was inoculated with graphite granules colonised by active biomass, the biomass was capable of very efficiently colonising the remainder of the electrode surface and the growth was extremely rapid. This was observed already in the enrichment experiments when mov-

ing colonised anodes from one reactor to another, and later again when inoculating the UGold reactors with the graphite granules used in the enrichment experiments. Even when the fraction of the colonised graphite granules was as low as 13.8 % of the complete mass of granules used as the electrode, growth was fast and enrichment could be carried out in 18 d.

It was also concluded here that simultaneous increase in TAN concentration and pH in batch mode resulted in inhibition of the biomass. The sudden increase in the pH from 7.5 to 9 seemed to be too much for the microbial community, and a better approach was to first increase the TAN concentration and only after that the pH, as was also done by Winkler (2009). If the enrichment is carried out in continuous mode, simultaneous TAN concentration and pH increase might be possible if the feed rate is kept low, allowing time for the biomass to adjust to the changing conditions.

6.2 Performance of the catalyst materials

Two important goals were set for the different catalyst materials tested at the air-cathodes: changing the ORR onset potential to a more positive direction and increasing the obtainable current densities. A slight change in the onset potential was observed with all studied materials, changing from -0.5 and 0 V vs. SHE (with the air-cathode without catalyst coating) in ammonia and phosphate buffers, respectively, to approximately +0.1 V vs. SHE in both buffers with all studied materials. The change was positive but not as notable as would have been needed for spontaneous ORR and completely power-free operation.

When comparing the onset potentials obtained with NCNTs here to those obtained with similar materials in the literature, the results vary quite significantly. When using a much more complex deposition technique that aligns the nanotubes in a more organised vertical position, the onset potentials were similar to the results of this study, remaining in the range from 0 to +0.1 V vs. SHE (Feng, Yan, et al. 2011a; Gong et al. 2009). The current densities, on the other hand, were actually significantly higher in this study (approximately 15 A m^{-2} at applied voltage -0.6 V vs. SHE) than e.g. in the study by Feng et al. (2011), where current production remained in the range of $2\text{--}4 \text{ A m}^{-2}$ at applied voltage -0.6 V vs. SHE.

In another study by Kundu et al. (2009), however, NCNTs grown at two different temperatures (550 and 850 °C) and tested conducting CVs in 0.5 M H_2SO_4 on a glassy carbon electrode were found to increase the onset potential from approximately +0.1 V (with a bare glassy carbon electrode) to +0.7 V vs. SHE. Highest current densities obtained were approximately 5.5 A m^{-2} at 0 V vs. SHE. When the N speciation of the NCNTs grown at the lower and the higher temperature was analysed, it was found that 42.8 and 20.3 %, respectively, of the NCNTs were present as pyridinic-like N. The high amount of pyridinic N was concluded to be responsible for the high onset potentials. This

could also be seen in the slightly higher onset potential (+0.74 V) of the NCNT grown at a lower temperature, having a higher amount of pyridinic N, compared to the onset potential (+0.7 V vs. SHE) of the NCNT grown at higher temperature. (Kundu et al. 2009) A similar trend was discovered by Lai et al. (2012) who also compared NCNTs grown at different temperatures (550, 850 and 1000 °C), even though the pyridinic N concentrations were lower (3.48, 4.08 and 0.96 %, respectively). Based on these results, it can also be estimated that an increasing growth temperature leads to decreased amount of pyridinic N (Kundu et al. 2009; Lai et al. 2012).

With NG, higher ORR onset potentials than those obtained in this study have been reported in the literature (Feng et al. 2013). With similar kind of NG, an onset potential of approximately 0.4 V vs. SHE was obtained and when implementing N active sites (mesoporous graphitic carbon nitride) to NG, the onset potential was even further increased to 0.6–0.7 V. However, the current densities reported were again rather low (2–4 A m⁻²), which was lower than obtained in this study with NG at similar voltages (5–7 A m⁻²). The notable variation in ORR onset potentials is most likely due to the speciation of the N compounds in the catalyst, i.e. the percentage of pyridinic N present.

For the same PAC studied in this project (Norit SX Plus, Cabot), an ORR onset potential was previously reported to be 0.37 V vs. SHE (Watson et al. 2013). The difference might be due to the different deposition techniques used in the study by Watson et al. (2013), using ink-like solutions spread on the cathode surface, which might result in a higher concentration of the catalyst on the electrode surface. Also the electrode materials were different (glassy carbon disc and stainless steel mesh). With Norit SX Plus, a maximum current density of approximately 9 A m⁻² was obtained at potentials -0.2 V vs. SHE and lower. (Watson et al. 2013)

In this study, the concentration of nanoparticles in the deposition liquid was clearly not the limiting factor for catalyst deposition since the liquid never cleared up during the deposition, meaning that a considerable amount of the nanoparticles remained in the solution even after the deposition. It is possible that EPD as the deposition technique was not effective enough or that the parameters used in the EPD could be optimised further. In general, it seems that high deposition voltages (in the range of 40–50 V or even up to 100–500 V) and short deposition times (1–5 min) have been found to provide the best results (Boccaccini et al. 2006; Du & Pan 2006; Thomas et al. 2005). However, the medium used in the EPD must be conductive enough to be able to reach high deposition voltages. In this study, for example, it was found out that deposition voltages >30 V were not possible when using Milli-Q as the medium, due to its low conductivity.

However, when considering the N-doped materials, it seems that the speciation of the N present in the catalyst material plays an important role (Kundu et al. 2009; Lai et al. 2012). Therefore, this might contribute to the relatively low ORR onset potentials obtained here more than the total amount of the catalyst deposited on the electrode surface.

The relatively small changes in the onset potentials suggest that the amount of pyridinic N in the NCNT and NG studied here is not especially high, whereas graphitic N is likely present at higher concentrations based on the relatively high current densities obtained. The speciation of N in the catalyst materials depends on the manufacturing methods (Feng et al. 2011a; Feng et al. 2011b) and could not be affected within this study.

6.3 Performance of PTFE as diffusion layer and operation of UGold reactor with air-cathode

The commercial PTFE sprays tested as the diffusion layers on the air-cathode showed promising results in the preliminary tests but proved to be less reliable already in slightly larger scale. A major issue was liquid leaking through the cathodes despite the PTFE layers, whereas excess PTFE seemed to simultaneously start blocking the cathode, hindering oxygen diffusion. When applying the PTFE by hand, as was done here, it is also very hard to make sure that the coating is uniform and each layer is sprayed in a similar way. Similar issues are related to the most commonly used method of painting PTFE layers on the air-facing side of the cathode (Cheng et al. 2006a).

The application of the PTFE spray could also be carried out with a more professional equipment, e.g. spray gun, rather than by hand, to obtain even diffusion layers. Methods for fixing the PTFE more efficiently on the electrode surface could also be studied. Sintering at high temperatures (340–350 °C or higher) is a commonly used method to fix PTFE on the electrode surface (Dong et al. 2012; Mathias et al. 2010). In this study, the PTFE sprays were either dried in room temperature overnight or at 100 °C for 1 h. The effect of using higher temperatures on the diffusion layer performance could be tested.

Other PTFE applying techniques could also be considered. A commonly used method for applying PTFE coating is to dip the electrode in an aqueous PTFE suspension, allow for the excess suspension to drip off, and fix the PTFE particles on the electrode surface by sintering. This might result in a more uniform layer of PTFE but cannot be applied in cases when the PTFE coating is only needed on one side of the electrode, which is the case with air-cathodes. When only wanted on one side of the electrode, using a PTFE paste and physically pressing it on the electrode surface might both make the layer more uniform and fix it more tightly to the surface. (Mathias et al. 2010)

Making the air-cathode more waterproof is a key factor in making use of the whole potential of the separately optimised anode and cathode in the UGold reactor. In this study, the constant leaking of the cathode and air accumulation between the cathode and the catholyte due to the reactor positioning were likely the most important reasons for low current generation.

This study did not provide any information on the concentration of the target nutrient N in the middle compartment of the UGold reactor. The reason for this was the low cur-

rent output of the UGold reactors operated with air-cathodes, which was assumed to lead to very low concentration of the nutrients. Therefore, concentration measurements were concluded unnecessary since the possible differences in nutrient concentrations between reactor chambers might not have been higher than the error limits of the analyses.

7 CONCLUSIONS

This study provided valuable information on both the anodic and the cathodic performance and was a step towards a low-energy bioelectrochemical nutrient recovery method. However, further optimisation will be required especially in regards to the air-cathode in order to reach completely power-free reactor in the future.

7.1 Concluding remarks

When enriching an acidophilic electroactive consortium for the anode, pH 7.5 was found to be more optimal than the two other studied pH, 6.5 and 5.5. Highest current density obtained at pH 7.5 was 15 A m^{-2} at $E_{\text{we}} = 0 \text{ V vs. SHE}$. This was in correlation with earlier studies, also showing that pH < 6 can inhibit anodic biomass and power generation tends to be higher at higher pH, even at high NH_3 concentrations. The largest activity-hindering factor at lower pH seemed to be the composition of the microbial community itself, rather than limitations in electrolyte buffer capacity. This was most likely due to the biomass inoculum being accustomed to the higher pH of hydrolysed urine (around pH 9.2). A metagenomics analysis would provide more detailed information on the development and behaviour of the microbial community at the anode, and might help in planning further optimisation of the anodic performance. Using a different start-up community, i.e. less optimised for certain conditions, for the enrichment might also have resulted in better performance at lower pH but might not have been feasible within the timeframe of this study.

The three studied catalyst materials at the air-cathode – NCNT, NG and PAC – increased the current densities obtainable with the carbon cloth electrode quite considerably compared to the electrode with no catalyst coating. In CV measurements, current densities up to 35 A m^{-2} at -0.6 V vs. SHE were obtained. All studied catalysts were also able to shift the ORR onset potential to a slightly more positive potential, from -0.5 and 0 V vs. SHE in ammonia (pH 9) and phosphate (pH 7) buffer, respectively, to $+0.1 \text{ V vs. SHE}$ in both buffers. This indicates that the studied catalyst materials are rather suitable for the basic pH commonly present at the cathode since the ORR onset potential obtained at pH 9 was identical compared to pH 7.

The shift in onset potential was, however, not enough for completely power-free operation of the UGold reactor. The best performance was obtained with NCNT pre-treated in acid, and the current production was further increased when adding diffusion layers on the air-facing side using a commercial PTFE spray WD-40. The number of layers

sprayed had a notable effect on the cathode performance, and four layers were found to be the optimal amount with the spray in question.

An air-cathode UGold reactor was able to reach current densities of 1–2 A m⁻² at $E_{\text{cell}} = 0$ V, and the power density was doubled when cell voltage was increased to 0.5 V. However, better performance could have been expected based on the preliminary tests as well as the individual CV and potential measurements of the electrodes in the reactor. The largest issue with the UGold reactor operated with an air-cathode was the inadequate performance of the PTFE diffusion layer on the air-facing side. This resulted in constant leaking through the cathode. Because of this, the reactors also had to be positioned horizontally, which resulted in air accumulating in the cathode chamber between the cathode and the catholyte, thus reducing the effective surface area.

7.2 Outlook

The first step towards improved performance of the air-cathode reactor would be to improve the waterproofing of the cathode. The effect of sintering at high temperatures on the fixation of the PTFE spray on the electrode surface could be tested. The application of the PTFE spray could also be carried out with a more professional equipment, e.g. a spray gun, rather than by hand, to obtain even and uniform diffusion layers. Replacing the Acid-NCNT catalyst coating with PVDF-PAC might also result in more waterproof end product since the PVDF contributes to the waterproofing similarly to PTFE. Furthermore, current densities obtained with PVDF-PAC as the catalyst layer were almost in the same range as with Acid-NCNT. If the cathode can be made completely waterproof, operation of the reactor in vertical position would be possible, which might also reduce the disturbance caused by the air bubbles in the system.

The effect of changing EPD parameters on the catalyst performance could be tested in order to obtain higher current densities. The deposition voltage could be further increased higher than 50 V and the deposition time conversely shortened from 5 min. However, the deposition medium might have to be changed to a more conductive solution to be able to reach higher voltages. A highly desired result would also be a further increase in the ORR onset potential. If this cannot be reached with a better deposition of the studied carbon nanomaterials, similar materials with higher pyridinic N content could be tested.

When these technical issues are solved and higher current densities obtained, the concentration of the target nutrients in the middle chamber should be studied. This part was completely lacking from this work. When the performance in laboratory-scale would be found satisfactory, the UGold concept should first be tested in pilot-scale and after that, it could hopefully be upscaled to full commercial use. The goal of UGold is to offer a decentralised nutrient recovery method that would target complexes with large enough wastewater stream, such as universities, airports and office blocks. This would require

implementation of source-separating sanitation system in the facilities, which is why UGold treatment unit could be more easily integrated to new buildings already during the construction.

UGold reactors would still release their effluent into the sewer network and thus be dependent on the centralised WWTP. However, removing most of the nutrients already at the source of the wastewater stream would drastically reduce the nutrient load arriving at the centralised WWTP. This would result in lower energy consumption of the treatment process and thus lower costs.

Naturally, the end product (in this case, a concentrated nutrient-rich liquid or possibly pure NH_4HCO_3 as a solid) needs to have a value for the recovery process to be feasible. The fertiliser market in agriculture is large but highly competitive, and the fertiliser volumes produced by UGold might not be sufficient to effectively compete against larger suppliers. A more realistic option could be to turn to horticulture and individual gardeners who use fertilisers in much smaller amounts. A good idea might be to target horticulturists nearby the location of the UGold treatment unit, which would lower transportation costs and make the fertiliser a truly local product, increasing its market value.

REFERENCES

- An, S.J., Zhu, Y., Lee, S., Stoller, M.D., Emilsson, T., Park, S., Velamakanni, A., An, J. & Ruoff, R.S. 2010. Thin film fabrication and simultaneous anodic reduction of deposited graphene oxide platelets by electrophoretic deposition. *Journal of Physical Chemistry Letters*, 1(8), pp. 1259–1263.
- Angelidaki, I. & Ahring, B.K. 1993. Applied Microbiology and Biotechnology. *Applied Microbiology and Biotechnology*, 38, pp. 560–564.
- Atkins, P. & de Paula, J. 2014. Atkins' Physical Chemistry. 10th edition, Oxford University Press.
- Bard, A.J. & Faulkner, L.R. 1944. Electrochemical methods. Fundamentals and Applications. 2nd edition, John Wiley & Sons, Inc.
- Boccaccini, A.R., Cho, J., Roether, J.A., Thomas, B.J.C., Minay, E.J. & Shaffer, M.S.P. 2006. Electrophoretic deposition of carbon nanotubes. *Carbon*, 44(15), pp. 3149–3160.
- Bolger, A.M., Lohse, M. & Usadel, B. 2014. Trimmomatic: A flexible trimmer for Illumina Sequence Data. *Bioinformatics*, 30(15), pp. 2114–2120.
- Booker, N.A., Priestley, A.J. & Fraser, I.H. 1999. Struvite Formation in Wastewater Treatment Plants: Opportunities for Nutrient Recovery. *Environmental Technology*, 20(7), pp. 777–782.
- Brenner, D.J., Krieg, N.R. & Staley, J.T. 2005. Bergey's Manual of Systematic Bacteriology, Volume Two, Part C: The Alpha-, Beta-, Delta- and Epsilonproteobacteria. 2nd edition, Springer.
- Cai, T., Park, S.Y. & Li, Y. 2013. Nutrient recovery from wastewater streams by microalgae: Status and prospects. *Renewable and Sustainable Energy Reviews*, 19, pp. 360–369.
- Cao, X., Huang, X., Liang, P., Xiao, K., Zhou, Y., Zhang, X. & Logan, B.E. 2009. A New Method for Water Desalination Using Microbial Desalination Cells. *Environmental Science & Technology*, 43(18), pp. 7148–7152.
- Caporaso, J.G., Kuczynski, J., Stombauch, J., Bittinger, K., Bushman, F.D., Costello, E.K., Fierer, N., Gonzalez Pena, A., Goodrich, J.K., Gordon, J.I., Huttley, G.A., Kelley, S.T., Knights, D., Koenig, J.E., Ley, R.E., Lozupone, C.A., McDonald, D., Muegge, B.D., Pirrung, M., Reeder, J., Sevinsky, J.R., Turnbaugh, P.J., Walter, W.A., Widmann, J., Yatsunenko, T., Zanevel, J. & Knight, R. 2010. QIIME allows analysis of high-throughput community sequencing data. *Nature Methods*, 7, pp. 335–336.
- Chen, X., Sun, D., Zhang, X., Liang, P. & Huang, X. 2015. Novel Self-driven Microbial

- Nutrient Recovery Cell with Simultaneous Wastewater Purification. *Scientific Reports*, 5(15744), pp. 1–10.
- Cheng, S., Liu, H. & Logan, B.E. 2006a. Increased performance of single-chamber microbial fuel cells using an improved cathode structure. *Electrochemistry Communications*, 8(3), pp. 489–494.
- Cheng, S., Liu, H. & Logan, B.E. 2006b. Power densities using different cathode catalysts (Pt and CoTMPP) and polymer binders (Nafion and PTFE) in single chamber microbial fuel cells. *Environmental Science and Technology*, 40(1), pp. 364–369.
- Cordell, D. 2013. Peak phosphorus and the role of P recovery in achieving food security. In T. A. Larsen, K. M. Udert, & J. Lienert, eds. *Source Separation and Decentralization for Wastewater Management*. IWA Publishing, pp. 29–44.
- Cordell, D., Drangert, J.O. & White, S. 2009. The story of phosphorus: Global food security and food for thought. *Global Environmental Change*, 19(2), pp. 292–305.
- DeSantis, T.Z., Hugenholtz, P., Larsen, N., Rojas, M., Brodie, E.L., Keller, K., Huber, T., Dalevi, D., Hu, P. & Andersen, G.L. 2006. Greengenes, a Chimera-Checked 16S rRNA Gene Database and Workbench Compatible with ARB. *Applied Environmental Microbiology*, 72(7), pp. 5069–5072.
- Dong, H., Yu, H., Wang, X., Zhou, Q. & Feng, J. 2012. A novel structure of scalable air-cathode without Nafion and Pt by rolling activated carbon and PTFE as catalyst layer in microbial fuel cells. *Water Research*, 46(17), pp. 5777–5787.
- Du, C. & Pan, N. 2006. Supercapacitors using carbon nanotubes films by electrophoretic deposition. *Journal of Power Sources*, 160(2 SPEC. ISS.), pp. 1487–1494.
- El-Shafai, S.A., El-Gohary, F.A., Nasr, F.A., van der Steen, N.P. & Gijzen, H.J. 2007. Nutrient recovery from domestic wastewater using a UASB-duckweed ponds system. *Bioresource Technology*, 98(4), pp. 798–807.
- Erisman, J.W., Galloway, J.N., Seitzinger, S., Bleeker, A., Dise, N.B., Petrescu, A.M.R., Leach, A.M. & de Vries, W. 2013. Consequences of human modification of the global nitrogen cycle. *Philosophical transactions of the Royal Society of London. Series B, Biological sciences*, 368(1621), pp. 1–9.
- Erisman, J.W. & Larsen, T.A., 2013. Nitrogen economy of the 21st century. In T. A. Larsen, K. M. Udert, & J. Lienert, eds. *Source Separation and Decentralization for Wastewater Management*. IWA Publishing, pp. 45–58.
- FAO. 2016. FAOSTAT. Available at: <http://faostat.fao.org/beta/en/#data/RF> [Accessed November 22, 2016].
- Feng, L., Yang, L., Huang, Z., Luo, J., Li, M., Wang, D. & Chen, Y. 2013. Enhancing

- electrocatalytic oxygen reduction on nitrogen-doped graphene by active sites implantation. *Scientific Reports*, 3(3306), pp. 1–8.
- Feng, L., Yan, Y., Chen, Y. & Wang, L. 2011a. Nitrogen-doped carbon nanotubes as efficient and durable metal-free cathodic catalysts for oxygen reduction in microbial fuel cells. *Energy & Environmental Science*, 4(5), pp. 1892–1899.
- Feng, L., Chen, Y. & Chen, L. 2011b. Easy-to-Operate and Low-Temperature Synthesis of Gram-Scale Nitrogen-Doped Graphene and Its Application as Cathode Catalyst in Microbial Fuel Cells. *ACS Nano*, 5(12), pp. 9611–9618.
- Franks, A.E., Nevin, K.P., Jia, H., Izallalen, M., Woodard, T.L. & Lovley, D.R. 2009. Novel strategy for three-dimensional real-time imaging of microbial fuel cell communities: monitoring the inhibitory effects of proton accumulation within the anode biofilm. *Energy & Environmental Science*, 2(January), pp.113–119.
- Freguia, S., Rabaey, K., Yuan, Z. & Keller, J. 2008. Sequential anode-cathode configuration improves cathodic oxygen reduction and effluent quality of microbial fuel cells. *Water Research*, 42(6–7), pp. 1387–1396.
- Friedler, E., Butler, D. & Alfiya, Y. 2013. Wastewater composition. In T. A. Larsen, K. M. Udert, & J. Lienert, eds. *Source Separation and Decentralization for Wastewater Management*. IWA Publishing, pp. 241–257.
- Galloway, J.N., Aber, J.D., Erisman, J.W., Seitzinger, S.P., Howarth, R.W., Cowling, E.B. & Cosby, B.J. 2003. The Nitrogen Cascade. *American Institute of Biological Sciences*, 53(4), pp. 341–356.
- Gong, K., Du, F., Xia, S., Durstock, M. & Dai, L. 2009. Nitrogen-Doped Carbon Nanotube Arrays with High Electrocatalytic Activity for Oxygen Reduction. *Science*, 323(5915), pp. 760–764.
- Hamelers, B., Sleutels, T., Jeremiasse, A.W., Post, J.W., Strik, D. & Rozendal, R.A. 2010. Technological factors affecting BES performance and bottlenecks towards scale up. In K. Rabaey, L. Angenent, U. Schröder & J. Keller, eds. *Bioelectrochemical Systems: From Extracellular Electron Transfer to Biotechnological Application*. IWA Publishing, pp. 205–223.
- Hansen, K.H., Angelidaki, I. & Ahring, B.K. 1998. Anaerobic digestion of swine manure: Inhibition by ammonia. *Water Research*, 32(1), pp. 5–12.
- Harnisch, F. & Freguia, S. 2012. A basic tutorial on cyclic voltammetry for the investigation of electroactive microbial biofilms. *Chemistry - An Asian Journal*, 7(3), pp. 466–475.
- Harnisch, F. & Schröder, U. 2010. From MFC to MXC: chemical and biological cathodes and their potential for microbial bioelectrochemical systems. *Chemical Society reviews*, 39(11), pp. 4433–4448.

- Harnisch, F., Schröder, U. & Scholz, F. 2008. The Suitability of Monopolar and Bipolar Ion Exchange Membranes as Separators for Biological Fuel Cells. *Environmental Science and Technology*, 42(April), pp. 1740–1746.
- Holt, J.G., Krieg, N.R., Sneath, P.H.A., Staley, J.T. & Williams, S.T. 1994. Bergey's Manual of Determinative Bacteriology. Ninth edition, Williams & Wilkins.
- Jönsson, H. & Vinnerås, B. 2013. Closing the loop: Recycling nutrients to agriculture. In T. A. Larsen, K. M. Uder, & J. Lienert, eds. *Source Separation and Decentralization for Wastewater Management*. IWA Publishing, pp. 163–178.
- Kissinger, P.T. & Heineman, W.R. 1983. Cyclic voltammetry. *Journal of Chemical Education*, 60(9), pp. 702–706.
- Kundu, S., Nagaiah, T.C., Xia, W., Wang, Y., van Dommele, S., Bitter, J.H., Santa, M., Grundmeier, G., Bron, M., Schuhmann, W. & Muhler, M. 2009. Electrocatalytic activity and stability of nitrogen-containing carbon nanotubes in the oxygen reduction reaction. *Journal of Physical Chemistry C*, 113(32), pp. 14302–14310.
- Kuntke, P., Zamora, P., Saakes, M., Buisman, C.J.N. & Hamelers, H.V.M. 2016. Gas-permeable hydrophobic tubular membranes for ammonia recovery in bio-electrochemical systems. *Environmental Science: Water Research & Technology*, 2, pp. 261–265.
- Kuntke, P., Sleutels, T.H.J.A., Saakes, M. & Buisman, C.J.N. 2014. Hydrogen production and ammonium recovery from urine by a Microbial Electrolysis Cell. *International Journal of Hydrogen Energy*, 39(10), pp. 4771–4778.
- Kuntke, P., Smiech, K.M., Bruning, H., Zeeman, G., Saakes, M., Sleutels, T.H.J.A., Hamelers, H.V.M. & Buisman, C.J.N. 2012. Ammonium recovery and energy production from urine by a microbial fuel cell. *Water Research*, 46(8), pp. 2627–2636.
- Kuntke, P., Geleji, M., Bruning, H., Zeeman, G., Hamelers, H.V.M. & Buisman, C.J.N. 2011. Effects of ammonium concentration and charge exchange on ammonium recovery from high strength wastewater using a microbial fuel cell. *Bioresource Technology*, 102(6), pp. 4376–4382.
- LaBelle, E. & Bond, D.R. 2010. Cyclic voltammetry for the study of microbial electron transfer at electrodes. In K. Rabaey, L., Angenent, U. Schröder & J. Keller, eds. *Bioelectrochemical Systems: From Extracellular Electron Transfer to Biotechnological Application*. IWA Publishing, pp. 137–151.
- Lai, L., Potts, J.R., Zhan, D., Wang, L., Poh, C.K., Tang, C., Gong, H., Shen, Z., Lin, J. & Ruoff, R.S. 2012. Exploration of the active center structure of nitrogen-doped graphene-based catalysts for oxygen reduction reaction. *Energy & Environmental Science*, 5(7), pp. 7936–7942.

- Larsen, T.A. & Gujer, W. 2013. Implementation of source separation and decentralization in cities. In T. A. Larsen, K. M. Udert, & J. Lienert, eds. *Source Separation and Decentralization for Wastewater Management*. IWA Publishing, pp. 135–150.
- Ledezma, P., Jermakka, J., Keller, J. & Freguia, S. 2017. Recovering Nitrogen as a Solid without Chemical Dosing: Bio-Electroconcentration for Recovery of Nutrients from Urine. *Environmental Science & Technology Letters*, 4(3), pp. 119–124.
- Ledezma, P., Kuntke, P., Buisman, C.J.N., Keller, J. & Freguia, S. 2015. Source-separated urine opens golden opportunities for microbial electrochemical technologies. *Trends in Biotechnology*, 33(4), pp. 214–220.
- Logan, B.E., 2010. Materials for BES. In K. Rabaey, L. Angenent, U. Schröder & J. Keller, eds. *Bioelectrochemical Systems: From Extracellular Electron Transfer to Biotechnological Application 2*. IWA Publishing, pp. 184–204.
- Logan, B.E. 2008. Microbial fuel cells. 1st edition, John Wiley & Sons.
- Logan, B.E., Hamelers, B., Rozendal, R., Schröder, U., Keller, J., Freguia, S., Aelterman, P., Verstraete, W. & Rabaey, K. 2006. Microbial fuel cells: Methodology and technology. *Environmental Science and Technology*, 40(17), pp. 5181–5192.
- Mathias, M.F. et al., 2010. Diffusion media materials and characterisation. In W. Vielstich, H.A. Gasteiger, A. Lamm, eds. *Handbook of Fuel Cells – Fundamentals, Technology and Applications, Volume 3: Fuel Cell Technology and Applications*. John Wiley & Sons, Ltd., pp. 517–537.
- Maurer, M., Pronk, W. & Larsen, T.A. 2006. Treatment processes for source-separated urine. *Water Research*, 40(17), pp. 3151–3166.
- Mehanna, M., Saito, T., Yan, J., Hickner, M., Cao, X., Huang, X. & Logan, B.E. 2010. Using microbial desalination cells to reduce water salinity prior to reverse osmosis. *Energy & Environmental Science*, 3(8), pp. 1114–1120.
- Mitchell, C., Fam, D. & Abeysuriya, K. 2013. Transitioning to sustainable sanitation: a transdisciplinary pilot project of urine diversion. Institute for Sustainable Futures, University of Technology Sydney.
- Nam, J.Y., Kim, H.W. & Shin, H.S. 2010. Ammonia inhibition of electricity generation in single-chambered microbial fuel cells. *Journal of Power Sources*, 195(19), pp. 6428–6433.
- Nicholson, R.S. 1965. Theory and Application of Cyclic Voltammetry for Measurement of Electrode Reaction Kinetics. *Analytical Chemistry*, 37(11), pp. 1351–1355.
- Pronk, W. & Koné, D. 2009. Options for urine treatment in developing countries.

- Desalination*, 248(1–3), pp. 360–368.
- Pronk, W., Biebow, M. & Boller, M. 2006. Electrodialysis for recovering salts from a urine solution containing micropollutants. *Environmental Science and Technology*, 40(7), pp. 2414–2420.
- Qi, Z. 2008. Electrochemical methods for catalyst activity evaluation. In J. Zhang, ed. *PEM Fuel Cell Electrocatalysts and Catalyst Layers: Fundamentals and Applications*. Springer, pp. 547–608.
- Rabaey, K. 2010. Bioelectrochemical systems: a new approach towards environmental and industrial biotechnology. In K. Rabaey, L. Angenent, U. Schröder & J. Keller, eds. *Bioelectrochemical Systems: From Extracellular Electron Transfer to Biotechnological Application*. IWA Publishing, pp. 1–16.
- Rabaey, K., Rodríguez, J., Blackall, L.L., Keller, J., Gross, P., Batstone, D., Verstraete, W. & Neelson, K.H. 2007. Microbial ecology meets electrochemistry: electricity-driven and driving communities. *The ISME Journal*, 1(1), pp. 9–18.
- Rabaey, K. & Verstraete, W. 2005. Microbial fuel cells: Novel biotechnology for energy generation. *Trends in Biotechnology*, 23(6), pp. 291–298.
- Rodríguez Arredondo, M., Kuntke, P., ter Heijne, A., Hamelers, H.V.M. & Buisman, C.J.N. 2017. Load ratio determines the ammonia recovery and energy input of an electrochemical system. *Water Research*, 111, pp. 330–337.
- Rozendal, R.A., Hamelers, H.V.M. & Buisman, C.J.N. 2006. Effects of Membrane Cation Transport on pH and Microbial Fuel. *Environmental Science & Technology*, 40(17), pp. 5206–5211.
- Saeed, H.M., Hussein, G.A., Yousef, S., Saif, J., Al-Asheh, S., Abu Fara, A., Azzam, S., Khawaga, R. & Aidan, A. 2015. Microbial desalination cell technology: A review and a case study. *Desalination*, 359, pp. 1–13.
- Schröder, U. & Harnisch, F. 2010. Electrochemical losses. In K. Rabaey, L. Angenent, U. Schröder & J. Keller, eds. *Bioelectrochemical Systems: From Extracellular Electron Transfer to Biotechnological Application*. IWA Publishing, pp. 119–133.
- Shi, X., Feng, Y., Wang, X., Lee, H., Liu, J., Qu, Y., He, W., Kumar, S.M.S. & Ren, N. 2012. Application of nitrogen-doped carbon powders as low-cost and durable cathodic catalyst to air-cathode microbial fuel cells. *Bioresour. Technol.*, 108, pp. 89–93.
- Siegrist, H., Laurenzi, M. & Udert, K.M. 2013. Transfer into the gas phase: ammonia stripping. In T. A. Larsen, K. M. Udert, & J. Lienert, eds. *Source Separation and Decentralization for Wastewater Management*. IWA Publishing, pp. 337–350.
- Song, C. & Zhang, J. 2008. Electrocatalytic oxygen reduction reaction. In J. Zhang, ed. *PEM Fuel Cell Electrocatalysts and Catalyst Layers: Fundamentals and*

Applications. Springer, pp. 89–134.

- Strathmann, H. 2010. Electrodialysis, a mature technology with a multitude of new applications. *Desalination*, 264(3), pp.268–288.
- Strathmann, H. 2004. Ion-Exchange Membrane Separation Processes. 1st edition, Elsevier B.V.
- Sutton, M., Bleeker, A., Howard, C.M., Bekunda, M., Grizzetti, B., de Vries, W., van Grinsven, H.J.M., Abrol, Y.P., Adhya, T.K., Billen, G., Davidson, E.A., Datta, A., Diaz, R., Erisman, J.W., Liu, X.J., Oenema, O, Palm, C., Raghuram, N., Reis, S., Scholz, R.W., Sims, T., Westhoek, H. & Zhang, F.S. 2013. Our Nutrient World: The challenge to produce more food and energy with less pollution. Global Overview of Nutrient Management. The Centre for Ecology and Hydrology (CEH), Edinburgh.
- Syers, J.K., Johnston, A.E. & Curtin, D. 2008. Efficiency of soil and fertilizer phosphorus use. Reconciling changing concepts of soil phosphorus behaviour with agronomic information. *Fao Fertilizer and Plant Nutrition Bulletin* 18.
- Tchobanoglous, G. & Leverenz, H. 2013. The rationale for decentralization of wastewater infrastructure. In T. A. Larsen, K. M. Udert, & J. Lienert, eds. *Source Separation and Decentralization for Wastewater Management*. IWA Publishing, pp. 101–115.
- Terrones, M., 2004. Carbon nanotubes: synthesis and properties, electronic devices and other emerging applications. *International Materials Reviews*, 49(6), pp. 325–377.
- Thomas, B.J.C., Boccaccini, A.R. & Shaffer, M.S.P. 2005. Multi-walled carbon nanotube coatings using Electrophoretic Deposition (EPD). *Journal of the American Ceramic Society*, 88(4), pp. 980–982.
- Udert, K.M., Brown-Malker, S. & Keller, J. 2013. Electrochemical systems. In T. A. Larsen, K. M. Udert, & J. Lienert, eds. *Source Separation and Decentralization for Wastewater Management*. IWA Publishing, pp. 321–335.
- Udert, K.M. & Jenni, S. 2013. Biological nitrogen conversion processes. In T. A. Larsen, K. M. Udert, & J. Lienert, eds. *Source Separation and Decentralization for Wastewater Management*. IWA Publishing, pp. 291–305.
- Udert, K.M. & Wächter, M. 2012. Complete nutrient recovery from source-separated urine by nitrification and distillation. *Water Research*, 46(2), pp. 453–464.
- Udert, K.M., Larsen, T.A. & Gujer, W. 2006. Fate of major compounds in source-separated urine. *Water Science and Technology*, 54(11–12), pp. 413–420.
- Udert, K.M., Larsen, T.A., Biebow, M. & Gujer, W. 2003a. Urea hydrolysis and precipitation dynamics in a urine-collecting system. *Water Research*, 37(11), pp. 2571–2582.

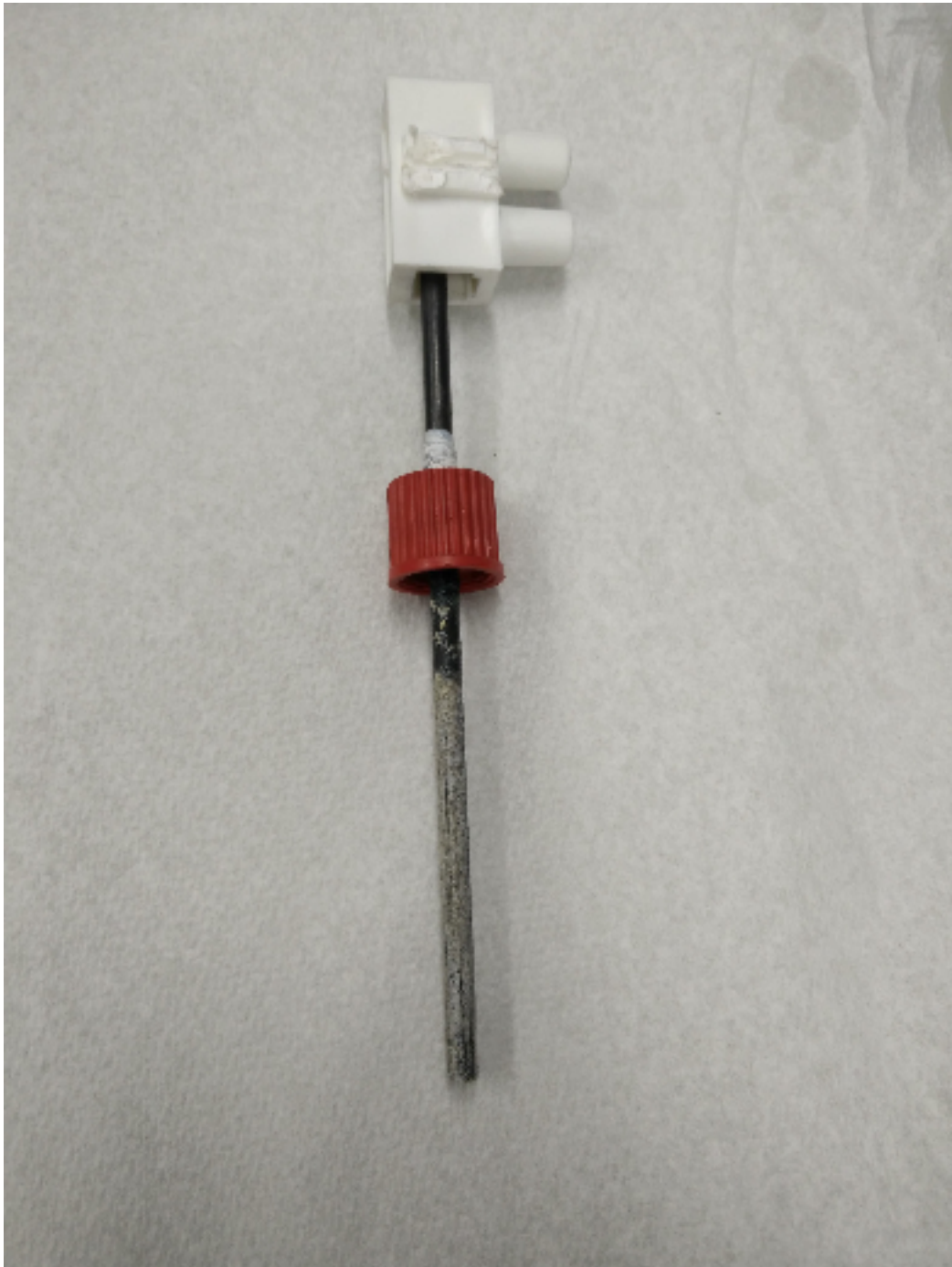
- Udert, K.M., Larsen, T.A. & Gujer, W. 2003b. Biologically induced precipitation in urine-collecting systems. *Water Science and Technology: Water Supply*, 3(3), pp. 71–78.
- Udert, K.M., Larsen, T.A. & Gujer, W. 2003c. Estimating the precipitation potential in urine-collecting systems. *Water Research*, 37, pp. 2667–2677.
- Vinnerås, B., Nordin, A., Niwagaba, C. & Nyberg, K. 2008. Inactivation of bacteria and viruses in human urine depending on temperature and dilution rate. *Water Research*, 42(15), pp. 4067–4074.
- Watson, V.J., Nieto Delgado, C. & Logan, B.E. 2013. Influence of chemical and physical properties of activated carbon powders on oxygen reduction and microbial fuel cell performance. *Environmental science & technology*, 47(12), pp. 6704–10.
- Winkler, R., 2009. *Urine Treatment with Microbial Fuel Cells: Inhibition Effects of Ammonia Compounds*. Master of Science thesis, Swiss Federal Institute of Aquatic Science and Technology (Eawag), Swiss Federal Institutes of Technology Domain, Switzerland.
- Zhang, F., Li, J. & He, Z. 2014. A new method for nutrients removal and recovery from wastewater using a bioelectrochemical system. *Bioresource Technology*, 166, pp. 630–634.
- Zhao, F., Harnisch, F., Schröder, U., Scholz, F., Bogdanoff, P. & Herrmann, I. 2006. Challenges and constraints of using oxygen cathodes in microbial fuel cells. *Environmental Science and Technology*, 40(17), pp. 5193–5199.

APPENDIX A: COMPOSITION OF THE TRACE ELEMENT SOLUTION

Constituent	Concentration (g/L)
EDTA (acid form)	10
NaOH ¹	
FeCl ₃ ·6H ₂ O	1.5
H ₃ BO ₃	0.15
CuSO ₄ ·5H ₂ O	0.03
KI	0.18
MnCl ₂ ·4H ₂ O	0.12
Na ₂ MoO ₄ ·2H ₂ O	0.06
ZnSO ₄ ·7H ₂ O	0.12
CoCl ₂ ·6H ₂ O	0.15
NiCl ₂ ·6H ₂ O	0.023

¹ used to adjust pH of EDTA to 7

APPENDIX B: PHOTO OF STRUVITE FORMATION ON THE CATHODE IN THE ENRICHMENT EXPERIMENTS



APPENDIX C: ION SPECIES DISTRIBUTION AT DIFFERENT PH

Compound	Species	Distribution (%)			
		pH 5.5	pH 6.5	pH 7.5	pH 8.9 (original recipe)
Na+1	Na+1	82.655	80.011	85.226	82.707
	Na-Acetate (aq)	3.518	3.738	4.151	4.046
	NaCl (aq)	4.545	4.397	2.048	0.37
	NaSO4-	0.965	0.943	1.092	1.147
	NaHPO4-	1.261	6.747	4.065	4.203
	Na2HPO4 (aq)	0.087	0.452	0.293	0.297
	NaH2PO4 (aq)	6.969	3.712	0.227	0
	NaCO3-	0	0	0.223	4.821
	NaHCO3 (aq)	0	0	2.674	2.384
K+1	K+1	83.556	82.136	90.019	91.522
	K-Acetate (aq)	2.518	2.717	3.104	3.17
	KCl (aq)	4.594	4.513	2.163	0.409
	KSO4-	1.256	1.247	1.486	1.635
	KHPO4-	0.823	4.472	2.772	3.003
	K2HPO4 (aq)	0.207	1.103	0.216	0.24
	KH2PO4 (aq)	7.045	3.811	0.24	0.011
NH4+1	NH4+1	97.764	97.642	96.443	75.689
	NH4SO4-	2.225	2.244	2.409	2.047
	NH3 (aq)	0.011	0.114	1.147	22.237
	CaNH3+2	0	0	0	0.02
Mg+2	Mg+2	45.632	31.046	33.515	27.827
	MgCl+	12.049	8.287	3.785	0.577
	MgSO4 (aq)	4.536	3.124	3.66	3.314
	MgPO4-	0	0	0.032	0.689
	MgHPO4 (aq)	9.617	36.257	22.099	19.691
	Mg-Acetate+	28.167	21.28	23.165	19.076
	MgCO3 (aq)	0	0	1.01	18.787
	MgHCO3+	0	0	12.731	9.59
	Mg2CO3+2	0	0	0	0.214
	MgOH+	0	0	0	0.032
	Mg(NH3)2+2	0	0	0	0.204
Ca+2	Ca+2	39.526	32.882	34.754	17.49
	CaCl+	6.585	5.538	2.476	0.229
	CaSO4 (aq)	4.946	4.165	4.779	2.622
	CaNH3+2	0	0.019	0.198	1.909
	Ca(NH3)2+2	0	0	0	0.064
	CaHPO4 (aq)	6.034	27.82	16.601	8.966
	CaPO4-	0	0.36	2.118	27.69
	CaH2PO4+	22.605	10.468	0.615	0.013
	Ca-Acetate+	20.293	18.747	19.98	9.972
	CaHCO3+	0	0	16.391	7.484
	CaCO3 (aq)	0	0	2.089	23.56

Compound	Species	Distribution (%)				
		pH 5.5	pH 6.5	pH 7.5	pH 8.9 (original recipe)	
Acetate-1	Acetate-1	83.79	92.177	95.133	94.7	
	Na-Acetate (aq)	2.94	3.124	3.469	3.382	
	K-Acetate (aq)	3.219	3.474	1.131	1.155	
	H-Acetate (aq)	9.877	1.082	0.113	0	
	Mg-Acetate+	0.101	0.076	0.083	0.545	
	Ca-Acetate+	0.072	0.067	0.071	0.214	
Cl-1	Cl-1	94.389	94.53	96.572	96.469	
	CaCl+	0.014	0.011	0.012	0.036	
	MgCl+	0.025	0.017	0.018	0.121	
	KCl (aq)	3.384	3.325	1.071	1.098	
	NaCl (aq)	2.188	2.117	2.326	2.276	
SO4-2	SO4-2	43.204	43.214	48.093	52.246	
	MgSO4 (aq)	0.133	0.092	0.108	0.78	
	CaSO4 (aq)	0.145	0.123	0.141	0.463	
	NaSO4-	6.639	6.489	7.516	7.894	
	KSO4-	13.228	13.129	4.458	4.906	
	NH4SO4-	36.644	36.953	39.686	33.712	
PO4-3	PO4-3	0	0	0	0.1	
	HPO4-2	3.838	24.108	59.313	63.423	
	H2PO4-	75.507	47.762	11.548	0.504	
	H3PO4	0.022	0	0	0	
	MgPO4-	0	0	0	0.115	
	MgHPO4 (aq)	0.041	0.178	0.46	3.282	
	CaHPO4 (aq)	0.026	0.136	0.346	1.121	
	CaPO4-	0	0	0.044	3.461	
	CaH2PO4+	0.097	0.051	0.013	0	
	NaHPO4-	1.261	7.74	19.817	20.489	
	KHPO4-	1.259	7.848	5.891	6.381	
	K2HPO4 (aq)	0.158	0.968	0.229	0.255	
	KH2PO4 (aq)	10.778	6.687	0.51	0.023	
	KPO4-2	0	0	0	0.019	
	Na2HPO4 (aq)	0.044	0.259	0.714	0.723	
	Na2PO4-	0	0	0	0.016	
	NaH2PO4 (aq)	6.969	4.258	1.107	0.047	
	NaPO4-2	0	0	0	0.039	
	CO3-2	CO3-2	0	0	0.352	7.869
		HCO3-	0	0	92.76	84.466
H2CO3* (aq)		0	0	4.352	0.164	
MgCO3 (aq)		0	0	0	0.537	
MgHCO3+		0	0	0.045	0.274	
CaHCO3+		0	0	0.059	0.16	
CaCO3 (aq)		0	0	0	0.505	
NaCO3-		0	0	0.187	4.029	
NaHCO3 (aq)		0	0	2.235	1.993	